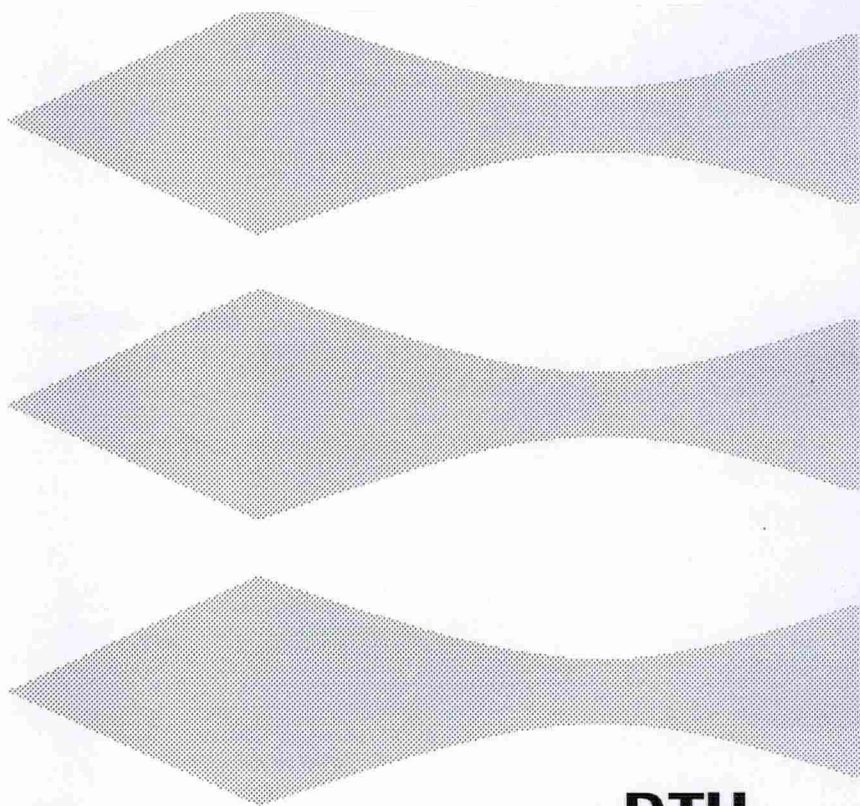


Wave Load Prediction - a Design Tool

Delft University of Technology
Ship Hydromechanics Laboratory
Library

Mekelweg 2, 2628 CD Delft
The Netherlands

Phone: +31 15 2786873 - Fax: +31 15 2781836



Tommy Pedersen
PhD thesis
January 2000

DEPARTMENT OF
NAVAL ARCHITECTURE
AND OFFSHORE ENGINEERING



Wave Load Prediction - a Design Tool

Tommy Pedersen

DEPARTMENT OF NAVAL ARCHITECTURE AND OFFSHORE ENGINEERING
TECHNICAL UNIVERSITY OF DENMARK · LYNGBY
JANUARY 2000

Department of Naval Architecture and Offshore Engineering
Technical University of Denmark
Building 101E, DK-2800 Lyngby, Denmark
Phone +45 4525 1360, Telefax +45 4588 4325
email ish@ish.dtu.dk, Internet <http://www.ish.dtu.dk>

Published in Denmark by
Department of Naval Architecture and Offshore Engineering
Technical University of Denmark

© T. Pedersen 2000
All right reserved

Publication Reference Data

Pedersen, T.

Wave Load Prediction - a Design Tool.

Ph.D. Thesis.

*Department of Naval Architecture and Offshore Engineering,
Technical University of Denmark, January, 2000.*

ISBN 87-89502-17-5

*Keywords: Non-Linear, Wave loads, Time Domain, Frequency
Domain, Quadratic Strip Theory, Linear Strip
Theory.*

Preface

This thesis is submitted as a partial fulfilment of the requirements for the Danish Ph.D. degree. The work has been performed at the Department of Naval Architecture and Offshore Engineering, (ISH), Technical University of Denmark, (DTU). The project has been supervised by Professor Jørgen Juncher Jensen and Associate Professor Poul Andersen, whose help and guidance has been highly appreciated.

The study has been financed by the Danish Technical Research Council (STVF), and additional funding for two stays abroad has been provided by the Danish Vetlesen Fellowship for Naval Architects and by the Department of Naval Architecture and Offshore Engineering, DTU.

Validation of the work has been made during a stay at Registro Italiano Navale, Italy. Dr. Mario Dogliani made this stay possible and the friendly cooperation with the staff at the Research and Development Department is gratefully acknowledged. Special thanks to Rasmus Folsø for our cooperation on parts of the programme and extensive feedback.

Also great thanks to Professor Alaa Mansour, Department of Naval Architecture and Offshore Engineering, U.C. Berkeley, California, who made my stay possible and met me with kindness.

Special thanks to my colleagues at ISH, friends and family for invaluable help and support.

Tommy Pedersen
Lyngby, March 26, 2000

This page is intentionally left blank.

Executive Summary

The objective of the present work has been to develop a computational design tool for calculation of wave loads on ships and implement it into a comprehensive program system. The program system, named I-ship, has been developed at the department and is used for conceptual design.

Based on a survey of available theoretical methods for determining wave loads on a ship, three have been selected. The criteria are

- Robustness of the method in as wide a range of applications as possible.
- Reasonable computational time on a state-of-the-art PC.
- Accuracy within engineering practice.
- Linear as well as non-linear predictions should be available.

The methods are a linear strip theory according to Salvesen, Tuck and Faltinsen [49] for calculations in five degrees of freedom, a quadratic strip theory based on Jensen and Pedersen [24] and, finally, a non-linear time-domain strip theory according to Petersen [44]. As all of these methods have the determination of the two-dimensional flow around the ship hull in common, a library of methods has been developed to include different types of effects. The structure of the program consists of three submodules, which is a preprocessor, a strip theory solver and a postprocessor.

Implementation of all the above-mentioned methods has proved to be too ambitious. The library of routines for determination of the two-dimensional flow around the hull consists of two mapping and three boundary element methods. However, due to a too simple grid generator, only the mapping methods and a single boundary element method have proved to be sufficiently robust for general use.

The linear strip theory has with respect to functionality been shown to require a more advanced method for including roll damping.

The quadratic strip theory has the full functionality with the possibility of including flexibility of the ship hull and determining fatigue damage. It has been shown to be a very robust method for determination of vertical wave loads on ships including second order effects.

The present implementation of the non-linear time-domain strip theory has the functionality of determining responses in regular waves.

The implemented theoretical methods have been verified and validated against results from model tests and other programs. The task of verifying and validating a complete application including hydroelasticity and fatigue damage prediction has been too ambitious. The emphasis has therefore been on a robust well tested application, including the linear strip theory and the rigid body part of the quadratic strip theory with the statistical facilities to perform short- and long-term predictions.

Generally, a fairly good agreement has been found. However, as been shown by reference to the work by the ITTC78 [17] and the ITTC81 [18] committee differences can be expected, which has also been the case in the present work.

The results from the linear strip theory have been shown generally to agree well with other programs and the agreement with model tests has been acceptable. However, disagreements have also been found for the roll motion in beam sea and for the vertical bending moment on a fast ferry.

Also the results from the quadratic strip theory have been shown generally to agree well with both other programs and model tests. The strip theory on which the quadratic strip theory is based and the methods for determining added mass and damping can be combined in a number of ways. One has been shown to deviate from the remaining. However, this is only a small part of the available combinations. For the second order part of the response, a comparison with the design values based on the IACS unified rules for classification [40] shows good agreement with the hogging bending moment but a 30% larger sagging bending moment.

The results from the present implementation of the non-linear time-domain strip theory have been shown to give heave motion in good agreement with other programs, but the pitch motion and vertical bending moment deviate from results from other programs. This method has therefore, in the present implementation, not been judged useful for analyses.

In general, the developed system has been shown to be a useful tool for determination of wave loads on ships. The included facilities have been more limited than first intended, however, suggestions for improving and extending the present version have been made.

Synopsis

Denne afhandling omhandler bestemmelsen af globale bølgelaste på et skibsskrog. Formålet har været at lave et designværktøj i form af et computer program til bestemmelse af designlaste på et skib og integrere dette i et omfattende programsystem. Programsystemet, benævnt I-ship, er udviklet på instituttet og kan benyttes til konceptuelt design af skibe.

Der er udført et litteraturstudie, af hvilket resultatet er en kort gennemgang af mulige teoretiske metoder. Baseret på denne gennemgang er der valgt tre metoder ud fra følgende kriterier:

- Metoderne skal i så vidt et omfang være robuste.
- Beregninger skal kunne udføres indenfor rimelig tid på en state-of-the-art PC.
- Metoderne skal give resultater indenfor ingeniørmæssig nøjagtighed.
- Lineære såvel som ikke-lineære metoder skal inkluderes.

De valgte metoder er en lineær stripteori af Salvesen, Tuck og Faltinsen [49] til beregninger i fem frihedsgrader, en anden-ordens stripteori baseret på Jensen og Pedersen [24] og endelig en ikke-lineær tidsdomæne stripteori af Petersen [44]. Disse metoder har alle bestemmelsen af den to-dimensionale strømning om skibets skrog, i form af medsvingende vand og dæmpning, til fælles. Derfor er der lavet et bibliotek af rutiner til bestemmelsen af disse, hvorved forskellige effekter kan inkluderes. Det udviklede program består af en præprocessor, en solver og en postprocessor og er således opdelt i tre dele.

Implementering af ovenstående har vist sig for ambitiøst. Biblioteket af rutiner til bestemmelsen af den to-dimensionale strømning om skibets skrog består af to 'mapping-metoder' og tre rand-element metoder. Da den implementerede metode til diskretisering af skibets skrog har vist sig for simpel, kan kun 'mapping-metoderne' og en enkelt rand-element metode benyttes generelt.

Den lineære stripteori har med hensyn til funktionalitet vist sig at kræve en mere avanceret metode til inkludering af rulledæmpning end den relativt simple metode, der er implementeret som en del af dette arbejde.

Den anden-ordens stripteori har den fulde funktionalitet, hvilket omfatter muligheden for at medtage effekter af skrogbjælkens elasticitet og ligeledes beregninger af udmattelse. Denne metode har vist sig meget robust til bestemmelse af vertikale bølgebelastninger, hvor der medtages anden-ordens effekter.

Den nærværende implementering af den ikke-lineære tidsdomæne stripteori har funktionaliteten til at bestemme gensvar i regelmæssige bølger

De implementerede metoder er blevet verificeret og valideret ved sammenligning med resultater fra andre programmer og ligeledes med resultater fra modelforsøg. Opgaven i at verificere og validere det komplette program inklusive delene der omfatter hydroelasticitet og udmattelse har vist sig for stor. Vægten er derfor blevet lagt på et gennemtestet program der inkluderer den lineære stripteori og den anden-ordens stripteori med skibet modelleret uden elasticitet og med de statistiske faciliteter der muliggør kort- og langtidsforudsigelser.

Generelt er resultatet af sammenligningerne, at der er fundet en rimelig overensstemmelse. Der er dog også fundet resultater der ikke stemmer så godt overens. En meget god overensstemmelse kan ikke altid forventes som det også er vist ved reference til arbejdet af ITTC78 [17] og ITTC81 [18].

Den lineære stripteori har generelt vist sig at give resultater i god overensstemmelse med de sammenlignede programmer og en acceptabel overensstemmelse med modelforsøg. Der er dog fundet resultater der ikke svarer så godt overens for rullebevægelsen i tværsøj og ligeledes for det vertikale bøjningsmoment på en hurtigtsejlende færge.

Også resultaterne fra den anden-ordens stripteori har generelt vist god overensstemmelse med de sammenlignede programmer og også med modelforsøg. Stripteorien, den anden-ordens metode baseres på, og metoderne til bestemmelse af medsvingende vand og dæmpning kan kombineres. En kombination af disse metoder har vist sig at give resultater der afviger fra de øvrige. Dette er dog kun en af flere mulige kombinationer. Med hensyn til gensvaret af anden orden er der lavet en sammenligning med IACS regler for klassificering [40], der giver god overensstemmelse for hogging bøjningsmomentet (kølløftning) men 30 % større sagging bøjningsmoment (kølsækning).

Den nærværende implementering af den ikke-lineære tidsdomæne stripteori har vist at kunne bestemme sætningsbevægelsen i god overensstemmelse med andre programmer, men for duvning og det vertikale bøjningsmoment er der ikke opnået tilfredsstillende resultater. Denne implementering af metoden er derfor ikke fundet egnet til praktisk brug.

Generelt er det vist at det udviklede system er et brugbart værktøj til bestemmelse af bølgelaste på et skib. Faciliteterne, der er til rådighed, er blevet knap så omfangsrige som den oprindelige intention, men forslag til forbedringer og inkludering af yderligere metoder er givet.

Contents

Preface	i
Executive Summary	iii
Synopsis (in Danish)	v
Contents	vii
Symbols and Nomenclature	xi
1 Introduction	1
1.1 Overview and Background	1
1.2 Objectives and Scope of the Work	2
1.3 Structure of the Thesis	2
2 Methods for Prediction of Wave Loads	5
2.1 Introduction	5
2.2 Strip Theory Methods	5
2.2.1 Linear Strip Theory	5
2.2.2 Non-Linear Strip Theories	6
2.3 Unified Slender Body Theory	7
2.4 $2\frac{1}{2}$ D Methods	7
2.5 3D Methods	8

2.5.1	Green Function Methods	8
2.5.2	Rankine Source Methods	8
2.6	Summary of the Methods for Prediction of Wave Loads	9
3	Strip Theory Formulations	11
3.1	Introduction	11
3.2	Linear Strip Theories	12
3.2.1	The Five Degree of Freedom Strip Theory	13
3.3	Non-Linear Strip Theories	19
3.3.1	The Quadratic Strip Theory	19
3.3.2	The Non-Linear Time-Domain Strip Theory	26
3.4	Limitations on the Strip Theory Methods	27
3.4.1	Slenderness	28
3.4.2	Speed	28
3.4.3	Frequency Range	31
4	Hydrodynamic Coefficients	35
4.1	Mapping Technique	36
4.1.1	The Lewis-Form Method	36
4.2	2D Green Function Methods	40
4.2.1	Simple Green Function	44
4.2.2	Frank Close Fit	47
4.2.3	Discretization of the Integral Equation	48
4.3	Irregular Frequencies	52
4.4	Roll Damping	52

5	Response Statistics	55
5.1	Introduction	55
5.2	Short-Term Response Statistics	55
5.2.1	Linear Frequency Response	56
5.2.2	Quadratic Frequency Response	59
5.2.3	Fatigue Analysis	61
5.3	Long-Term Response Statistics	63
6	Verification and Validation of the Code	67
6.1	Analysis of a Container Ship	68
6.1.1	Geometry	69
6.1.2	Weight Condition	70
6.1.3	Motions	70
6.1.4	Loads	73
6.1.5	Long-Term Predictions	75
6.1.6	Results from the Non-linear Time-domain Strip Theory	77
6.2	Analysis of a VLCC	81
6.2.1	Geometry	82
6.2.2	Weight Condition	82
6.2.3	Motions	83
6.2.4	Loads	86
6.3	Analysis of a Fast Ferry	89
6.3.1	Weight Condition	89
6.3.2	Motions	90
6.3.3	Accelerations	91
6.3.4	Loads	94
6.4	Summary of the Verification and Validation	95

7	System Design	97
7.1	Introduction	97
7.2	General	97
7.3	The Preprocessor	99
7.3.1	General Input	100
7.3.2	Load Case Related Input	101
7.3.3	Short-Term Related Input	103
7.3.4	Long-Term Related Input	103
7.4	The Strip Theory Solver	104
7.5	The Postprocessor	104
8	Conclusion and Recommendations	107
8.1	Conclusion	107
8.2	Recommendations for Future Work	109
	Bibliography	111
	List of Figures	121
	List of Tables	123
A	Additional Results on the Container Ship	125
B	Documentation of the User Interface	127
B.1	The Preprocessor	127
B.1.1	Input Ship Data	128
B.1.2	Input Operational Parameters	129
B.1.3	Specify Analysis	130
B.2	The Strip Theory Solver	136
B.3	The Postprocessor	136
	List of Ph.D. Theses Available from the Department	139

Symbols and Nomenclature

The symbols used in this thesis are explained when they are first introduced. The following list contains the main symbols used.

Latin Letters

A	Sectional submerged area of station
B	Waterline breadth
C_1, C_2	Lewis mapping coefficients
C_M	Sectional area coefficient
G	Green function
H_s	Significant wave height
L_{pp}	Length between perpendiculars
$P(\omega)$	Phase function
$P(x, y)$	Field point
$Q(\xi, \eta)$	Singularity point
$R(\omega)$	Response amplitude operator
S_η	Wave spectrum as a function of ω
S_η^e	Wave spectrum as a function of ω_e
$S_R(\omega)$	Response spectrum
S_0	Body boundary
S_F	Free-surface boundary
S_B	Seabed boundary
S_L, S_R	Radiation boundaries
T	Draught
T_z	Mean zero crossing period
T_{aft}	Draught at aft perpendicular
T_{fore}	Draught at fore perpendicular
U	Velocity
U_{rel}	Relative velocity between wave and ship

V	Variance
a	Amplitude
a_w	Wave amplitude
c	Wave phase velocity
d	Water depth
g	Acceleration of gravity
h	Wave elevation
k	Wave number
k_2, k_4	Lewis transformation parameters
m_n	n th spectral moment
r	Distance between two points $P(y, z)$ and $Q(\xi, \eta)$
t	Time
t_k	Sectional force referring to the k th mode
y_R, y_L	Horizontal position for the radiation conditions on the right and left side of the domain

Greek Letters

ϕ	Potential
Φ	Potential
β	Wave heading direction relative to the ship
κ	Smith correction factor
κ_3	Skewness
κ_4	Kurtosis
λ	Wave length
σ	Standard deviation
μ	Mean value
ρ	Density of fluid
ν_p	Peak rate
ν_0	Zero upcrossing rate
ω	Angular wave frequency
ω_e	Angular frequency of encounter
Ω	Eigenvalue
ς	Structural damping
ζ	Response level in general
ζ_j	Complex amplitude of the j th mode of motion

Abbreviations

AP	Aft perpendicular
COG	Centre of gravity
DOF	Degree of freedom
Fn	Froude number, $F_n = U / \sqrt{gL_{pp}}$
FP	Fore perpendicular
FCF	Frank Close Fit
FRF	Frequency response function
GB	Gerritsma and Beukelman
GFM	Green function method
HAC	Horizontal acceleration
HBM	Horizontal bending moment
HSF	Horizontal shear force
IACS	International Association of Classification Societies
JONSWAP	Joint North Sea Wave Project
LCB	Longitudinal centre of buoyancy (measured positively forward of $L_{pp}/2$)
LGTM	Long-term response statistics
LIST	Linear strip theory
LT	Lewis transformation
NSM	New strip method
NLST	Non-linear time-domain strip theory
OS	Order statistics
OSM	Ordinary strip method
PM	Pierson Moskowitz
PU	Poisson upcrossing
RINA	Registro Italiano Navale
RMS	Root mean square
RSM	Rankine source method
SHTM	Short-term response statistics
SOST	Second order strip theory
STF	Salvesen, Tuck and Faltinsen
TM	Torsional moment
VAC	Vertical acceleration
VLCC	Very large crude carrier
VBM	Vertical bending moment
VSF	Vertical shear force

This page is intentionally left blank.

Chapter 1

Introduction

1.1 Overview and Background

The prediction of wave loads on ships is a broad field as regards methods and type of results. The latter because the definition of wave loads covers a wide range of more specific definitions.

In a structural analysis of a ship, the initial steps are to determine the still-water and wave-induced loads on the hull. Both the extreme loads the hull will be exposed to during its lifetime and load sequences, which can lead to fatigue damages are of interest. The wave loads are in general considered in terms of the global loads and the local loads. The global loads act on the ship considered as a beam. Local loads are dealt with, when a more detailed analysis is in question, such as pressure on a plate panel or stresses in a stiffener. These loads have previously been taken mainly from Classification rules but, recently, novel designs have been made using direct calculations.

The rigid body motions experienced by the ship on the sea are denoted surge, sway, heave, roll, pitch and yaw. From these motions the derived wave loads become horizontal and vertical shear forces, bending moments and a torsional moment.

Design loads on a ship are defined as levels accepted to be exceeded with a certain probability during the lifetime of the ship. To obtain these design loads the wave environment is discretized into stationary sea states. Stationary in the sense that the statistical properties of the ship speed, the heading and the wave kinematics are constant. Usually, this can be achieved in durations of three hours, and it is in this context denoted short-term statistics.

For frequency-domain methods the load prediction involves the determination of a response amplitude operator. With a given wave spectrum, the response can be determined as a response spectrum. As regards the alternative time-domain methods, the response is determined by means of a transformation of the wave spectrum into a wave signal in time and to

perform a simulation of the behaviour of the ship. For both methods the response are usually described statistically by the average value, the variance, the skewness, and the kurtosis.

The wave environment the ship will encounter during its lifetime can now be compiled as combinations of the short-term durations, and the sum of these will add up to the entire lifetime of the ship at sea. The result in terms of extreme values becomes a distribution of the peak values of the response. For fatigue, the result will be an accumulated damage based on the number of load cycles and associated stress amplitudes the ship will be exposed to.

For light and moderate sea states linear methods in general predict the wave loads fairly well but the prediction becomes less good for the severe sea states as the loads then show some non-linearities with respect to the wave height. Non-linear methods should be applied to these sea states as the effects they capture can be pronounced. The drawback is that the non-linear methods are far more time-consuming with respect to computer time. This implies, a combination of the methods to evaluate the ship responses in all the sea states would be favourable from a practical point of view. In ISSC '94 [15] the recommendations for the long-term prediction of the wave loads state that it should be based on a combination of linear and non-linear methods. Linear methods are appropriate to describe low or moderate sea conditions and non-linear methods are needed to describe severe sea conditions.

1.2 Objectives and Scope of the Work

The objective of this work is to develop a rational software system to determine design wave loads on ships and integrate it into a design package for conceptual design.

On the basis of a survey of available methods for determining wave loads on ships, some will be selected and implemented in the system.

Simple methods are usually fast and can give preliminary estimates of the response levels in question. More advanced methods require more skilled users and often also take longer time for the computations. This should be taken into account. It implies in this context the possibility of making linear calculations as a basic analysis and of including non-linear effects by more advanced methods.

The load modelling analysis will be performed in the frequency as well as in the time-domain. The ship types of interest are monohull, displacement vessels with the emphasis on the low to moderate Froude number range. The system will be structured as modules using routines from a library to be implemented.

1.3 Structure of the Thesis

The contents of the thesis are presented in eight chapters composed as follows. In Chapter 2 an overview is given of the available theories for the prediction of wave loads. The overview

includes advantages and drawbacks of the different methods. This is followed by a description of which methods are selected and the motivation for the choices.

Chapter 3 and Chapter 4 contain the theoretical background to the hydrodynamic methods implemented to determine the wave loads. Chapter 3 outlines the hydrodynamic approach without going into details about the hydrodynamics used to determine the hydrodynamic coefficients. In Chapter 4 a more detailed description of the methods for determination of the hydrodynamic coefficients is given. Next, in Chapter 5, a description of the implemented statistical methods is given. It is general for the three chapters that the principles of the procedures and the main assumptions are described. The more detailed derivations are referred to in references.

In Chapter 6 a validation and a verification of the developed software system are given on the basis of the results from calculations of three types of ships. Chapter 7 describes the system developed and, finally, Chapter 8 contains the conclusions and recommendations for further work.

The present work focuses on practical methods for estimating wave loads and much effort has been made as regards the implementation in a comprehensive integrated rational ship design package. Therefore, a part of the thesis is devoted to the description of the implementation philosophy. The more detailed documentation is divided into two parts. One is the comments in the code, which is too extensive to be included in this thesis. The other part is the documentation of the user interface, which is included in Appendix A.

This page is intentionally left blank.

Chapter 2

Methods for Prediction of Wave Loads

2.1 Introduction

Seakeeping computations have advanced significantly since the fundamental paper by Weinblum and St. Denis [65]. A few years later St. Denis and Pierson [55], inspired from the electromagnetic field, introduced the superposition principle to the seakeeping problem and the use of spectral technique opened the door to the determination of responses to random waves. The development of the seakeeping theory has taken several directions. One is extension of linear 2D strip theories to include non-linear effects. These have been applied to some extent to methods derived in the frequency domain and even more for methods in the time domain. Another direction has been the development of three-dimensional theories. The non-linearities in seakeeping problems become significant in severe sea states, mainly because of the immersion dependence on the restoring and hydrodynamic forces. A short overview of the commonest methods available will be given in the following sections.

2.2 Strip Theory Methods

2.2.1 Linear Strip Theory

Linear strip theories have been developed both from intuitive and theoretical viewpoints. An example of the first is the theory by Gerritsma and Beukelman [6], which uses the relative motion between the ship and the waves to determine the vertical motions and loads. An example of the latter is the theory developed by Salvesen, Tuck and Faltinsen (STF) [49]. They determine the excitation force from the sum of the incoming wave potential and the diffracted wave potential. This theory is normally called the classical strip theory. A variant of this method generally using the same approach but deviating at some points is e.g.

ordinary strip theory denoted (OSM) [59]. The linear strip theories is simple to implement and although they are based on the linear slender body assumption, they predict with good accuracy most of the linear wave loads, which comprise a major portion of the wave load encountered by a ship. This can be attributed to the fact that strip theory provides a good estimate of the Froude-Krylov force, the restoring force and the inertial force, which dominate the wave loads for most sea conditions. Due to the generally good accuracy of the predictions obtained by linear strip theory and the simplicity in the procedure, it is widely used. These linear strip theory results are, however, questionable at a low frequency of encounter, for full-form ships as tankers and for ships with large Froude numbers. Moreover, the pressure distribution on the hull is not well predicted. Nevertheless, it is stated in ITTC 94 [15] that the strip theories, which provide simple expressions for the transfer functions, still dominate in practice.

2.2.2 Non-Linear Strip Theories

For Froude numbers below 0.4 and light sea states, the classical linear strip theory usually gives satisfactory results. However, for severer sea states this is not always the case. Here non-linearities become significant. The non-linearities taken into account in the non-linear strip theories are mainly the variation of the section shape with respect to the instantaneous immersion. These effects lead to different absolute values of negative and positive responses, which are particularly significant for the vertical shear forces and bending moments. Elastic vibrations resulting from hydrodynamic impacts can increase this effect further. The extension of the linear strip theory to include non-linear effects has mainly been applied to time-simulation methods. An exception is the quadratic strip theory developed by Jensen and Pedersen [24]. Their theory is based on a perturbation procedure introducing second order terms in the linear strip theory formulation of Gerritsma and Beukelman [7]. Due to the quadratic terms, the theory is able to predict differences between sagging and hogging bending moments and it has the advantage of being formulated in the frequency-domain yielding an easy determination of statistical values of the response. The alternative to the frequency-domain approach is time-domain formulations. An example is the theory proposed by Meyerhoff and Schlachter [31] based on the relative motion concept. In this theory no memory effects are included. The memory effects are due to the continuous excitation by the waves and lead to dependence on the past history in the force terms. By use of time convolution as discussed by Cummins [5] memory effects can be included, but time-domain simulations for irregular sea states then become very time-consuming. An alternative to the time convolution has been developed by Söding [54] by describing the fluid force by a higher order differential equation as introduced by Tick [60]. This procedure has been used among others by Xia et al. [67], who reported good comparison with experimental values for the prediction of vertical wave loads on a container vessel.

Although all these non-linear procedures are based on the strip theory assumption, they are still subject to certain requirements of computers in order to calculate design values within reasonable time.

2.3 Unified Slender Body Theory

The unified slender body theory was developed by Newman [37] and later improved by Newman and Sclavounos [39] and by Kashiwagi [26]. The theory is unified in the sense that it does not have the limitation in the frequency range as the strip theory has. This is due to a different radiation condition. The complete solution of the seakeeping problem consists of a homogeneous and a particular solution and only the latter is considered in ordinary strip theory. The concept of dividing the domain into a near and a far field characterises the unified slender body theory. The principle is that the potential in the fluid domain surrounding the ship is divided into two terms, a near-field solution and a far-field solution. In the near field the details of the ship geometry are important and solved similarly to the strip theory problem. The solution for the potential ϕ consists of a particular and a homogeneous solution:

$$\phi_j(x, y, z) = \phi_{j,F}(x, y, z) + C_j(x)\phi_{j,H}(x, y, z) \quad (2.1)$$

where $j = 1, 2, \dots, 6$ signifies the mode of motion. The far-field velocity potential is influenced by the ship as a line distribution of three-dimensional sources. The method uses matched asymptotic expansions by matching the far-field behaviour of the near field and the near-field behaviour in the far field in a region, and relations are established to determine the homogeneous solution to the near-field problem. Although the solution is more consistent in a physical sense, it is not widely used. This might be due to the more complicated scheme for the determination of the 3D correction in terms of the homogeneous part of the solution. It should be noted that Sclavounos [52], [51] reported results from calculations on two realistic ship hulls at the Froude numbers 0.2 and 0.35. The conclusion was that the exciting force was predicted more accurately, but not to an extent which made the prediction of the motion better than that of the linear strip theory. In ITTC 1987 [20] it is concluded that the slender body theory does not seem to possess overall advantages over strip theories for the vertical motions of a ship at forward speed, whereas it seems to provide better predictions for sway and yaw motions.

2.4 $2\frac{1}{2}$ D Methods

The $2\frac{1}{2}$ D method is also called the high-speed slender-body theory because it treats high forward speeds in a more correct way than the strip theory. In the classical strip theory, the velocity potential satisfies a linearised 2D free-surface condition while the velocity potential in the high-speed slender-body theory satisfies a linear 3D free-surface condition. The difference can be explained in a physical way, as the waves generated from the motions of the ship in strip theory will travel away from the ship parallel to a longitudinal axis. This is not the case for the $2\frac{1}{2}$ D method where the 3D free surface condition is applied. The 3D effect taken into

account leads to a downstream interaction between the steady and the unsteady flow around the ship, which is neglected in the 2D strip theory. The theory is slightly more complicated than the 2D strip theory and cannot be used for low to moderate Froude numbers due to the neglect of the transverse wave pattern.

2.5 3D Methods

The three-dimensional methods can be divided into two groups: Green function methods (GFM) and Rankine source methods (RSM).

2.5.1 Green Function Methods

The Green function method (GFM) determines the velocity potential by distributing sources over the hull surface. It is based on an integral formulation with a Green's function, which satisfies all boundary conditions, except for the body boundary condition. From Green's second identity, the potential can be determined from a surface integral over the submerged body and a line integral over the intersection between the hull and the water surface. LAMP-1 is an example of an application using this approach in a linear version and LAMP-2 and LAMP-4 [53] are non-linear versions.

2.5.2 Rankine Source Methods

The Rankine source methods (RSM) have been used both in frequency-domain and in time-domain. The perhaps most well known applications of this type of method are SWAN-1 [34] in frequency-domain and SWAN-2 [35] in time-domain.

In frequency domain the velocity potential is determined by distributing Rankine sources ($1/r$) over the body. As the Rankine source does not satisfy the free surface condition a source distribution on the free surface is needed as well. A difficulty using this approach [3] is to ensure the proper physics of the radiated and diffracted waves in the ranges below and above $\tau = \frac{U\omega_e}{g} = 0.25$ where different wave patterns occur. In the time domain the method is even less mature than in the frequency domain. Some results have been reported on real ship types but the major part of the computations has been carried out with well-behaved hull forms. Bertram et al. [3] state in an evaluation that the RSM and the GFM do not yet seem mature for practical applications both in terms of robustness and in terms of computational time. Moreover, the ISSC 1997 [16] states at the time of the work by the committee that the situation was so that significant work needed to be done to establish practically dependable three-dimensional computation methods.

2.6 Summary of the Methods for Prediction of Wave Loads

From the previous description of the methods available a number of methods need to be selected for this work. The criteria for the selection are

- Robustness of the method in as wide a range of applications as possible.
- Reasonable computational time on a state-of-the-art PC.
- Accuracy within engineering practice.
- Linear as well as non-linear predictions should be available.

The strip theory is in general the most robust method available. Compared to 3D methods, which must be considered less robust and more time-consuming, the robustness is achieved at the expense of accuracy in particular cases and at the expense of the local pressure distribution. The latter, can however, be estimated from strip theory results using approximate methods.

It is possible that, as the 3D methods become more developed in the sense of robustness and the computers become faster, these methods will show superiority over strip theory methods. Presently, the time for this seems some years ahead so strip theory methods will be applied. Another argument is the simplicity of the input for the strip theory, especially the description of the hull form. Strip theory requires the offset data on the longitudinal cross-sections, so-called stations, while the three-dimensional panel codes need three-dimensional surface data. Most ship types have complicated surfaces at the bow and at the stern and the discretization into three-dimensional panels is a complicated task. This discretization can be done after the hull has been defined in a CAD code. Therefore, concerning analysis of wave loads on ships, strip theory is an appropriate tool at the initial stage of ship design, while three-dimensional panel codes seem more suitable in the detailed design phase. Three methods are left, 2D strip theory, the $2\frac{1}{2}$ D method and the unified slender body theory. As this work is focused on traditional ship types and not high-speed crafts, which is the area of application of the $2\frac{1}{2}$ D, this theory is omitted here. Finally, unified slender body theory is in a sense an extension to the strip theory, which justifies the selection of a strip theory method with the possibility of extending it to slender body theory.

Regarding non-linear effects, the computational time becomes a very clear matter where the non-linear strip theories show superiority over 3D codes. As the non-linear strip theories are formulated as extensions to linear strip theories, the basic tool will be linear strip theory. A non-linear, frequency-domain theory which is fast and includes the most important non-linear effects is the quadratic strip theory by Jensen and Pedersen [24]. As an additional feature, it also predicts the hydroelastic behaviour of the ship hull. For the moderate sea

states, the quadratic strip theory appears to be the best method. First of all because it is formulated in the frequency domain, which makes the calculation of the statistical values of the response much faster as for time-domain methods.

In severe sea states time-domain strip theories appear to be superior for practical applications. In this project only a simple time-domain strip theory neglecting memory effects will be implemented.

A drawback of the selected non-linear methods is the fact that they only include the vertical motions and loads. However, as these degrees of freedom in a lot of cases are also the most important considering wave loads, it is accepted here that the horizontal motions and loads only can be predicted by linear strip theory. Thus, the following theories are to be a part of the present wave load module: the linear strip theory by Gerritsma and Beukelman [6] and the linear strip theory by Salvesen, Tuck and Faltinsen [49], the quadratic strip theory by Jensen and Pedersen [24] and, finally, a time-domain strip theory according to the theory by Petersen [44]. However, it should be emphasized that the system architecture of the developed software system is such that other strip theories can be implemented, e.g. $2\frac{1}{2}$ D and non-linear asymmetric strip theories, Pereira [43] and Wang [62].

Chapter 3

Strip Theory Formulations

3.1 Introduction

The idea of applying a strip theory approach to a sailing ship was first published by Krylov [27] in 1896 to calculate the heave and pitch motions in regular head waves. Basically, the concept is to approximate the three-dimensional hydrodynamic coefficients by an integration over the length of the ship of two-dimensional coefficients, each valid for a cross-section of an infinitely long cylinder. In the following, a brief description will be given of various strip theory formulations.

A general feature of the strip theory methods described in this chapter is the right-hand Cartesian coordinate system with a positive z -axis upwards and origo placed in the water surface above the centre of gravity of the ship as shown in Figure 3.1. The coordinate system is fixed with respect to the mean position of the ship. This is in agreement with the recommendation of ITTC [21], although it might sometimes be more favourable to use a geometrically defined point, such as midship, rather than the mass centre, as origo.

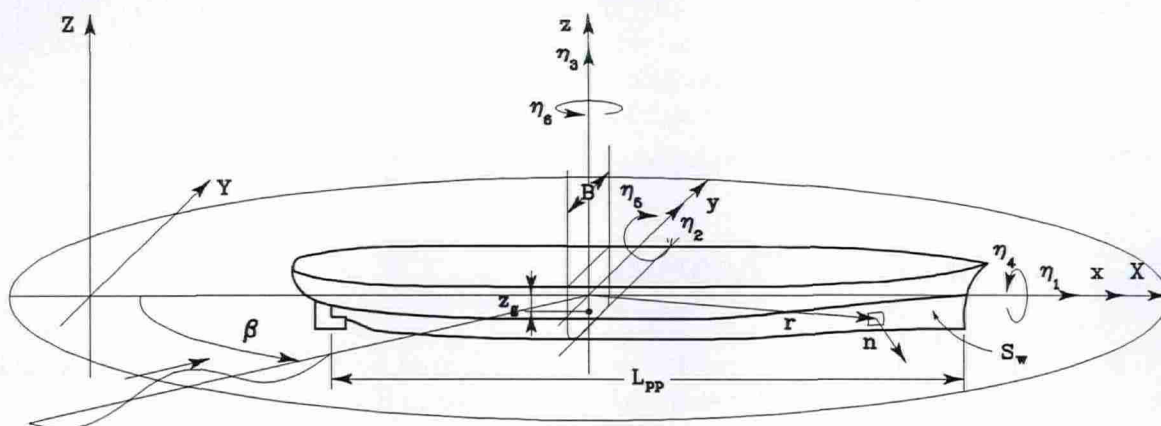


Figure 3.1: Sign convention for translatory and angular displacements.

The coordinate system, (x, y, z) , is fixed with respect to the mean position of the ship. The sway and heave motions of the centre of gravity are denoted η_2 and η_3 , and roll, pitch and yaw η_4 , η_5 and η_6 , respectively. The vertical distance from the origo of the coordinate system to the centre of gravity is denoted z_g . Moreover, an inertial coordinate system, (X, Y, Z) , is used. The incoming wave refers to this coordinate system. The relation between the two coordinate systems is $x = X - Ut$, where U is the forward speed of the ship. Finally, the definition of the heading angle β is shown, indicating 0 degrees as following sea and 180 degrees as head sea.

The generalised surface normal to the submerged hull n_j is defined by

$$(n_1, n_2, n_3) = n \quad \text{and} \quad (n_4, n_5, n_6) = r \times n \quad (3.1)$$

with n being the outward unit normal vector on the hull surface and r the position vector with respect to the origin of the coordinate system. The wetted surface of the hull is denoted S_w . The sign convention for the loads on the ship is shown in Figure 3.2. Here HSF and

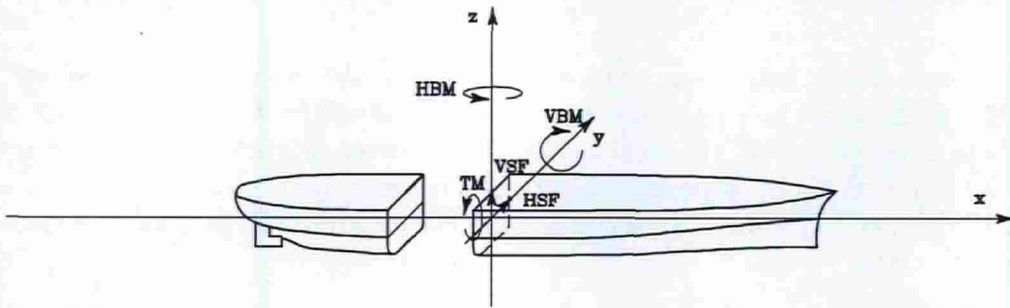


Figure 3.2: Sign convention for loads on the hull

HBM refer to loads acting horizontally on the hull and are therefore denoted horizontal shear force and bending moment. Similarly, for the vertical loads, VSF and VBM denote vertical shear force and bending moment. Finally, the torsional moment is referred to by TSM. In the following, two degrees of freedom are referred to as the motions and loads in the vertical plane. Not to be mistaken by two-dimensional (2D) described in the previous chapter. Five degrees of freedom consist of motions and loads in the horizontal and vertical planes, which also comprise the torsional moment.

3.2 Linear Strip Theories

The linear strip theories exist in approaches developed from both intuitive and theoretical points of departure. The quadratic strip theory described in Section 3.3.1 is extended from the linear strip theory by Gerritsma and Beukelman [6] and represents an example of the former. The following section presents an example of the latter.

3.2.1 The Five Degree of Freedom Strip Theory

The implemented linear strip theory in five degrees of freedom is based on the theory by Salvesen, Tuck and Faltinsen [49]. In the following, it is denoted (LIST). It deviates from the theory by Gerritsma and Beukelman [6] described in Section 3.3.1 by the determination of the wave-excitation force in a theoretically more consistent way as a sum of a radiation and a diffraction solution. Also, the inclusion of forward speed is different and is addressed further in this section. The hydrodynamic force on a ship travelling in waves can generally be determined by integrating the pressure over the hull. By use of the Bernoulli equation and integration over the hull the following is obtained:

$$H_k = - \int_{S_w} p n_k ds = -\rho \int_{S_w} \left(\frac{\partial \Phi}{\partial t} + \frac{1}{2} |\nabla \Phi|^2 + gz \right) n_k ds \quad (3.2)$$

where H_k is the hydrodynamic force in the direction $k = 2, 3, \dots, 6$, referring to sway, heave, roll, pitch and yaw. The potential Φ is the total velocity potential in the fluid. The integration is over the wetted surface S_w of the hull at rest with the normal n_k oriented positively in the direction into the fluid domain. The velocity potential can be decomposed into the potentials

$$\Phi(x, y, z; t) = [-Ux + \phi_S(x, y, z)] + \phi_T(x, y, z)e^{i\omega_e t} \quad (3.3)$$

which can be interpreted as a time-independent steady velocity potential $-Ux + \phi_S$, due to the forward motion of the ship in calm water and a time-dependent velocity potential $\phi_T e^{i\omega_e t}$. Here ω_e is the frequency of encounter experienced on the ship and different from the wave frequency due to forward speed and heading. The potentials must each satisfy the Laplace equation and appropriate conditions at infinity. In addition to these general requirements, each of the potentials must satisfy the hull boundary condition and the linearised free-surface condition. The steady potential contributes with a steady force component, which may be used to determine the dynamic sinkage and trim. As only the unsteady wave-induced force is of interest in a linear formulation, the steady potential can be neglected by assuming that there is no interaction between the two. The time-dependent velocity potential is associated with two problems. An incoming and a diffracted wave potential around the constrained ship and a radiated wave potential due to a forced oscillation of the ship in calm water. The procedure is then to decompose the amplitude of the time-dependent potential ϕ_T as

$$\phi_T = \phi_I + \phi_D + \sum_{j=2}^6 \zeta_j \phi_j \quad (3.4)$$

where ϕ_I is the incident wave potential, ϕ_D the diffracted wave potential and ϕ_j is the contribution to the velocity potential from the j th mode of motion, denoted the radiation

potential. Finally, ζ_j is the complex amplitude of the j th mode of motion, related to the displacements $\eta_j(t) = \text{Re}[\zeta_j e^{i\omega t}]$.

The incident wave potential, ϕ_I , and the diffraction potential, ϕ_D , must satisfy the free surface condition and the hull boundary condition on the mean position of the hull, given by

$$\frac{\partial \phi_I}{\partial n} + \frac{\partial \phi_D}{\partial n} = 0 \quad \text{on } S_w \quad (3.5)$$

The diffraction potential ϕ_D can be eliminated by using a relation proposed by Haskind [13] and Hanaoka [11] and later extended to include forward speed by Newman [36]. The procedure is to use Green's second identity and the boundary condition on the hull to express the diffraction potential from the radiation and the incident wave potential. The expense of using this relation is that the pressure distribution on the hull is lost. Only the total force becomes known. However, the pressure distribution can be recovered in an approximate way as described by Tanizawa [57].

The oscillatory potential components ϕ_j ($j = 2, \dots, 6$) must satisfy the free-surface condition and the condition that the fluid on the hull surface must move identically to the hull surface.

$$\left(i\omega_e - U \frac{\partial}{\partial x} \right)^2 \phi_j + g \frac{\partial \phi_j}{\partial z} = 0 \quad \text{on } z = 0 \quad (3.6)$$

$$\frac{\partial \phi_j}{\partial n} = i\omega_e n_j + U m_j \quad \text{on } S_w \quad (3.7)$$

In Eq. (3.7) $m_j = 0$ for $j = 2, 3, 4$ and $m_5 = n_3$ and $m_6 = -n_2$.

By dividing the oscillatory potential into two parts, a speed-independent part ϕ_j^0 , still dependent on the frequency of encounter though, and a speed-dependent ϕ_j^U , as

$$\phi_j = \phi_j^0 + \frac{U}{i\omega_e} \phi_j^U \quad (3.8)$$

the hull boundary condition in Eq. (3.7) can be rewritten to the two conditions

$$\frac{\partial \phi_j^0}{\partial n} = i\omega_e n_j \quad \text{and} \quad \frac{\partial \phi_j^U}{\partial n} = i\omega_e m_j \quad (3.9)$$

which shows the potentials for $j = 2, 3, 4$ to be speed-independent, denoted ϕ_j^0 :

$$\phi_j = \phi_j^0 \quad j = 1, 2, 3, 4 \quad (3.10)$$

Using the boundary condition for the speed dependent part of the two potentials gives $\phi_5^U = \phi_3^0$ and $\phi_6^U = -\phi_2^0$, and thus

$$\phi_5 = \phi_5^0 + \frac{U}{i\omega_e} \phi_3^0 \quad (3.11)$$

$$\phi_6 = \phi_6^0 - \frac{U}{i\omega_e} \phi_2^0 \quad (3.12)$$

This limits the speed dependence to the free-surface condition. By assuming that the frequencies of encounter are high, $\omega_e \gg U\partial/\partial x$, this dependence is eliminated by rewriting the free-surface condition in Eq. (3.6) to

$$\left[-\omega_e^2 + g \frac{\partial}{\partial z} \right] \phi_j = 0 \quad \text{on } z = 0 \quad (3.13)$$

This is one of the critical assumptions, which limits the theory to short waves and relatively low to moderate Froude numbers. For heave and pitch, the restoring force is the dominant part in the range disregarded by the assumption. Hence, the theory might also then be used in the low-frequency range. For motions without restoring force, surge, sway and yaw, the consequence of this assumption is severer.

From the Bernoulli equation

$$p = -\rho \left(\frac{\partial \Phi}{\partial t} + \frac{1}{2} |\nabla \Phi|^2 + gz \right) \quad (3.14)$$

interaction between the different components of the total velocity potential can be found in the quadratic terms in the velocity-squared part of Bernoulli's equation. However, on the assumption of small wave amplitudes and small motion amplitudes, these terms are neglected. Thus,

$$p = -\rho \left(i\omega_e - U \frac{\partial}{\partial x} \right) \phi_T e^{i\omega_e t} - \rho g (\zeta_3 + \zeta_4 y - \zeta_5 x) e^{i\omega_e t} \quad (3.15)$$

Integrating the pressure over the hull gives the total force and moment components on the ship. The first term in Eq. (3.15) gives the hydrodynamic force and moment amplitude and the second term the restoring force and moment amplitude.

First the hydrodynamic force and moment amplitudes are considered:

$$H_j = -\rho \int_{S_w} n_j \left(i\omega_e - U \frac{\partial}{\partial x} \right) \phi_T ds \quad j = 2, 3, \dots, 6 \quad (3.16)$$

The unsteady force component H_j consists of two potentials due to the decomposition. One from the excitation F_j where the incident wave is diffracted by the fixed hull and another contribution G_j due to the motion of the ship radiating waves away from the hull.

By use of Eq. (3.4) the exciting force can be written

$$F_j = -\rho \int_{S_w} n_j \left(i\omega_e - U \frac{\partial}{\partial x} \right) (\phi_I + \phi_D) ds \quad (3.17)$$

As described before, use of the Haskind-Hanaoka relation eliminates the diffraction potential ϕ_D and F_j becomes a function of the incoming wave and the radiation potential. The incoming wave potential is known and the radiation potential is determined in Chapter 4.

The force due to the motion of the hull is given by

$$G_j = -\rho \int_{S_w} n_j \left(i\omega_e - U \frac{\partial}{\partial x} \right) \sum_{k=1}^6 \zeta_k \phi_k ds = \sum_{k=1}^6 T_{jk} \zeta_k \quad (3.18)$$

where

$$T_{jk} = -\rho \int_{S_w} n_j \left(i\omega_e - U \frac{\partial}{\partial x} \right) \phi_k ds \quad (3.19)$$

The hydrodynamic force or moment T_{jk} is acting in the j th direction due to a motion in the k th mode. By use of Stokes' theorem the surface integral in Eq. (3.19) is rewritten to

$$T_{jk} = -\rho i\omega_e \int_{S_w} n_j \phi_k ds + U\rho \int_{S_w} m_j \phi_k ds - U\rho \int_{C_A} n_j \phi_k dl \quad (3.20)$$

neglecting the line integral along the intersection between the hull and the water surface. This divides the force into a speed-dependent part and a speed-independent part. The definition of m_j is the same as in Eq. (3.7). The last term means the line integral over the aft station indicated by C_A . To describe the principle only the cases for $i, j = 2, 3, 4$ are given. In these cases m is zero, which gives

$$T_{jk} = T_{jk}^0 + \frac{U}{i\omega_e} t_{jk}^A \quad (3.21)$$

The term t_{jk} is generally given by

$$t_{jk} = -\rho i\omega_e \int_{C_x} n_j \phi_k^0 ds \quad (3.22)$$

The superscript A on t_{jk}^A in Eq. (3.21) indicates that the line integral is along the cross-section of the hull at the aftermost section. However, as noted in Salvesen et al. [49], the elimination of the speed dependence does not exclusively come from the derivations above, but requires also that the high-frequency assumption is used in the free-surface condition. T_{jk}^0 indicates the speed-independent part of the force T_{jk} given by

$$T_{jk}^0 = -\rho i \omega_e \int_{S_w} n_j \phi_k^0 ds \quad (3.23)$$

The force T_{jk} can be separated into a real and an imaginary part:

$$T_{jk} = \omega_e^2 A_{jk} + i \omega_e B_{jk} \quad (3.24)$$

where A_{jk} and B_{jk} are denoted the added mass and damping coefficients, respectively.

If the expression in Eq. (3.15) is returned to, integration of the second term gives the amplitude of the restoring force:

$$R_j = -\rho g \int_{S_w} n_j (\zeta_3 + \zeta_4 y - \zeta_5 x) ds \quad j = 2, 3, \dots, 6 \quad (3.25)$$

This expression can be written as

$$R_j = \sum_{k=1}^6 C_{jk} \zeta_k \quad (3.26)$$

For a ship symmetric around a longitudinal axis the non-zero hydrostatic restoring coefficients C_{jk} are C_{33} , C_{44} , C_{55} and C_{35} , which is equal to C_{53} .

By taking the sum of the inertia force, the restoring force and the hydrodynamic force, the equations of motion in the frequency domain become

$$\sum_{k=1}^6 [-\omega_e^2 (M_{jk} + A_{jk}) + i \omega_e B_{jk} + C_{jk}] \zeta_k = F_j \quad (3.27)$$

where M_{jk} is the generalised mass matrix for the ship.

The potentials $\phi_k^0 = \phi_k^0(x, y, z)$ are still 3D potentials. If the beam and draught of the ship are small compared to the length of the ship, the so-called slenderness assumption can be used to approximate the surface integral by setting $ds \simeq d\xi dl$, which gives

$$T_{jk}^0 = -\rho i \omega_e \int_{S_w} n_j \phi_k^0 ds = -\rho i \omega_e \int_L \int_{C_x} n_j \phi_k^0 dl d\xi = \int_L t_{jk} d\xi \quad (3.28)$$

where L indicates integration over the length of the hull and t_{jk} the sectional force given in Eq. (3.22).

If the normal vector n is considered, it follows from the slenderness assumption that the x -component n_1 is small compared to n_2 and n_3 . This is valid except at the bow and the stern. Because these parts of the ship normally constitute a relatively small part of the ship it can be justified to consider n_2 and n_3 as the components of a two-dimensional normal vector. For n_5 and n_6 this gives

$$n_5 = zn_1 - xn_3 \simeq -xn_3 \quad (3.29)$$

$$n_6 = xn_2 - yn_1 \simeq xn_2 \quad (3.30)$$

From these assumptions the three-dimensional Laplace equation and the boundary conditions are simplified to the two-dimensional Laplace equation and the conditions for the two-dimensional hull cross-section C_x oscillating in the free surface. The potentials ϕ_2 , ϕ_3 and ϕ_4 are now considered two-dimensional potentials. It follows from the hull boundary condition that

$$\phi_5(x, y, z) = -x\phi_3(y, z) \quad \text{and} \quad \phi_6(x, y, z) = x\phi_2(y, z) \quad (3.31)$$

For $j, k = 2, 3, 4$ this simplifies the sectional force terms to the following two expressions:

$$t_{jk} = -\rho i \omega_e \int_{C_x} n_j \phi_k^0 dl = \omega_e^2 a_{jk} - i \omega_e b_{jk} \quad (3.32)$$

where a_{jk} and b_{jk} are the two-dimensional added mass and damping coefficients, respectively.

The determination of the two-dimensional potentials ϕ_2 , ϕ_3 and ϕ_4 and thus the sectional added mass and damping coefficients a_{jk} and b_{jk} is described in Chapter 4. From Eq. (3.27) the motions can be determined. The relative vertical motion between the undisturbed wave and the ship as well as the horizontal and vertical accelerations are found from rigid body dynamics.

In Figures 3.3 and 3.4 examples of the output from the linear strip theory are shown. The output has been compared with results given in Salvesen et al. [49]. The present results are based on the design draught of the ship and the hydrodynamic coefficients are determined by use of the Frank Close Fit method, described in Chapter 4. The reference lacks detailed data on the loading condition of the ship and also the method used to determine the hydrodynamic coefficients. Therefore, a certain discrepancy could be expected. However, when this is taken into account both amplitude and phase correspond reasonably well with the calculations by Salvesen et al. [49].

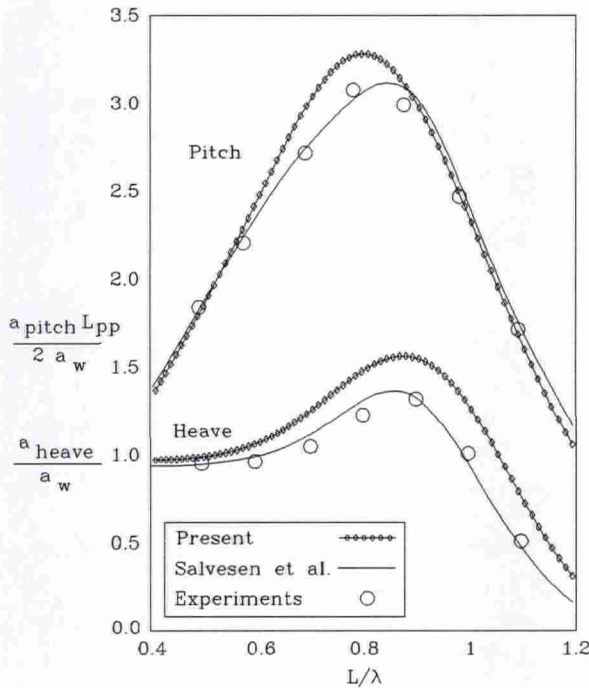


Figure 3.3: *Linear frequency response function for heave and pitch determined in head sea at $F_n = 0.2$ for Mariner [48].*

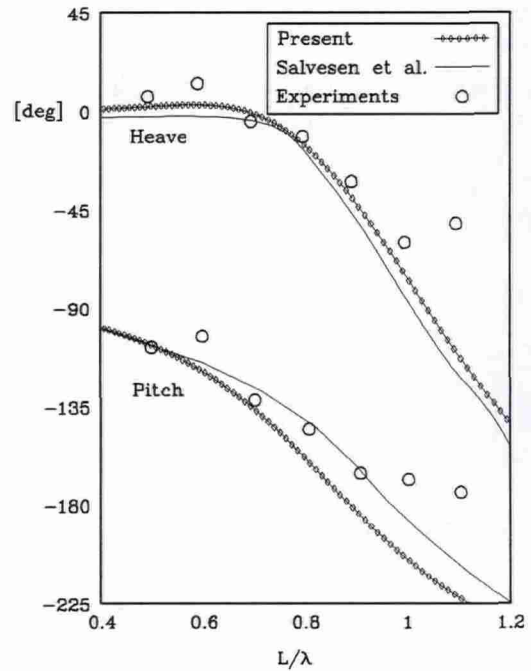


Figure 3.4: *Linear frequency phase function for heave and pitch determined in head sea at $F_n = 0.2$ for Mariner [48].*

3.3 Non-Linear Strip Theories

The non-linear methods can be separated into frequency-domain perturbation methods and time-domain methods, in which non-linear hull boundary conditions and free-surface conditions are satisfied up to a certain degree of accuracy. The non-linear methods in general include two degrees of freedom, therefore motions in the following mean heave and pitch, further loads are referred to as vertical shear force and bending moment.

3.3.1 The Quadratic Strip Theory

The quadratic strip theory (SOST) was developed by Jensen and Pedersen [24] based on a perturbation procedure for predicting wave loads and ship responses in light to moderate seas. The theory is formulated in the frequency domain and the statistical moments can therefore be easily obtained. The theory has been shown to predict very well the difference between hogging and sagging bending moments, Jensen et al. [25]. The first order fluid forces are determined by classical strip theory methods: Salvesen, Tuck and Faltinsen [49] or Gerritsma and Beukelman [6], while the quadratic terms are due to a second order exciting Stokes wave and the perturbation of the restoring force and the two-dimensional hydrodynamic

coefficients. The calculation of the hydrodynamic forces is based on the time derivative of the momentum of the added mass. The theory furthermore takes into account the flexibility of the ship by modelling the ship hull as a free-free Timoshenko beam and uses modal analysis to predict hull deflections. In this section the method and the solution scheme will be outlined. The complete derivation can be found in Jensen and Pedersen [24].

The equation of motion in the vertical plane of a non-prismatic Timoshenko beam is

$$\frac{\partial}{\partial x} \left[EI \left(1 + \varsigma \frac{\partial}{\partial t} \right) \frac{\partial \varphi}{\partial x} \right] + \mu GA \left(1 + \varsigma \frac{\partial}{\partial t} \right) \left(\frac{\partial w}{\partial x} - \varphi \right) = m_s r^2 \frac{\partial^2 \varphi}{\partial t^2} \quad (3.33)$$

$$\frac{\partial}{\partial x} \left[\mu GA \left(1 + \varsigma \frac{\partial}{\partial t} \right) \left(\frac{\partial w}{\partial x} - \varphi \right) \right] = m_s \frac{\partial^2 w}{\partial t^2} - H(x, t) \quad (3.34)$$

where $EI(x)$ and $\mu GA(x)$ are the vertical rigidities of the hull girder for bending and shear, respectively. The slope due to bending is denoted $\varphi(x, t)$ and the vertical deflection $w(x, t)$. This includes both the rigid body displacement as well as the elastic deflection of the beam. Finally, ς is the structural damping of the hull, $m_s(x)$ the hull mass per unit length, and $m_s r^2(x)$ the mass moment of inertia about the horizontal y -axis. The boundary conditions for the hull beam state that the shear force and the bending moment are zero at the ends. The solution is expressed in the form

$$\varphi(x, t) = \sum_{i=0}^N u_i(t) \alpha_i(x) \quad (3.35)$$

$$w(x, t) = \sum_{i=0}^N u_i(t) \nu_i(x) \quad (3.36)$$

where u_i are time-dependent coefficients. The eigenfunctions, $\alpha_i(x)$ and $\nu_i(x)$, are arranged so that $i = 0$ indicates heave, $i = 1$ pitch and $i > 1$ indicates elastic vibration modes. Furthermore, the eigenfunctions are orthogonalised and normalised so that the orthogonality relation becomes

$$\int_0^L [m_s r^2 \alpha_i \alpha_j + m_s \nu_i \nu_j] dx = \delta_{ij} \quad (3.37)$$

where δ_{ij} denotes Kronecker's delta. From Eqs. (3.33) and (3.37) it follows that the coefficients $u_i(t)$ must satisfy

$$\ddot{u}_j + \varsigma \Omega_j^2 \dot{u}_j - \Omega_j^2 u_j = \int_0^L \nu_j H(x, t, \sum_{i=0}^N u_i \nu_i) dx \quad (3.38)$$

where Ω_j^2 is the eigenvalue corresponding to the j th eigenfunction. The hydrodynamic force $H(x, t)$ is determined from the expression proposed by Gerritsma and Beukelman [6], in a slightly modified version where the hydrodynamic coefficients and the breadth depend on the sectional immersion:

$$H(x, t) = - \left[\frac{D}{Dt} \left\{ a_{33}(x, \tilde{z}) \frac{D\tilde{z}}{Dt} \right\} + b_{33}(x, \tilde{z}) \frac{D\tilde{z}}{Dt} + \int_{-T}^{-\tilde{z}} B(x, \tilde{z}) \frac{\partial p}{\partial z} \Big|_{z+w} dz \right] \quad (3.39)$$

In Eq. (3.3.1) the added mass is denoted $a_{33}(x, \tilde{z})$, the damping $b_{33}(x, \tilde{z})$, both per unit length, and the vertical motion is indicated by index three. Finally, the sectional breadth is represented by $B(x, \tilde{z})$. The relative immersion, denoted \tilde{z} , is given by the difference between the wave surface elevation $h(x, t)$ and the displacement of the ship in the vertical direction determined as $\tilde{z} = w(x, t) - \kappa(x)h(x, t)$.

The added mass term can as before be expanded as follows:

$$\begin{aligned} \frac{D}{Dt} \left\{ a_{33}(x, \tilde{z}) \frac{D\tilde{z}}{Dt} \right\} &= \frac{Da_{33}(x, \tilde{z})}{Dt} \frac{D\tilde{z}}{Dt} + a_{33}(x, \tilde{z}) \frac{D^2\tilde{z}}{Dt^2} \\ &= \frac{Da_{33}(x, \tilde{z})}{D\tilde{z}} \left(\frac{D\tilde{z}}{Dt} \right)^2 + a_{33}(x, \tilde{z}) \frac{D^2\tilde{z}}{Dt^2} \end{aligned} \quad (3.40)$$

An important effect, which is included, is momentum slamming. The first term in Eq. (3.40) represents this effect.

The perturbed parameters are the added mass a_{33} , the hydrodynamic damping b_{33} , and the waterline breadth B , given by

$$a_{33}(x, \tilde{z}) \simeq a_{33}(x, 0) + \tilde{z} \frac{\partial a_{33}}{\partial \tilde{z}} \Big|_{\tilde{z}=0} \equiv a_{33,0}(x) + \tilde{z}(x, t) a_{33,1}(x) \quad (3.41)$$

$$b_{33}(x, \tilde{z}) \simeq b_{33}(x, 0) + \tilde{z} \frac{\partial b_{33}}{\partial \tilde{z}} \Big|_{\tilde{z}=0} \equiv b_{33,0}(x) + \tilde{z}(x, t) b_{33,1}(x) \quad (3.42)$$

$$B(x, \tilde{z}) \simeq B(x, 0) + \tilde{z} \frac{\partial B}{\partial \tilde{z}} \Big|_{\tilde{z}=0} \equiv B_0(x) + \tilde{z}(x, t) B_1(x) \quad (3.43)$$

The first order wave elevation is given as a series of unidirectional waves:

$$h^{(1)}(x, t) = \sum_{i=1}^n a_i \cos(\psi_i), \quad \text{where} \quad \psi_i = -k_i(x - Ut \cos(\beta)) - \omega_{e_i} t + \theta_i \quad (3.44)$$

The wave number k_i refers in this case to the x-direction. Due to the non-linear free-surface condition, also a second order incident wave contribution $h^{(2)}$ is introduced in the total elevation h :

$$h(x, t) = h^{(1)} + h^{(2)} \quad (3.45)$$

with

$$h^{(2)} = \frac{1}{4} \sum_{i=1}^n \sum_{j=1}^n a_i a_j [(k_i + k_j) \cos(\psi_i + \psi_j) - |k_i - k_j| \cos(\psi_i - \psi_j)] \quad (3.46)$$

and similar expressions for the exciting wave potential.

The expression for the hydrodynamic force is divided into a restoring part $H_R \simeq H_R^{(1)} + H_R^{(2)}$ and a hydrodynamic part $H_H \simeq H_H^{(1)} + H_H^{(2)}$, both with the terms organised as first and second order. The solution given by the time-dependent coefficients in Eq. (3.35) and Eq. (3.36) is found in the form

$$u_i(t) = u_i^{(1)} + u_i^{(2)} \quad (3.47)$$

where $i = 0, 1$ as before, refers to heave and pitch and $i > 1$ indicates the elastic vibration modes. Each of the $u_i(t)$ are determined from two sets of equations. One for the determination of the linear part $u_i^{(1)}$, and another for the determination of the quadratic part $u_i^{(2)}$.

The wave elevation in Eq. (3.44) is manipulated after integration along the length of the ship to the more convenient form $a_i \cos(\omega_{e_i} t + \theta_i) = a_i (\cos(\omega_{e_i} t) \cos(\theta_i) - \sin(\omega_{e_i} t) \sin(\theta_i)) = \xi_i \cos(\omega_{e_i} t) - \xi_{i+n} \sin(\omega_{e_i} t)$ and similarly for the second order elevation. The linear part of the response thus becomes

$$u_i^{(1)}(t) = \sum_{r=1}^n \{ [\xi_r u_{ir}^c - \xi_{r+n} u_{ir}^s] \cos(\omega_{e_r} t) + [\xi_r u_{ir}^s + \xi_{r+n} u_{ir}^c] \sin(\omega_{e_r} t) \} \quad (3.48)$$

where e.g. u_{0r}^c and u_{0r}^s can be interpreted as the real and the complex part of the heave frequency response function for the frequency of encounter number r . The second order part becomes

$$u_i^{(2)}(t) = \sum_{r=1}^n \sum_{t=1}^n \{ [\xi_r \xi_t - \xi_{r+n} \xi_{t+n}] u_{irt}^{c+}(x) - [\xi_r \xi_{t+n} + \xi_{r+n} \xi_t] u_{irt}^{s+}(x) \} \cos((\omega_{e_r} + \omega_{e_t})t) \\ + [\xi_r \xi_t + \xi_{r+n} \xi_{t+n}] u_{irt}^{c-}(x) + [\xi_r \xi_{t+n} - \xi_{r+n} \xi_t] u_{irt}^{s-}(x) \} \cos((\omega_{e_r} - \omega_{e_t})t) \\ + [\xi_r \xi_t - \xi_{r+n} \xi_{t+n}] u_{irt}^{s+}(x) + [\xi_r \xi_{t+n} + \xi_{r+n} \xi_t] u_{irt}^{c+}(x) \} \sin((\omega_{e_r} + \omega_{e_t})t) \\ + [\xi_r \xi_t + \xi_{r+n} \xi_{t+n}] u_{irt}^{s-}(x) - [\xi_r \xi_{t+n} - \xi_{r+n} \xi_t] u_{irt}^{c-}(x) \} \sin((\omega_{e_r} - \omega_{e_t})t) \} \quad (3.49)$$

The wave-induced loads on the hull can be determined both from the elastic deflections and from an integration of the forces. The former requires the inclusion of a large number of elastic modes to represent the deflection properly. As this is not the case for the latter, this method has been applied. From the equilibrium equations for the beam a relation between the wave-induced force and the sectional loads on the hull can be established. These loads can also be divided into linear and second order parts, e.g. the bending moment $M(x, t)$ at $x = x$ becomes

$$M(x, t) = M^{(1)}(x, t) + M^{(2)}(x, t) \quad (3.50)$$

with

$$M^{(1)}(x, t) = \sum_{r=1}^n \{ [\xi_r M_r^c(x) - \xi_{r+n} M_r^s(x)] \cos(\omega_{e_r} t) + [\xi_r M_r^s(x) + \xi_{r+n} M_r^c(x)] \sin(\omega_{e_r} t) \} \quad (3.51)$$

and

$$M^{(2)}(x, t) = \sum_{r=1}^n \sum_{t=1}^n \{ [\xi_r \xi_t - \xi_{r+n} \xi_{t+n}] M_{rt}^{c+}(x) - [\xi_r \xi_{t+n} + \xi_{r+n} \xi_t] M_{rt}^{s+}(x) \} \cos((\omega_{e_r} + \omega_{e_t})t) \\ + [\xi_r \xi_t + \xi_{r+n} \xi_{t+n}] M_{rt}^{c-}(x) + [\xi_r \xi_{t+n} - \xi_{r+n} \xi_t] M_{rt}^{s-}(x) \} \cos((\omega_{e_r} - \omega_{e_t})t) \\ + [\xi_r \xi_t - \xi_{r+n} \xi_{t+n}] M_{rt}^{s+}(x) + [\xi_r \xi_{t+n} + \xi_{r+n} \xi_t] M_{rt}^{c+}(x) \} \sin((\omega_{e_r} + \omega_{e_t})t) \\ + [\xi_r \xi_t + \xi_{r+n} \xi_{t+n}] M_{rt}^{s-}(x) - [\xi_r \xi_{t+n} - \xi_{r+n} \xi_t] M_{rt}^{c-}(x) \} \sin((\omega_{e_r} - \omega_{e_t})t) \} \quad (3.52)$$

The solution contains a linear part equivalent to the linear methods described in the previous section. In addition, also the quadratic terms are included. The linear frequency response function in terms of $M_r^c(x)$ and $M_r^s(x)$ refers to the r th frequency of encounter and can also be denoted $M^c(\omega_e, x)$ and $M^s(\omega_e, x)$. They represent the coefficients to the $\cos(\omega_e t)$ and $\sin(\omega_e t)$ in the linear response. The response can be rewritten to the response amplitude operator $M_1 = \sqrt{(M_r^c(x))^2 + (M_r^s(x))^2}$ and the corresponding phase function, relative to the phase of the wave, θ_r .

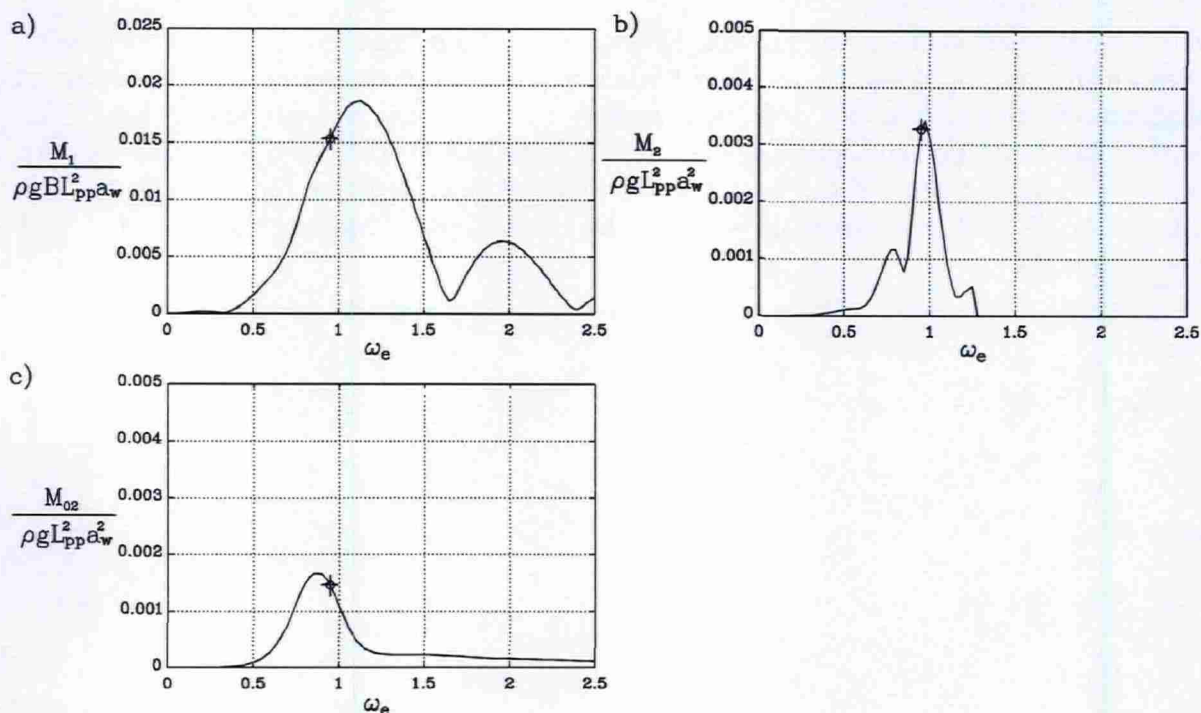


Figure 3.5: Example of the response in terms of the midship bending moment for the container ship S175. The ship is advancing in head sea at a forward speed of 22 knots.

From these frequency response functions the response to a regular wave can be found. The quadratic response to an irregular sea state includes summations of sum and difference frequencies. If a regular wave of the amplitude a is considered the sum frequency becomes the double frequency of the equivalent linear one. The difference frequency becomes zero and leads to a mean shift of the response. This makes it possible to express the second order response, $M_{rt}^{\alpha\pm}$; $\alpha = c, s$, in terms of $M_2 = \sqrt{(M_{rr}^{c+})^2 + (M_{rr}^{s+})^2}$ and the phase function. The shift of the response is denoted $M_{02} = M_{rr}^{c-}$. To clarify the theory in a more physical way, an example from a calculation on a container ship is shown in the following. The container ship is denoted S175 and characterised by a relatively high design speed ($F_n=0.275$) and bow flare. The principal particulars can be found in Section 6. The second order contribution mainly originating from the restoring force will be pronounced due to the bow flare.

The linear part of the frequency response function is shown in Figure 3.5a. The quadratic parts are shown in Figure 3.5b and c. The corresponding frequency range for M_2 is half of the linear transfer function.

The form of the results shown in Figure 3.5 makes it difficult to identify and quantify the difference from a linear calculation. This becomes more obvious if, as an example, the rigid body response in a regular sea is considered. The phase angle of the wave is set to zero. The

linear part in Eq. (3.51) becomes

$$M^{(1)}(x, t) = a[M_r^c(x) \cos(\omega_{e_r} t) + M_r^s(x) \sin(\omega_{e_r} t)] \quad (3.53)$$

and the quadratic given term in Eq. (3.52):

$$M^{(2)}(x, t) = a^2[M_{rr}^{c+}(x) \cos(2\omega_{e_r} t) + M_{rr}^{s+}(x) \sin(2\omega_{e_r} t) + M_{rr}^{c-}(x)] \quad (3.54)$$

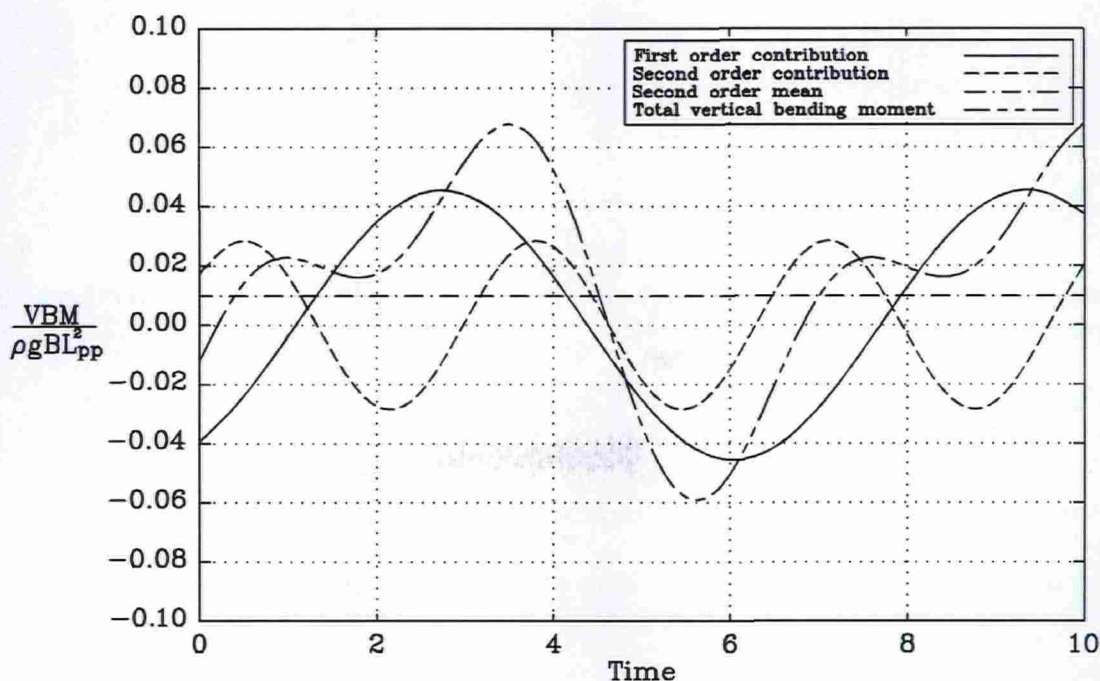


Figure 3.6: An example of the midship vertical bending moment for the container ship S175. The frequency of encounter corresponds to $L/\lambda = 1.1$ and the wave amplitude a_w is 3m. The ship is advancing in head sea at a forward speed of 22 knots.

In Figure 3.6 the response has been plotted for the wave frequency, which corresponds to the ratio of $L/\lambda = 1.1$. This has been marked in Figure 3.5. It is seen that the second order contribution is at its maximum at this frequency. In Figure 3.6 the three parts of the response are shown.

Springing and whipping are typical flexible response modes for ship hull. Springing denotes the continuous wave-induced two-node vertical vibration. The excitation forces for springing are active along the entire hull. Whipping is due to an impulsive wave-induced two-node vertical vibration. The exciting forces for whipping occur only on certain parts of the hull and are mainly due to slamming and to shipping green water at the bow region. In the quadratic theory springing is included whereas transient effects as whipping cannot be included in the frequency-domain approach. For most ships springing and whipping do not

significantly affect the extreme values but may, in long slender hulls with low natural frequencies, contribute significantly to the fatigue loading. Figure 3.7 shows some measured natural frequencies for ships with different lengths and of different types.

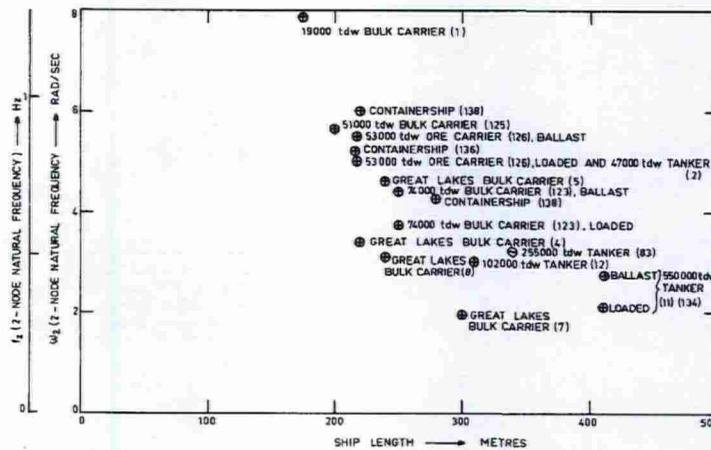


Figure 3.7: Measured natural frequency of the 2-node vertical vibration as a function of ship length (van Gunsteren [10]).

The excitation of springing is mainly due to the second order terms, which gives a high frequency contribution to the response. This is the reason why it is of limited interest to implement hydroelasticity in linear formulations.

The quadratic approach described here is based on the theory by Gerritsma and Beukelman. It is also available to analyses based on Salvesen, Tuck and Faltinsen with a modified method.

3.3.2 The Non-Linear Time-Domain Strip Theory

The point of departure for the time-domain approach is the linear equations of motion of Gerritsma and Beukelman [6] in the frequency domain. The program is based on the work by Petersen [44] and later by Hansen [12] and includes only rigid body motions. The basic expression for the hydrodynamic force H is the expression

$$H(x, t) = - \left[\frac{D}{Dt} \left\{ a_{33}(x, \tilde{z}) \frac{D\tilde{z}}{Dt} \right\} + b_{33}(x, \tilde{z}) \frac{D\tilde{z}}{Dt} + \rho g A(x, \tilde{z}) - m_s(x)g \right]. \quad (3.55)$$

The immersion dependence on the added mass, the damping and the restoring term form the extension from the Gerritsma and Beukelman [6] formulation. Symbols are similar to the cases described previously in this chapter. In the linear and quadratic frequency-domain formulations, the equilibrium condition in still water is assumed to be predetermined and only

motions from this initial condition are considered. In the time domain, the determination of the equilibrium condition in still water is included. This is the reason for the two terms in Eq. (3.55) including A and m_s , which is the sectional immersed area and the sectional mass respectively. However, the steady state dynamic sinkage and trim are not included.

The added mass term can be expanded similarly to Eq. (3.40) and as all terms are included also momentum slamming is taken into account. In the quadratic strip theory the immersion dependence is described by a Taylor expansion around the equilibrium position, while in the time-domain strip theory the terms are evaluated at the instantaneous immersion.

Green water on deck is included. A possibility of including the green water in the d'Alembert force is an option.

A time signal of the motions is determined by solving the equations of motion using the force expression in Eq. (3.55) with an Adams predictor corrector scheme. The relative motions and the loads are found similarly to what has been described previously in this chapter.

3.4 Limitations on the Strip Theory Methods

In general, the derivation of the equations is based on some approximations for the free surface and the hull boundary condition. The strip theory is based on the following assumptions:

- The hull is slender with only gradual change of form in the longitudinal direction.
- The forward speed of the ship should be relatively low (Froude number less than 0.4).
- The frequency of encounter should not be too low or too high.

In addition, for the linear strip theory:

- The motions are small.
- The ship hull sections are wall-sided at the waterline.

For the quadratic strip theory the slope of the hull section in the waterline is taken into account. However, if the motions are large the slope is extended under the keel and above the deck line. This limits the quadratic strip theory to small to mediate sea states.

More specific limits on the assumptions are difficult to determine in general. The agreement between model experiments and theory depends first of all on the type of result in question. Different extent of agreement is found for motions, relative motions, accelerations and

loads. As noted by Newman [38], strip theory usually underpredicts heave and pitch and overpredicts vertical bending moments. Normally, better agreement is found for head sea calculations. In addition, results related to motion in the vertical plane are better predicted than in the horizontal plane, mainly due to the dominating and well predicted restoring force.

Published results with comparisons of transfer functions made with strip theory are available. In the following, a few will be shortly reviewed to give an impression of the applicability of the strip theory.

3.4.1 Slenderness

For the assumption about slenderness, reference is made to Gerritsma et al. [8]. Good agreement between model experiments and calculated vertical response in head waves was found for $Fn = 0.3$ and ratios of L/B as low as 4. The Seakeeping Committee of the 18th ITTC [20] concludes that strip theory appears remarkably effective for prediction of vertical motions of ships with length to beam ratios as low as $L/B = 2.5$. This conclusion was based on eleven reported studies comparing theoretical results and model experiments for small vessels.

3.4.2 Speed

With respect to speed, Blok and Beukelman [4] reported good agreement between strip theory results and model experiments for a series of models, which were tested in head waves with a length/beam ratio of $L/B = 8$. For heave, pitch and vertical acceleration good agreement was found up to $Fn = 1.14$. For relative motions good agreement was found up to $Fn = 0.57$. In the outline of the derivation of the linear strip theory in Section 3.2.1 the steady potential ϕ_S is discarded as negligible and assumed not to interact with the unsteady potential ϕ_T . The steady contribution will in this case lead to wave pattern around the ship and a dynamic sinkage and trim. It is possible to take parts of these effects into account by modifying the equilibrium condition of the ship to the condition observed including dynamic sinkage and trim. This has a small effect on the motions shown in Figures 3.8 and 3.9 and therefore also on the vertical acceleration as shown in Figure 3.10. Since the pressure distribution leading to the sinkage and trim may contribute to the loads it is not used for analyses where loads are considered.

For the pitch motion shown in Figure 3.9 the response amplitude operator does not approach unity as the frequency decreases. This problem has been found where the speed is high. However, because no wave energy is present at these frequencies it usually has no effect on the calculation.

FCF denotes as indicated the Frank Close Fit method and includes one of the methods for determining added mass and damping. The method is described in detail in Chapter 4.

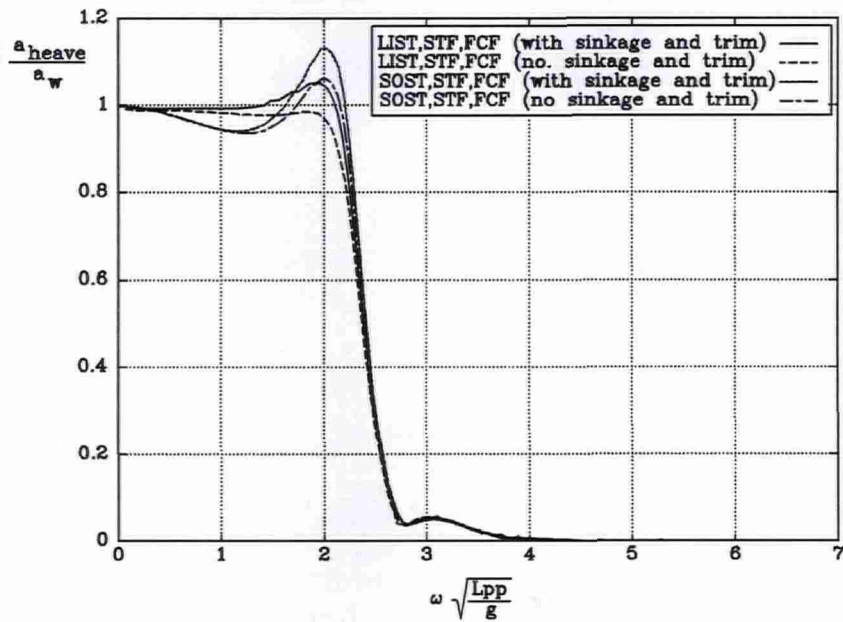


Figure 3.8: Comparison of heave frequency response functions for a fast ferry (Froude number=0.55) with and without dynamic sinkage and trim. LIST: Linear strip theory. SOST: Quadratic strip theory. STF: Salvesen, Tuck and Faltinsen. FCF: Frank Close Fit.

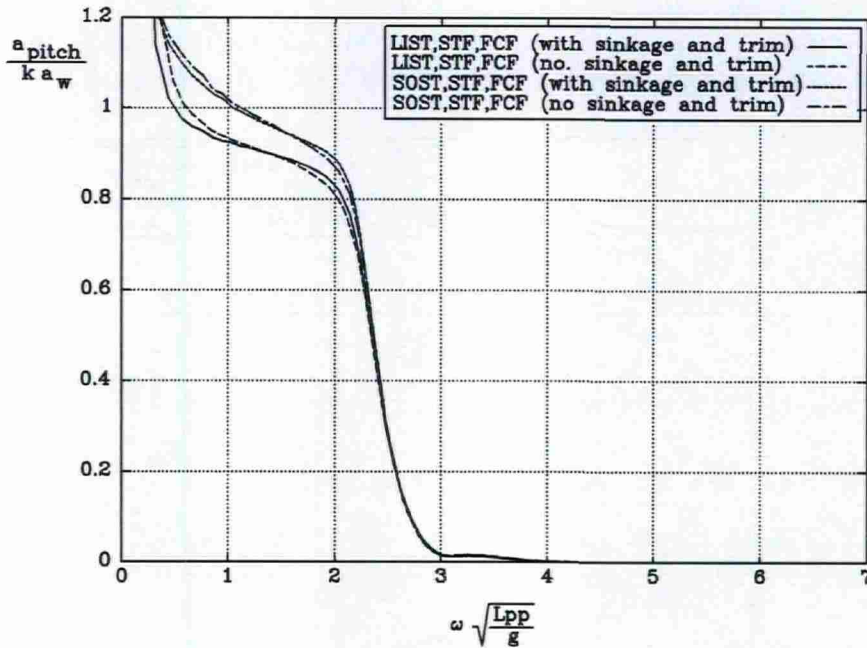


Figure 3.9: Comparison of pitch frequency response functions for a fast ferry (Froude number=0.55) with and without dynamic sinkage and trim. LIST: Linear strip theory. SOST: Quadratic strip theory. STF: Salvesen, Tuck and Faltinsen. FCF: Frank Close Fit.

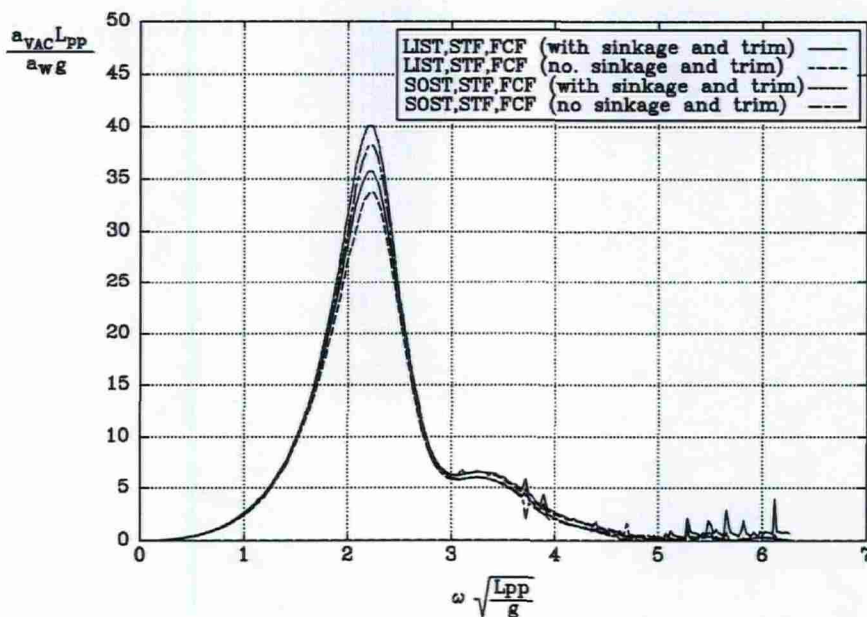


Figure 3.10: Comparison of acceleration frequency response functions at $3/4L_{pp}$ for a fast ferry (Froude number=0.55) with and without dynamic sinkage and trim. LIST: Linear strip theory. SOST: Quadratic strip theory. STF: Salvesen, Tuck and Faltinsen. FCF: Frank Close Fit.

3.4.3 Frequency Range

The theory by Gerritsma and Beukelman [6] is theoretically restricted to a medium range of frequencies. For the short waves the Froude-Krylov hypothesis, assuming the ship to be small compared to the wave, is violated and for the very long waves the strip theory assumption of $\omega_e \gg U\partial/\partial x$ fails. As the theory by Salvesen et al. [49] is not based on the Froude-Krylov hypothesis, it has only the restriction on the long waves. However, the low-frequency range is governed by the restoring force, so this limitation can in most cases be neglected.

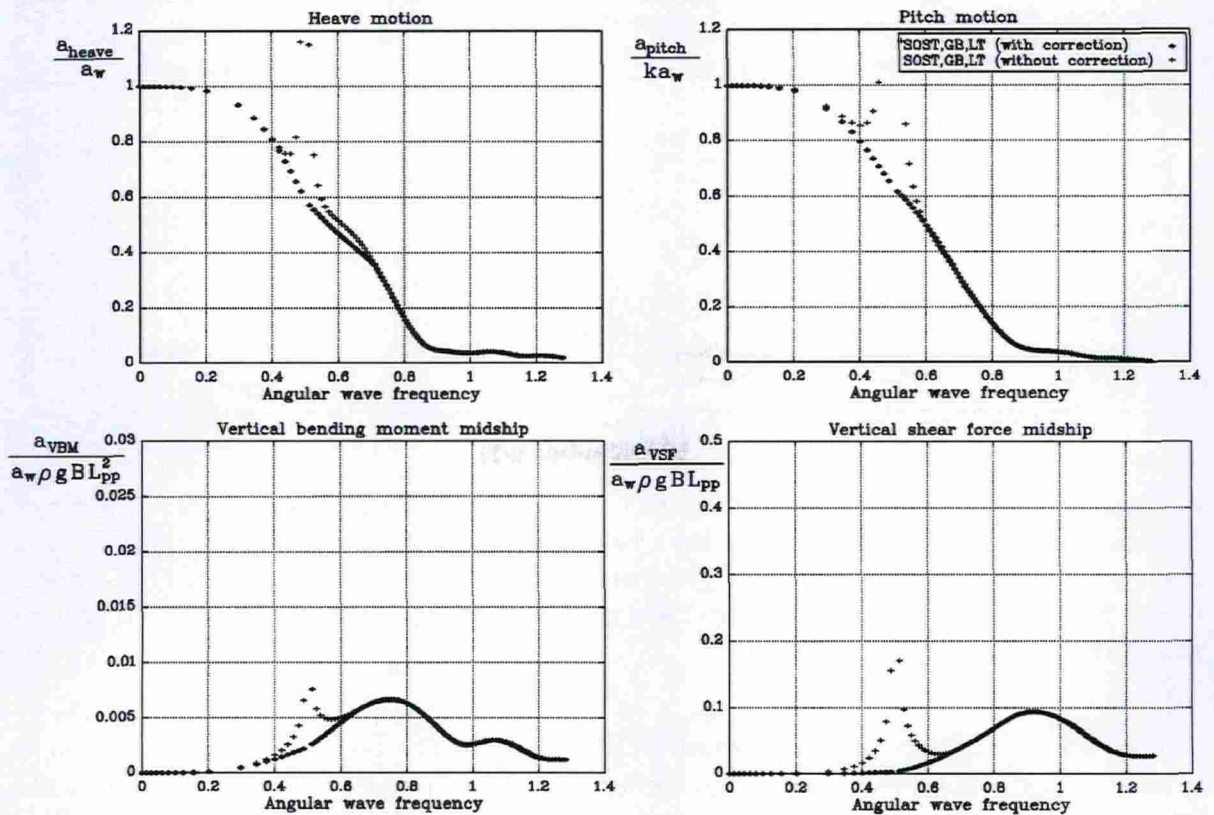


Figure 3.11: Response amplitude operators for heave, pitch, vertical shear force and vertical bending moment. The calculations have been performed for a fast ferry with a Froude number of 0.55 and a heading of 0 degrees with and without the low frequency of encounter modification. (SOST: Quadratic strip theory. GB: Gerritsma and Beukelman. LT: Lewis transformation).

The strip theories predict motions and loads less well for quartering and following seas. This is particularly the case when the frequency of encounter tends to zero while the wave frequency has a larger value. From head to beam seas, the frequency of encounter is greater than or equal to the wave frequency, avoiding the problem. However, for quartering and following seas the frequency of encounter may become zero, leading to unrealistically predicted results. This is mainly because the two-dimensional hydrodynamic mass in the heaving

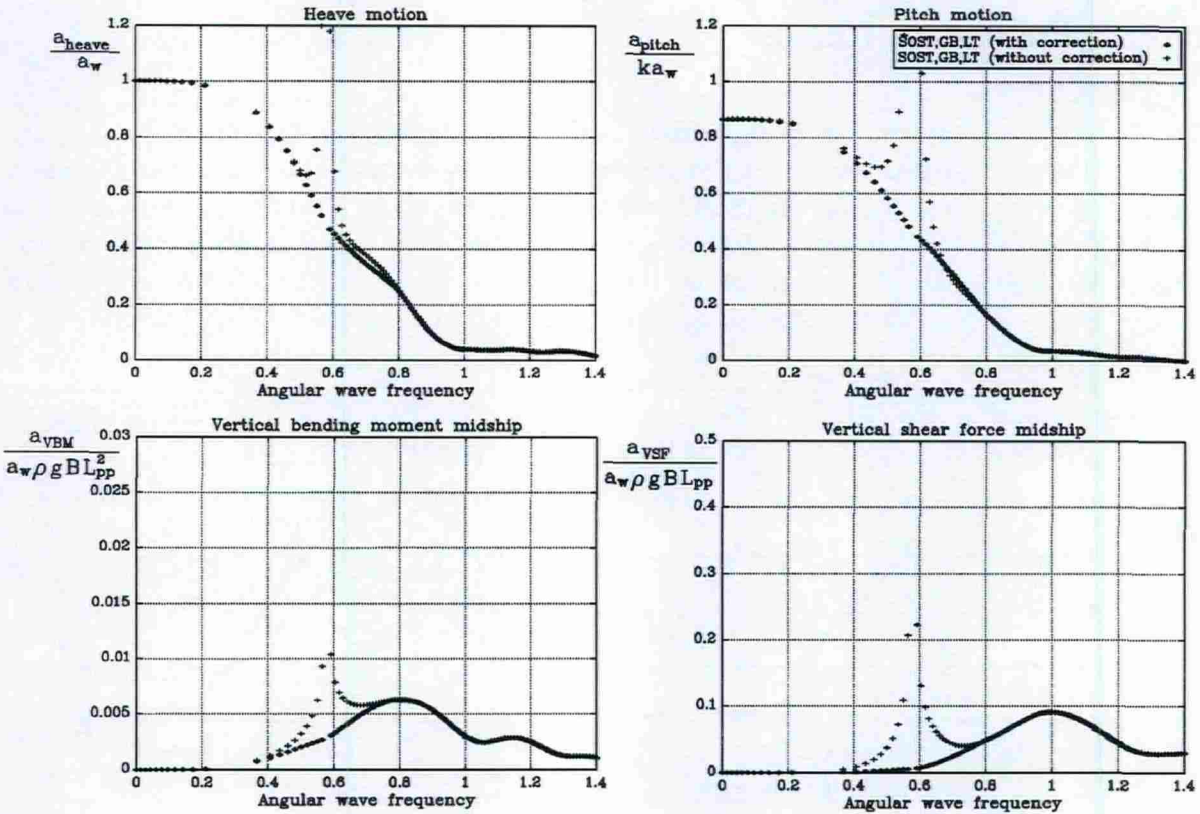


Figure 3.12: Response amplitude operators for heave, pitch, vertical shear force and vertical bending moment. The calculations have been performed for a fast ferry with a Froude number of 0.55 and a heading of 30 degrees with and without the low frequency of encounter modification. (SOST: Quadratic strip theory. GB: Gerritsma and Beukelman. LT: Lewis transformation).

mode tends to infinity when the frequency tends to zero. The problem is that in the equations of motion all frequency-dependent coefficients on the motion parameters depend on the frequency of encounter, whereas the excitation force depends on the wave frequency. ITTC 84 [19] addressed this subject and drew the conclusion that for following and quartering seas, where the frequency of encounter is very low, a significant improvement of the results could be achieved by using the hydrodynamic coefficients corresponding to the wave frequency instead of the frequency of encounter. This has no physical background and serves only the purpose to avoid that the results go to infinity.

For the quadratic strip theory, a very simple procedure has been used. An upper limit for the added mass is taken simply by limiting the parameter k_4 in Eq. (4.6) to 2.0 for each section. The problem observed at low frequencies of encounter as indicated in Figures 3.11, 3.12 and 3.13 presents itself over a relatively wide wave frequency band. At low speeds the wave spectral density in the corresponding frequency band is small, which makes modifications less important. However, for higher speeds the wave spectral density may have its maximum

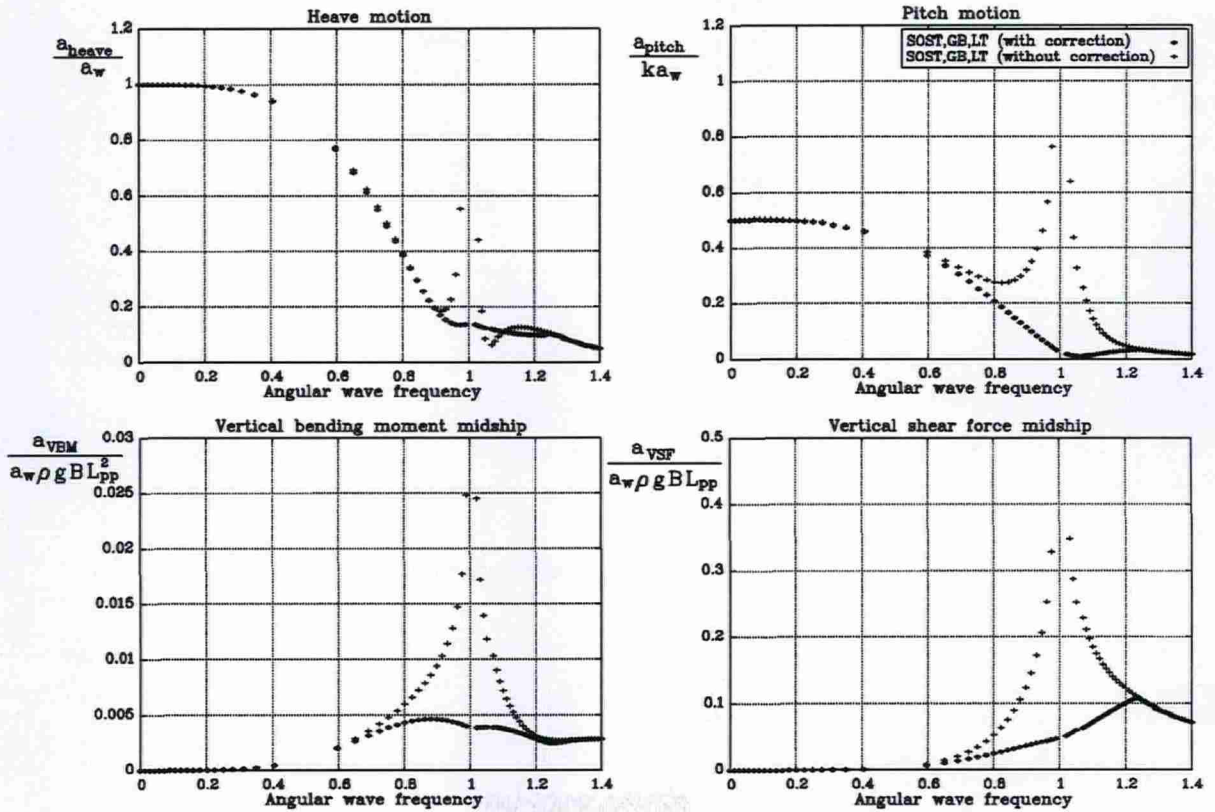


Figure 3.13: Response amplitude operators for heave, pitch, vertical shear force and vertical bending moment. The calculations have been performed for a fast ferry with a Froude number of 0.55 and a heading of 60 degrees with and without the low frequency of encounter modification. (SOST: Quadratic strip theory. GB: Gerritsma and Beukelman. LT: Lewis transformation).

value where the frequency of encounter tends to zero, which makes modifications vital. From Figures 3.11, 3.12 and 3.13 the modification is seen to improve the results toward what is intuitively more reasonable in a physical sense. The modification has no effect on results for headings from head to beam sea.

LT denotes, as indicated Lewis transformation and includes one of the methods for determining added mass and damping. The method is described in detail in Chapter 4.

This page is intentionally left blank.

Chapter 4

Hydrodynamic Coefficients

The hydrodynamic coefficients are found by solving the problem of calculating the fluid response to a forced harmonic oscillation. The physical problem is shown in Figure 4.1 for the

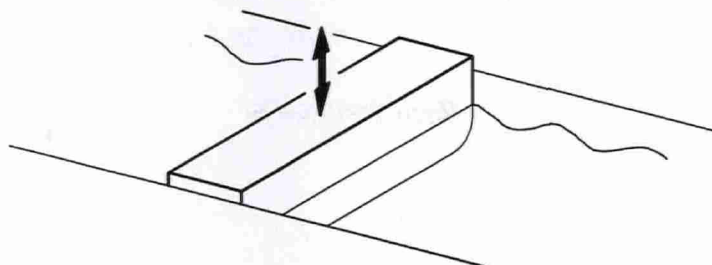


Figure 4.1: *Experimental set-up to determine the hydrodynamic coefficients for heave.*

heave mode. The prismatic model has a cross-sectional shape as the ship in the longitudinal position in question, and it is forced to oscillate sinusoidally at a given frequency. In the linear case, the force with respect to time can be described by a trigonometric function as well. The measured force includes the hydrodynamic, the restoring, and the inertia force. In this case, only the hydrodynamic part is considered. The added mass is defined as the coefficient to the term in phase with the acceleration of the motion, and the damping is defined as the coefficient to the term in phase with the velocity, both normalised to unit amplitude of acceleration and velocity, respectively. This procedure is repeated until the frequency range of interest is covered. A more advanced experimental method is to perform transient oscillations to include a range of frequencies in one experiment.

Different theoretical approaches have been applied to this problem. A simplified method uses the solution to the potential flow around a circular cylinder and in addition a frequency correction due to the free surface. In 1949 Ursell [61] determined the velocity potential around a semi-submerged heaving circular cylinder and reported the added mass and damping. The

velocity potential was based on an infinite series of non-orthogonal polynomials (multipoles) and a wave source at the origin. It is referred to as the method of multipoles. Based on the solution to the circular cylinder case the mapping methods were developed to determine the potential around a wider range of geometries. The known potential around the circular cylinder is mapped onto the cross-section in question and the pressures are integrated to determine the forces and thus the hydrodynamic coefficients. These so-called mapping methods strongly depend on the shape of the mapped sections and an increased number of parameters are required to map certain cross-sections properly. An alternate approach to obtaining a solution for bodies of a more arbitrary shape is the use of integral equations, also called panel methods. These methods use Green's third identity on two potential functions. One is a source function, which contains a singularity, and the other potential function is the unknown potential.

In Chapter 3 the potentials in terms of the added mass and damping coefficients A_{jk} and B_{jk} were left as unknowns to be described in this chapter. To recapture the denotations, the upper case coefficients, e.g. A_{jk} , refer to the entire ship and the lower case coefficients, a_{jk} , refer to the sectional values. Further, the frequency of the oscillation refers to the frequency of encounter. Finally, the superscript '0' on the potential, ϕ^0 , indicating speed-independence, has been omitted in this chapter because no speed dependence is considered in this chapter. However, following the notation strictly would imply the superscript '0' on all potentials in this chapter.

4.1 Mapping Technique

The mapping procedure is generally a transformation of a known potential around a given geometry into a flow around a contour in question by use of suitable mapping functions. The transformation consists of an expansion of parameters to determine the transformation. By truncating the transformation series to only three terms the mapped cross-sections will become so-called Lewis forms, after Lewis [29], who first proposed their use.

4.1.1 The Lewis-Form Method

The Lewis transformation has some limitations on the mapped geometries. The cross-section needs to be symmetric and semi-submerged and the hull surface needs to intersect the water surface perpendicularly. Further, the deep-water assumption has been applied. Only the transformation for heave has been implemented.

The three parameter transformation ensure the beam-draught ratio B/T , and the section area coefficient $A/(BT)$ is the same for the two cross-sections.

The added mass per cross-sectional length can be written

$$a_{33}(x) = \rho k_2 k_4 A(x) \quad (4.1)$$

Here k_2 is the non-dimensional coefficient which determines the mapping of the geometry into the flow around a circular cylinder without any free surface. The non-dimensional coefficient k_4 is a frequency correction for the free surface. The density of the water is denoted ρ and $A(x)$ is the sectional immersed area. The non-dimensional coefficient k_2 becomes in accordance with Lewis [29]:

$$k_2 = \frac{(1 + C_1)^2 + 3C_2^2}{1 - C_1^2 - 3C_2^2} \quad (4.2)$$

Here C_1 and C_2 are Lewis' mapping coefficients given by

$$\begin{aligned} C_1 &= \frac{B}{B_0}(1 - \Lambda) & C_2 &= \frac{B}{B_0}(1 + \Lambda) - 1 \\ \frac{B}{B_0} &= \frac{1}{2} \left(3(1 + \Lambda) - \sqrt{(1 + \Lambda)^2 + 8\Lambda \left(1 - 4\frac{C_M}{\pi}\right)} \right) \\ \Lambda &= \frac{2T}{B} & C_M &= \frac{A}{BT} \end{aligned} \quad (4.3)$$

where B and T are the sectional waterline breadth and draught, respectively. If the argument under the square root sign in Eq. (4.3) is negative, the actual draught $T(x)$ is replaced by a new, larger draught, so that the argument becomes zero. The non-dimensional coefficient k_4 reflects the free-surface effects. This value depends on the cross-sectional shape and the non-dimensional frequency:

$$\xi_0 = \frac{\omega_e^2 B}{2g}$$

For small values of the non-dimensional frequency ($\xi_0 < 0.2$), Ursell [61] has given the following expression for elliptic cross-sections:

$$k_4 = k_{4,1} = -\frac{8}{\pi^2} \ln \left(0.795 \left(1 + \frac{2T}{B} \xi_0 \right) \right), \quad \xi_0 < 0.2 \quad (4.4)$$

Tasai [58] showed that this expression could be used for other than elliptic body plans. For larger values of the non-dimensional frequency $\xi_0 > 0.2$, k_4 does not vary very much as a

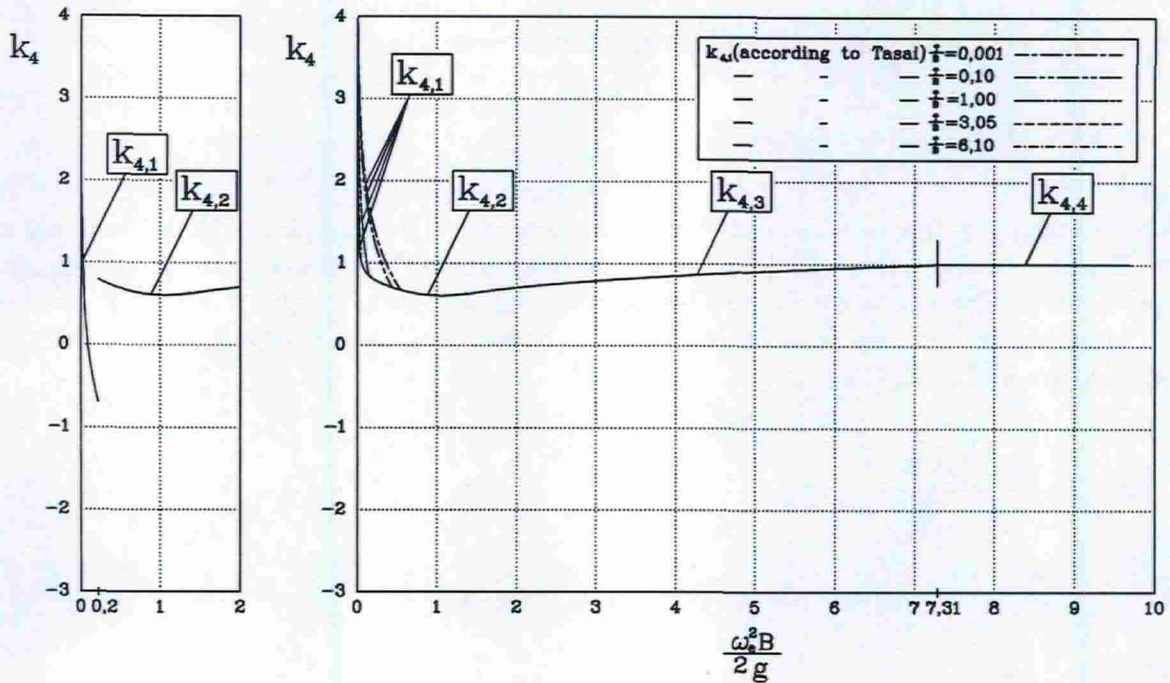


Figure 4.2: The non-dimensional coefficient k_4 as a function of $\frac{T}{B}$ and the non-dimensional frequency of encounter.

function of the shape of the cross-section. Therefore, in this frequency range k_4 is expressed by

$$k_4 = \begin{cases} k_{4,2} = 0.2367\xi_0^2 - 0.4944\xi_0 + 0.8547 + \frac{0.01}{\xi_0 + 0.0001}, & 0.2 \leq \xi_0 < 1.388 \\ k_{4,3} = 0.4835 + \sqrt{-0.0484 + 0.0504\xi_0 - 0.001\xi_0^2}, & 1.388 \leq \xi_0 \leq 7.31 \\ k_{4,4} = 1.0, & \xi_0 > 7.31 \end{cases} \quad (4.5)$$

The expressions in Eq. (4.5) are found by fitting numerical results for a circular cross-section given by Ursell. This gives four expressions, each defined within the ranges given above. However, use of these limits does not always lead to a proper match between $k_{4,1}$ and $k_{4,2}$. An example of this is shown on the left side of Figure 4.2. The reason is that the intersection between the two curves depends on the ratio of $\frac{T}{B}$, as it can be seen in Figure 4.2. It has therefore been changed so that the limit between $k_{4,1}$ and $k_{4,2}$ is determined by

the intersection between the two curves. For $\frac{T}{B} \leq 6.1$ this gives

$$k_4 = \begin{cases} k_{4,1} = -\frac{8}{\pi^2} \ln \left(0.795 \left(1 + \frac{2T}{B} \right) \xi_0 \right) & \xi_0 < -\frac{1.3503}{\frac{T}{B} - 0.9846} + 2.3567 + 0.5497 \\ k_{4,2} = 0.2367\xi_0^2 - 0.4944\xi_0 + 0.8547 + \frac{0.01}{\xi_0 + 0.0001} & -\frac{1.3503}{\frac{T}{B} - 0.9846} + 0.5497 \leq \xi_0 \leq 1.388 \\ k_{4,3} = 0.4835 + \sqrt{-0.0484 + 0.0504\xi_0 - 0.001\xi_0^2} & 1.388 < \xi_0 \leq 7.31 \\ k_{4,4} = 1.0 & \xi_0 > 7.31 \end{cases}$$

For $\frac{T}{B} > 6.1$ no intersection between $k_{4,1}$ and $k_{4,2}$ exists, so $k_{4,2}$ has been extended to describe this frequency range as well, which gives

$$k_4 = \begin{cases} k_{4,2} = 0.2367\xi_0^2 - 0.4944\xi_0 + 0.8547 + \frac{0.01}{\xi_0 + 0.0001} & \xi_0 \leq 1.388 \\ k_{4,3} = 0.4835 + \sqrt{-0.0484 + 0.0504\xi_0 - 0.001\xi_0^2} & 1.388 < \xi_0 \leq 7.31 \\ k_{4,4} = 1.0 & \xi_0 > 7.31 \end{cases} \quad (4.6)$$

These expressions give continuous values of k_4 as a function of the non-dimensional frequency ξ_0 .

The damping coefficient per unit length of the cross-section $b_{33}(x)$ can be written as

$$b_{33}(x) = \rho g^2 \frac{\bar{A}^2}{\omega_e^3} \quad (4.7)$$

where \bar{A} is the non-dimensional amplitude ratio between the amplitude of the forced oscillation and the amplitude of the generated wave. Grim [9] derived an expression for the circular cross-section and Tasai [58] presented the expression for a Lewis form:

$$\bar{A} = \frac{2\xi_0}{1 + C_1 + C_2} \int_1^\infty \left(\frac{1 + C_1}{\beta^2} + \frac{3C_2}{\beta^4} \right) \cos \left(\xi_0 \left(\frac{\beta^4 + C_1\beta^2 + C_2}{(1 + C_1 + C_2)\beta^3} - 1 \right) \right) d\beta \quad (4.8)$$

This expression has been derived consistently based on the potential theory. A simpler expression have been given by Yamamoto et al. [68]:

$$\bar{A} = 2 \sin \left(\frac{\omega_e^2 B}{2g} \right) e^{\left(\frac{-\omega_e^2 \tau}{g} \right)} \quad (4.9)$$

Both expressions for the damping have been implemented.

Although the Lewis forms cover a wide range of cross-sections of ships, inaccurate transformations can occur, especially for the bow and the stern. To overcome this problem there are two possible solutions: to include more parameters in the mapping technique or to resort to a Green function method. The latter has been chosen as it has a wider range of applicability, however, at the expense of complexity and computer time.

4.2 2D Green Function Methods

In the following, three applications will be outlined which cover

- Unsymmetrical cross-sections in shallow water.
- Unsymmetrical cross-sections in deep water.
- Symmetric cross-sections in deep water.

Some of the items listed above could seem to be subcases of each other. The reason why each case is handled separately is to reduce computational time. If for instance the method listed first was to be used for a deep-water analysis, segments from the surface down to a large depth would be needed. This requires a long calculation time compared to a method intended for deep-water calculations. The symmetry condition reduces the calculation time similarly.

The procedure can be divided into three steps. First, the boundary conditions are stated. Then, the use of the Green's function in Green's second identity is described and leads to an integral equation. Finally, the integral equation is converted into a set of algebraic equations. This last step is in principle the same for all the methods. Therefore, a separate section is dedicated to a short description of this.

The general problem is considered to be solution of the deep-water case, which is the typical one and subsequently the case for restricted water depth is described, as an extension of the former. Further, only modes of motion in the transverse plane of the ship are considered because the solutions for the remaining modes can be determined from these modes.

The semi-infinite domain is shown in Figure 4.3, bounded by the free surface at its mean level and by the hull contour. The boundary of the domain is referred to as S and the hull contour is denoted C_x . For simplicity only translations are shown in the figure. In accordance with Figure 3.1 the coordinate system (y, z) is fixed with respect to the mean position of the hull, while the coordinate system (y', z') is fixed in the hull. The two systems coincide at rest and the motions are described by the two translations η_2 and η_3 and the rotation η_4 . The

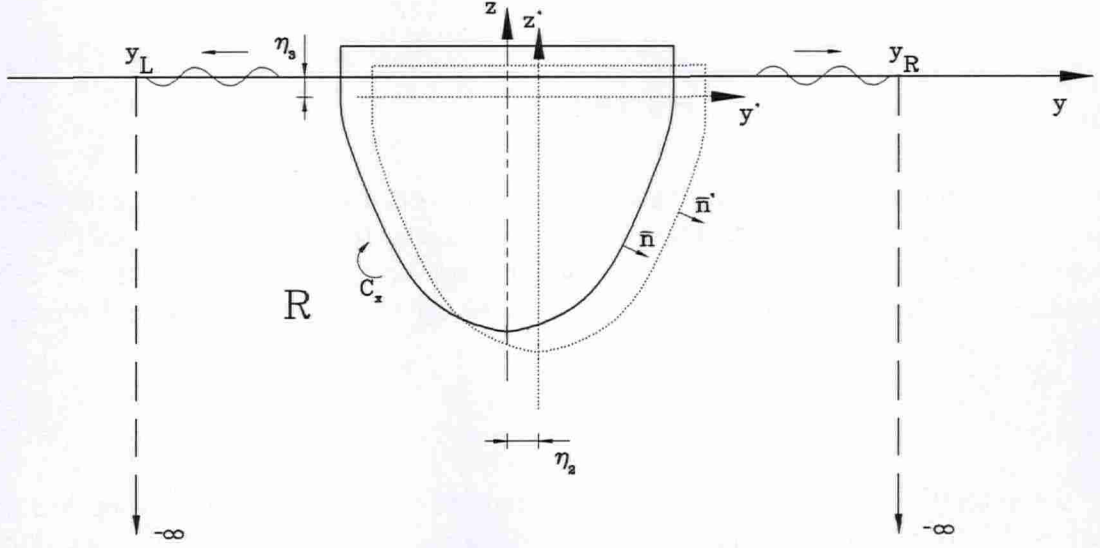


Figure 4.3: The fluid domain and the boundaries for the deep-water case.

rotation refers to the origo of the coordinate system (y', z') . The generalised normal vector n is normalised with respect to the transverse plane, neglecting the longitudinal component. The generalised normal vector n_k is given by $(n_2, n_3, n_4) = (n_y, n_z, yn_z - zn_y)$.

On the assumption about small rotations, the relation between the two systems becomes

$$y = y' + \epsilon\eta_2(t) - z'\eta_4(t) \quad (4.10)$$

$$z = z' + \epsilon\eta_3(t) + y'\eta_4(t) \quad (4.11)$$

The transient response is neglected and the solution will then depend harmonically on time. The motion of the hull cross-section is defined as:

$$\eta_k(t) = \text{Re}[\zeta_k e^{-i\omega_\epsilon t}] \quad k = 2, 3, 4 \quad (4.12)$$

The potentials must satisfy the Laplace equation given by

$$\nabla^2 \phi_k(y, z) = 0, \quad k = 2, 3, 4, \quad (y, z) \in R \quad (4.13)$$

Next, the linearised combination of the kinematic and the dynamic free-surface condition evaluated at the mean water level from Eq. (3.13) yields

$$g \frac{\partial \phi_k}{\partial z}(y, 0; t) + \frac{\partial^2 \phi_k}{\partial t^2}(y, 0; t) = 0, \quad k = 2, 3, 4 \quad (4.14)$$

or

$$\frac{\partial \phi_k}{\partial z}(y, 0) - \frac{\omega_e^2}{g} \phi_k(y, 0) = 0, \quad k = 2, 3, 4 \quad (4.15)$$

The kinematic hull boundary condition states that the normal velocity on the hull determined from the potential is identical to the prescribed motion of the surface. Two complications present themselves here as both the hull contour and the normal change with time. The potential can be given in both coordinate systems by use of the transformation given in Eq. (4.10):

$$\phi_k(y, z; t) = \phi'_k(y', z'; t) \quad (4.16)$$

Here the potential ϕ_k has been primed, which indicates that the transformation has been substituted into it. This gives two possibilities with respect to the boundary condition on the hull:

$$\dot{\eta}_k(t)n_k = \left. \frac{\partial \phi_k(y, z; t)}{\partial n_k(y, z; t)} \right|_{C_x} \quad (4.17)$$

$$= \left. \frac{\partial \phi'_k(y', z'; t)}{\partial n'_k(y', z')} \right|_{C_x} \quad (4.18)$$

In the inertial coordinate system (y, z) the normal depends on time, while in the coordinate system on the hull (y', z') there is no time dependence. By use of the Kirchhoff decomposition in the primed coordinate system given by

$$\phi'_k(y', z'; t) = \phi_k(y', z')\dot{\eta}_k(t) \quad (4.19)$$

which replaces the time dependence in the potential by a product of a space-dependent potential and velocity. The result is that the kinematic hull boundary condition now has to be satisfied in the mean position of the hull and that the time dependence has been eliminated, which gives

$$\dot{\eta}_k(t)n_k = \left. \frac{\partial \phi_k(y', z')\dot{\eta}_k(t)}{\partial n'_k(y, z)} \right|_{C_x} \rightarrow n_k = \left. \frac{\partial \phi_k(y', z')}{\partial n'_k(y', z')} \right|_{C_x} \quad (4.20)$$

The radiation condition states that a wave of constant amplitude radiates away from the oscillating hull. This implies

$$\frac{\partial \phi_k}{\partial z}(y_R, 0) = ik_R \phi_k, \quad y_R \gg 0 \quad (4.21)$$

$$\frac{\partial \phi_k}{\partial z}(y_L, 0) = -ik_L \phi_k, \quad y_L \ll 0 \quad (4.22)$$

In this equation, referring to Figure 4.3, k_R and k_L denote the wave number of the waves progressing away from the hull in the right and left direction, respectively. The y_L and y_R are the horizontal positions where these conditions are applied. They must be at a relatively large distance from the hull to ensure that the transient behaviour of the wave has disappeared. For deep water the wave number k is given by $k = \omega_e^2/g$ and for restricted water by $k \tanh(kd) = \omega_e^2/g$, where d is the water depth.

Moreover, a condition related to the bottom has to be applied. For restricted water depth the kinematic condition evaluated on the seabed becomes

$$\frac{\partial \phi_k}{\partial n} = 0 \quad (4.23)$$

and alternatively for deep water, implying that the disturbance will vanish as the potential is evaluated at increasingly negative z -coordinates:

$$\lim_{z \rightarrow -\infty} \phi_k = 0 \quad (4.24)$$

Depending on which case is considered the boundary conditions listed above can be combined to pose a boundary value problem for the space-dependent potentials.

By use of Green's second identity this can be converted to an integral equation. Considering two points of interest in a fluid domain $P(y, z)$ and $Q(\xi, \eta)$. The point $Q(\xi, \eta)$ refers to the position of the Green function and the point $P(y, z)$ refers to a point at which the potential is to be evaluated.

Green's second identity yields the following theorem for a point P on the boundary:

$$\begin{aligned} \phi_k(P) = & \int_R \nabla^2 \phi_k(s) G(P, Q) dA + \\ & \frac{1}{\pi} \int_S \phi_k(s) \frac{\partial G(P, Q)}{\partial n} ds - \frac{1}{\pi} \int_S G(P, Q) \frac{\partial \phi_k(s)}{\partial n} ds \end{aligned} \quad (4.25)$$

Due to the field equation, Eq. (4.13), the expression reduces to

$$\phi_k(P) = \frac{1}{\pi} \int_S \phi_k(s) \frac{\partial G(P, Q)}{\partial n} ds - \frac{1}{\pi} \int_S G(P, Q) \frac{\partial \phi_k(s)}{\partial n} ds \quad (4.26)$$

The π in Eq. (4.26) refers to a point on the boundary. This is changed to 2π for a similar expression for an internal point in the domain and for a knuckle point the angle between the two segments connected to the knuckle point. The Green functions $G(P, Q)$ are distributed over the boundary of the hull. The potential is determined from an integration of the

potential function along the boundaries of the domain. The potentials can be determined from Eq. (4.26), which becomes a set of linearly coupled Fredholm integral equations of the second kind.

A number of Green functions can be applied. The general form is

$$G(y, z; \xi, \eta) = -\ln(r) + H(y, z; \xi, \eta) \quad (4.27)$$

where r is the distance between the two points $P(y, z)$ and $Q(\xi, \eta)$. H is any function that as a minimum satisfies the Laplace equation. If, in addition, the function H satisfies the free-surface, the radiation condition and the bottom boundary condition, the integral equation will only include integration over the hull boundary C_x .

This leaves the choice between evaluating a complicated Green function only over the hull boundary or evaluating a simpler Green function over the entire boundary of the fluid.

4.2.1 Simple Green Function

The Green function is in its simplest form $G(P, Q) = -\ln(r)$, where r is the distance from the point $P(y, z)$ to the location of the singularity $Q(\xi, \eta)$. This rather simple function makes it necessary to integrate around the entire boundary. Inserting the Green function in Eq. (4.26) gives

$$\pi\phi_k(P) = \int_S \phi_k(s) \frac{\partial}{\partial n}(\ln(r)) ds - \int_S \ln(r) \frac{\partial \phi_k(s)}{\partial n} ds \quad (4.28)$$

The subsequent subdivision of this contour refers to the symbols indicated in Figure 4.3. The two vertical contours S_R and S_L are located in the horizontal positions y_L and y_R , respectively. The contour on the free surface is denoted S_F , and the contour describing the seabed, S_B . By integration over the boundary of the domain and use of the boundary conditions Eqs. (4.15), (4.20), (4.21), (4.22) and (4.23) give

$$\begin{aligned} \pi\phi_k(P) = & \int_{C_x} \phi_k(s) \frac{\partial}{\partial n}(\ln(r)) ds - \int_{C_x} n_k(s) \ln(r) ds + \\ & \int_{S_F} \phi_k(s) \left[\frac{\partial}{\partial n}(\ln(r)) - k \ln(r) \right] ds + \\ & \int_{S_R} \phi_k(s) \left[\frac{\partial}{\partial n}(\ln(r)) - ik \ln(r) \right] ds + \\ & \int_{S_B} \phi_k(s) \frac{\partial}{\partial n}(\ln(r)) ds + \\ & \int_{S_L} \phi_k(s) \left[\frac{\partial}{\partial n}(\ln(r)) + ik \ln(r) \right] ds \end{aligned} \quad (4.29)$$

In the case where the domain is semi-infinite in terms of the distance to the seabed, the equations are simplified to some extent. In the following, two cases are treated.

Infinite Water Depth

If the distance to the seabed is infinite or at least of an order of which the deep-water wave approximation can be justified ($d/\lambda \gg 0.5$), then the disturbance from the motion will vanish as z approaches $-\infty$. This makes the fifth term in Eq. (4.29) negligible. Following the approach by Yeung [69] with the right radiation boundary as an example, the term associated with this boundary can be replaced by $\phi(\xi_R, 0)e^{k\eta}$ on the assumption that the distribution of the potential is an exponentially decaying function of the vertical distance from the free surface.

The corresponding integral in Eq. (4.29) for the point $P(y_i, z_i)$ becomes

$$\begin{aligned} \int_{s_R} \phi_k \left[\frac{\partial}{\partial n} \ln(r) - ik \ln(r) \right] ds &= \phi_k(\xi_R, 0) \int_{-\infty}^0 e^{k\eta} \left[\frac{\partial}{\partial \xi} \ln(r) - ik \ln(r) \right] d\eta \\ &= \phi_k(\xi_R, 0) [F_i^R - iG_i^R] \end{aligned} \quad (4.30)$$

The derivative with respect to the generalised normal n becomes equal to $\partial/\partial\xi$, because the radiation boundaries are vertical. The integrals F_i^R and G_i^R are defined by

$$F_i^R(k, \xi_R) = \int_{-\infty}^0 e^{k\eta} \frac{\partial}{\partial \xi} \ln \left[\sqrt{(y_i - \xi)^2 + (z_i - \eta)^2} \right] \Big|_{\xi=\xi_R} d\eta \quad (4.31)$$

$$G_i^R(k, \xi_R) = k \int_{-\infty}^0 e^{k\eta} \ln \left[\sqrt{(y_i - \xi_R)^2 + (z_i - \eta)^2} \right] d\eta \quad (4.32)$$

Using a similar approach on the left radiation boundary leaves only the integral on the hull boundary and the free surface. The unknowns on the radiation boundary are hereby replaced by a single unknown $\phi_k(\xi_R, 0)$ on the free surface on each side of the hull.

Finite Water Depth

For finite water depth the general approach is the same as before except for the integral on the seabed is not being negligible and, moreover, the way the radiation condition is treated is also different. The radiation conditions given by Eqs. (4.21) and (4.22) require that the distance from the section they are applied is sufficiently large so that transients have died out. However, this also leads to a larger domain which is not beneficial. Therefore, the

possibility of taking these transients into account in the posed condition is advantageous. Following the approach by Yeung [69] and also used by Andersen and He [1], the potential in the outer region of the radiation boundary on the right side of the domain R can be written as a sum of potentials

$$\psi_R = \sum_{n=0}^{\infty} C_{nR} \psi_{nR} \quad (4.33)$$

where C_{nR} are unknown coefficients. For $n = 0$ the unit potential is given by

$$\psi_{0R} = e^{ik_{0R}(y-y_R)} \frac{\cosh[k_{0R}(z+h_R)]}{\cosh[k_{0R}h_R]} \quad (4.34)$$

The depth is indicated by h_R , and y_R is the horizontal position of the radiation boundary, both corresponding to the right side of the domain. k_{0R} is the positive solution to the equation:

$$k_0 \tanh(k_0 h_R) = \frac{\omega_e^2}{g} \quad (4.35)$$

This corresponds to the potential of an outgoing shallow water wave. If decaying transients occur, they are included by the additional terms given by

$$\psi_{nR} = e^{k_{nR}(y-y_R)} \cos[k_{nR}(z+h_R)] \quad (4.36)$$

The constant k_n is given as the n -th positive solution to

$$k_n \tanh(k_n h_R) = -\frac{\omega_e^2}{g} \quad (4.37)$$

The terms, ψ_{nR} are a set of eigenfunctions satisfying the Laplace equation, the free-surface condition and the bottom boundary condition. At the radiation boundary the potentials are matched ($\psi_R = \phi_R$), which gives

$$\phi_R = \sum_{n=0}^{N_R} C_{nR} \psi_{nR} \quad (4.38)$$

Finally, the condition on the right side becomes

$$\left(\frac{\partial\phi}{\partial n}\right)_{S_R} = -\left(\frac{\partial\phi}{\partial y}\right)_{S_R} \quad (4.39)$$

$$= -ik_{0R}C_{0R}\psi_{0R} - \sum_{n=1}^{N_R} k_{nR}C_{nR}\psi_{nR} \quad (4.40)$$

Using the same procedure on the left side of the domain gives

$$\left(\frac{\partial\phi}{\partial n}\right)_{S_L} = -\left(\frac{\partial\phi}{\partial y}\right)_{S_L} \quad (4.41)$$

$$= -ik_{0L}C_{0L}\psi_{0L} - \sum_{n=1}^{N_L} k_{nL}C_{nL}\psi_{nL} \quad (4.42)$$

Applying these radiation conditions to Eq. (4.29) leads to the boundary value problem for restricted depth.

4.2.2 Frank Close Fit

The Frank Close Fit method, or what has earlier been referred to as application of a complicated Green function, uses a source distribution on the boundary of the hull and solves for the source strength. The implemented method is in accordance with Potash [45] and uses a Green function to solve for the potential. As it is shown in [45], this approach becomes equivalent to the Frank Close Fit method. This involves a more complicated Green function satisfying the required boundary conditions. In this case it is the infinite water depth boundary condition, the radiation condition and the free-surface condition corresponding to Eqs. (4.24), (4.21), (4.22) and (4.15). The Green function is given for the infinite water depth in Wehausen and Laitone [64] as the potential for a point source of unit strength located at (ξ, η) :

$$G(y, z, t) = \left\{ \frac{1}{2\pi} \ln \sqrt{\frac{(y-\xi)^2 + (z-\eta)^2}{(y-\xi)^2 + (z+\eta)^2}} - \frac{1}{\pi} \int_0^\infty \frac{e^{k(z+\eta)} \cos(u(y-\xi))}{u-k} du \right\} \cos(\omega_e t) - \left\{ e^{k(z+\eta)} \cos(k(y-\xi)) \right\} \sin(\omega_e t) \quad z, \eta \leq 0 \quad (4.43)$$

By application of this Green function to Eq. (4.26) it can be shown that the integrals vanishes as the depth approaches infinity except on the hull surface. The numerical details about the solution of principal value integral in Eq. (4.43) can be found in e.g. Yeung [69].

The remaining procedure for determining the potentials is similar to the description in the previous sections.

4.2.3 Discretization of the Integral Equation

The integral equation in a form dependent on the methods described in the previous sections consists of a curve integral along parts of or the entire boundary of the domain. This curve is approximated by straight-line segments. The segments are described by geometry points, which form the endpoints of the segments. The midpoints of the segments are considered to be potential points, which represent the constant potential on the segment. The potential on the i th segment ϕ_{k_i} , which forms the linear connection between (ξ_i, η_i) and (ξ_{i+1}, η_{i+1}) , is given by

$$\phi_{k_i} = \phi_{k_i} \left(\frac{\xi_i + \xi_{i+1}}{2}, \frac{\eta_i + \eta_{i+1}}{2} \right) \quad (4.44)$$

It is conceivable that this is reasonably accurate if the subdivisions are fine. For each potential point the integral along the boundary can be rewritten as a sum of all the contributions from the segments in question with the constant potential corresponding to each segment as a coefficient. This can be rearranged to a number of equations equal to the number of potential points. This discretization reduces the integral equation to a set of linear algebraic equations. The unknowns become the values of the potentials at a discrete set of control points along the boundary.

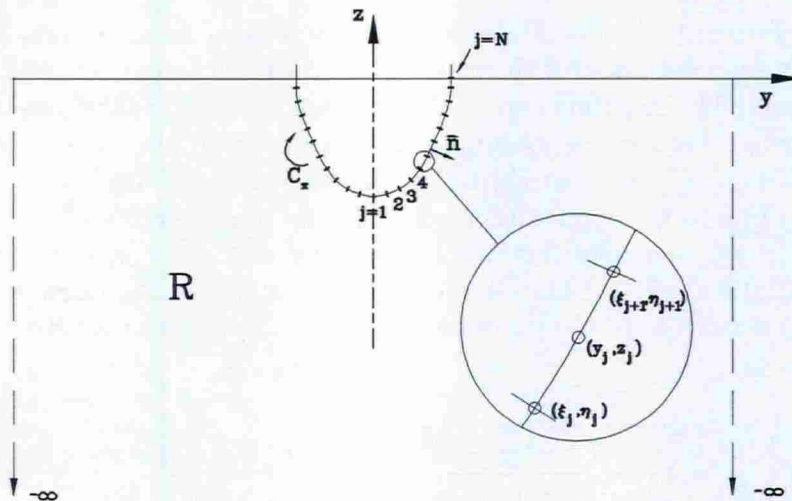


Figure 4.4: Example of the discretization of the boundary for the infinitely deep-water case.

This set of equations is solved for each of the modes sway, heave and roll and the potentials are determined.

The potential determined in this chapter is the space-dependent part of the decomposed potential $\phi_k(y, z; t) = \phi_k(y, z) i\omega_e e^{i\omega_e t}$. The sectional hydrodynamic force and moment $t_2(t)$

$t_3(t)$ and $t_4(t)$, due to the oscillation, can be expressed as

$$t_j(t) = -\rho \int_{C_x} \frac{\partial \phi_k(y, z, t)}{\partial t} n_j ds \quad k = 2, 3, 4 \quad (4.45)$$

by neglecting higher order terms in the Bernoulli equation. In Eq. (4.45) the sectional force or moment related to a certain mode j includes coupling terms from other modes. For the determination of the added mass and damping coefficients, only the amplitudes of the force and moment components are required. They can therefore be expressed specifically as t_{jk} , which means the amplitude of the force or moment corresponding to the j th mode due to motion corresponding to the i th mode.

$$t_{jk} = \rho \omega_e^2 \int_{C_x} \phi_k(y, z) n_j ds \quad (4.46)$$

Eqs. (4.46) and (3.32) deviate from Eq. (3.22) by a factor of $i\omega$. The reason for this is that in Chapter 3 the potential ϕ_k^0 denotes the amplitude of the potential, while in this chapter the derivations have been simplified by expressing the potential as a factor on the velocity. This leads to the relation between the potentials in Eqs. (3.32) and (4.46) given by $\phi_k^0(y, z) = i\omega \phi_k(y, z)$.

The expression in Eq. (3.32) relates the sectional added mass and hydrodynamic damping to the potentials

$$\rho \omega_e^2 \int_{C_x} n_j \phi_k dl = \omega_e^2 a_{jk} - i\omega_e b_{jk} \quad (4.47)$$

From this, the added mass and the damping become

$$a_{jk} = -\rho \int_{C_x} n_j \operatorname{Re}(\phi_k) dl \quad (4.48)$$

$$b_{jk} = \rho \frac{1}{\omega_e} \int_{C_x} n_j \operatorname{Im}(\phi_k) dl \quad (4.49)$$

In Figure 4.5a 4.5b and 4.5c examples of results for different depths are shown. The general tendency is that in the low-frequency area the hydrodynamic mass is increasing with decreasing clearance between the keel and the bottom. On the contrary as regards the higher frequencies where the hydrodynamic mass is decreasing with decreasing clearance. An exception is the hydrodynamic mass for heave in Figure 4.5c, which increases in the entire frequency range as the clearance decreases.

The effect of the water depth was considered by ITTC 1978 [17], which concluded that the influence of the water depth on ship motions becomes noticeable when the depth is shallower than twice the ship draught. However, the effect manifests itself both through the hydrodynamic coefficients and through the shallow water exciting wave, the latter has not been implemented here.

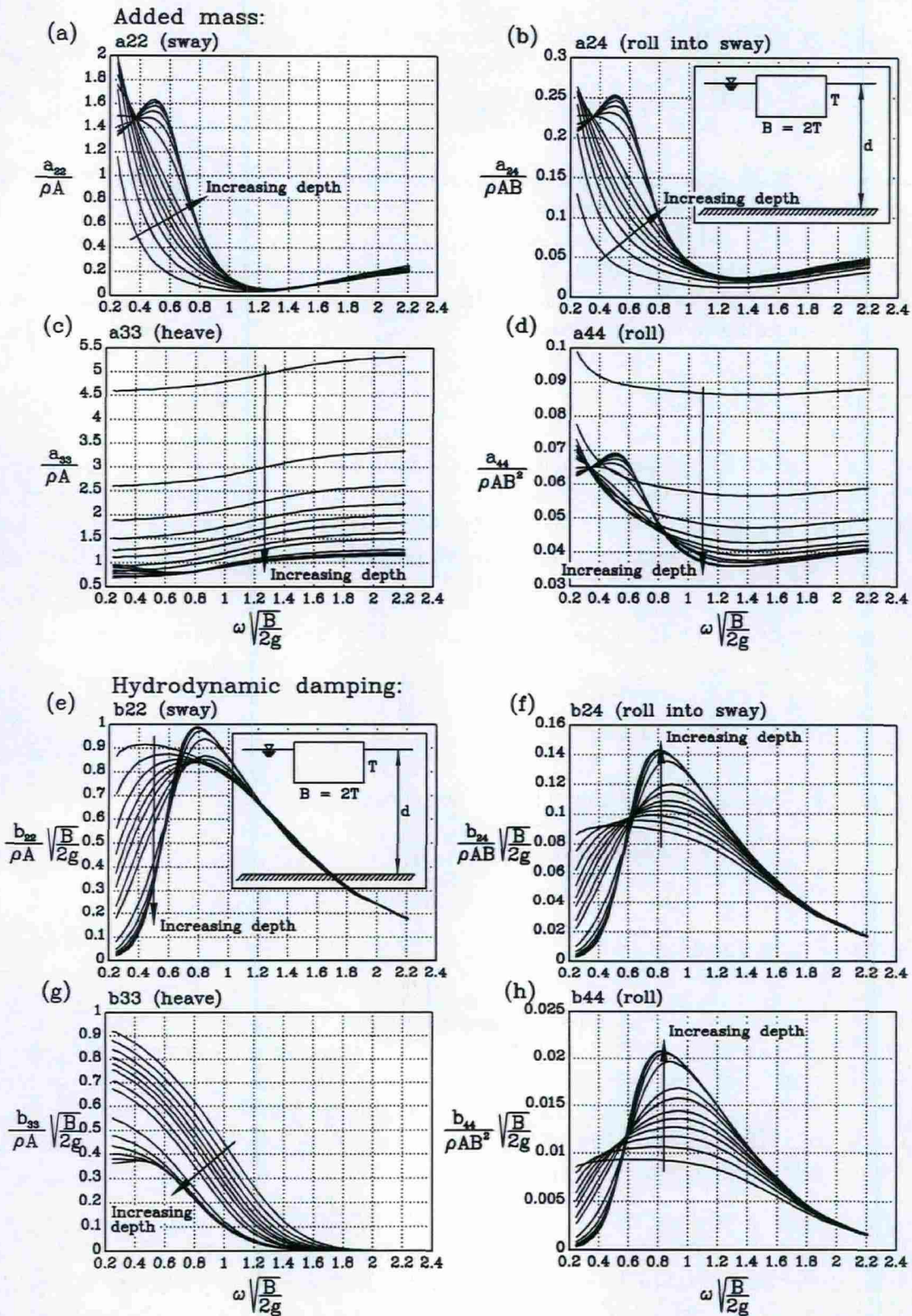


Figure 4.5: Non-dimensional added mass and damping of a rectangular symmetric section with $B/T = 2$ and different depth/draught-ratios.

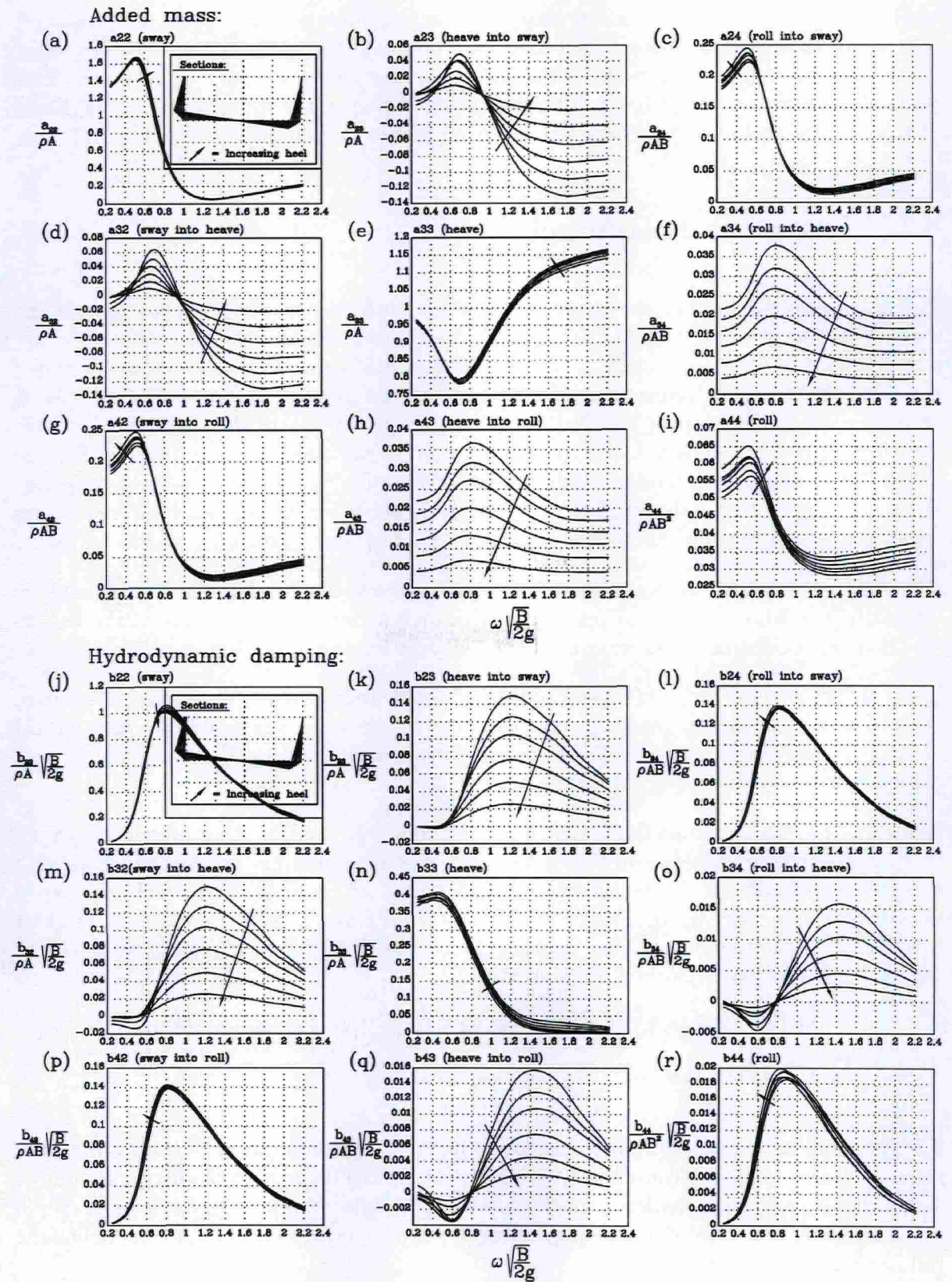


Figure 4.6: The non-dimensional added mass and damping for a rectangular symmetric section with $B/T = 2$ and different heeling angles.

In Figure 4.6 examples of the added mass and damping for a heeling section are presented. Nine terms are shown for both added mass and damping due to the asymmetry. For sway, heave, roll and the coupling between roll and sway, no significant change is observed. This is mainly due to the relatively small heeling angle. However, the remaining coupling terms increase as the heel angle increases and approach zero as the ship becomes upright.

4.3 Irregular Frequencies

It is a distinct advantage of the Green function approach that it solves the problem for the cross-section in question without the requirement of a proper transformation as for the mapping methods. At first sight there appears to be no restrictions on the cross-sectional shape. However, the matrix of influence coefficients can become singular for certain frequencies. A frequency where this happens is called an irregular frequency. Normally it happens at rather high frequencies and does not affect the calculation in the wave frequency range. For the simple Green function methods described above no irregular frequencies have been observed. For the Frank Close Fit the irregular frequencies do occur but usually for high frequencies where the wave spectrum contains less energy so the response spectrum is unaffected by it.

Different authors have proposed modifications to remove the frequencies. An example is Ohmatsu [42], who proposed to put a hydrodynamic lid on the water plane of the hull to suppress the oscillation of the interior of the hull, causing the irregularities.

Lee et al. [28] review this problem and add that discretization errors in the numerical solution of panel methods translate into large errors in the solution over a substantial frequency band around the irregular frequencies. Furthermore, that the width of the polluted frequency band can be reduced by increasing the number of panels.

Regarding the use of the methods the irregular frequencies usually occur at relatively high frequencies with no influence on the calculation. A regular ship motion problem even with a rather dense grid can be solved in reasonable time, which makes it possible to narrow the polluted frequency band. Finally, use of the Lewis transformation avoids the irregular frequencies. Therefore, it has been concluded that the ship motion problem can be solved without modifications regarding irregular frequencies.

4.4 Roll Damping

The damping in ship motion problems comes mainly from radiating waves away from the ship. This wave damping constitutes the major part of the dissipation of energy. Rolling of a ship, however, is an exception from this. In this case, the wave-making damping is only a small fraction of the total roll damping, which the ship experiences in reality. The remaining roll damping arises from

-
- Eddy shedding from e.g. a sharp keel or bilges when the ship rolls.
 - Skin friction as forces on the surface when the ship rolls.
 - Appendage forces, which oppose the rolling motion.

All these effects are due to the viscosity of the fluid, which is neglected in the strip theory. The wave-making damping is linear and proportional to the roll velocity. However, this is not the case for the viscous roll damping, which is generally proportional to the square of the roll velocity. A lot of more or less empirical relations have been developed, e.g. Schmitke [50] and Tanaka [56], to determine the three contributions listed above and make a linearisation with respect to a proper point of roll velocity.

In this work a simple procedure has been selected, in which it is possible to choose a percentage of the critical damping to add to the wave-making damping in order to get at least realistic values of the roll amplitude.

This page is intentionally left blank.

Chapter 5

Response Statistics

5.1 Introduction

The description of the ship response in waves in the previous chapters aims at regular waves only. However, the ocean wave climate is stochastic. The wave signal and the ship response must therefore be considered as stochastic processes subdivided into durations where they can be considered as stationary in a statistical sense. Stationary means in this context that the statistical properties characterising the stochastic process do not depend on time. A duration in which the process can be considered as stationary is denoted short-term and it is typically of the order of hours. The use of the definition long-term covers the 'in-service' lifetime of the ship and can be described by a large number of short-term periods. The outcome of the statistical analysis of the response is a distribution of the extreme values in terms of probabilities of exceedance for different levels of the response. Based on this distribution, design loads can be determined. In addition, the fatigue damage due to the stress amplitude distribution and number of cycles to which a detail on the ship has been exposed can be determined from these statistical results. The statistical procedure to be applied depends on the form of the response described in the previous chapters. In the following sections the procedure for each type will be addressed.

5.2 Short-Term Response Statistics

In the linear analysis the wave kinematics in a stationary sea state is modelled as Gaussian distributed processes. Due to the linear relation between waves and ship responses, also the responses are Gaussian distributed processes. The Gaussian process is described by its mean value and variance. As only wave-induced response is considered the mean value in the linear analysis is zero. The non-linear analyses introduce responses which deviate from the Gaussian distribution. These deviations can be determined on the basis of the statistical

moments and expressed approximately in terms of mean μ , variance $V \equiv \sigma^2$, skewness κ_3 and kurtosis κ_4 . As shown in Figure 5.1 the skewness causes an asymmetry to the Gaussian

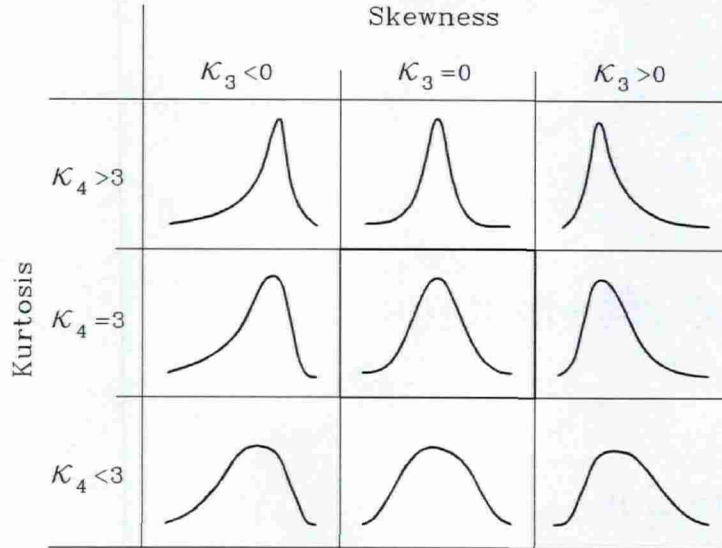


Figure 5.1: The effect of skewness and kurtosis in the Gaussian distribution.

distribution, while the kurtosis increases the probability in the 'tails' of the distribution.

5.2.1 Linear Frequency Response

The procedure for the linear response in the frequency domain is a standard linear spectral analysis. The response is known in terms of a complex frequency response function or a response amplitude operator $R(\omega|U, \beta)$ and the corresponding phase function $P(\omega|U, \beta)$. The vessel experiences the load sequences with respect to a frequency of encounter ω_e , which is the wave frequency measured from a moving reference placed on the ship. The response spectrum $S_R(\omega_e)$ is given as

$$S_R(\omega_e|H_s, T_z, U, \beta) = R(\omega_e|U, \beta)^2 S_\eta^e(\omega_e|H_s, T_z, U, \beta) \quad (5.1)$$

where $S_\eta^e(\omega_e)$ is the wave spectrum as a function of the frequency of encounter, the significant wave height H_s and the zero upcrossing period T_z . The relation between the frequency of encounter and the wave frequency is given in Eq. (5.2).

The transformation of the spectrum from the wave frequency to the frequency of encounter is described e.g. in Price and Bishop [46]. If a wave spectrum is considered, it can be expressed in terms of both the wave frequency and the frequency of encounter by the relation

$$\omega_e = \left| \omega - \frac{\omega^2}{g} U \cos(\beta) \right| \quad (5.2)$$

The relation between the wave spectrum given as a function of the wave frequency and as a function of the frequency of encounter is found by using energy conservation. This states that the energy of the waves in a frequency band must be the same whether it is expressed in terms of the wave frequency ω or the frequency of encounter ω_e :

$$S_{\eta}(\omega)d\omega = S_{\eta}^e(\omega_e)d\omega_e \quad (5.3)$$

so that

$$S_{\eta}^e(\omega_e) = \frac{S_{\eta}(\omega)}{|d\omega_e/d\omega|} = \frac{S_{\eta}(\omega)}{|1 - \frac{2\omega U}{g} \cos(\beta)|} \quad (5.4)$$

for the real, positive value of ω given by

$$\omega = \frac{1 \pm [1 - 4\frac{U}{g}\omega_e \cos(\beta)]^{\frac{1}{2}}}{2\frac{U}{g} \cos(\beta)}. \quad (5.5)$$

As stated in Jensen and Dogliani [23], Eq. (5.2) has up to three solutions of the wave frequency for each frequency of encounter for following and quartering seas. This makes integration with respect to the wave frequency less straightforward.

From the response spectral density S_R , the spectral moments

$$m_{Rn} = \int_0^{\infty} \omega_e^n S_R(\omega_e) d\omega_e, \quad n=0,1,2,\dots \quad (5.6)$$

can be determined.

Given these spectral moments of the response the distribution of the peak values can be determined. By assuming the response to be narrow-banded the distribution can be approximated by the Rayleigh distribution:

$$F_p(z) = 1 - e^{-\frac{z^2}{2m_{R0}}} \quad (5.7)$$

To determine the rate at which peaks occur the upcrossing rates must be determined. By use of the results derived by Rice [47], the zero upcrossing rate is determined by

$$\nu_0 = \frac{1}{2\pi} \frac{\dot{\sigma}}{\sigma} \quad (5.8)$$

where σ is the standard deviation of the response and $\dot{\sigma}$ is the standard deviation of the time derivative of the response. The latter enters through the condition of upcrossing. For a linear response the spectral moments of the derivatives are related by $m_{\dot{R}n} = m_{Rn+2}$ for $n = 0, 1$, which gives

$$\nu_0 = \frac{1}{2\pi} \frac{\sqrt{m_{R2}}}{m_{R0}} \quad (5.9)$$

Similarly, the peak rate becomes

$$\nu_p = \frac{1}{2\pi} \frac{\sqrt{m_{R4}}}{m_{R2}} \quad (5.10)$$

For a narrow-banded response the peak rate can be approximated by the zero upcrossing rate.

The number of peaks occurring within a given duration T is determined by $N = \nu_p T$. The distribution of the extreme values of the response with the duration T in the form of the probability of exceeding a given response level ζ can be determined by use of different methods. Often order statistics are used with the relation

$$F_{max}(\zeta) = 1 - \{F_p(\zeta)\}^N = 1 - \left\{1 - e^{-\frac{\zeta^2}{2m_{R0}}}\right\}^{\nu_p T} \quad (5.11)$$

assuming statistically independent peaks. An alternative is to consider the response as a Poisson process. The Poisson distribution has been derived on the assumption that the individual peaks are uncorrelated. This implies a not too narrow-banded response spectrum. The distribution of the extreme value of the response within a given period T is then given by

$$F_{max}(\zeta) = 1 - e^{-\nu T} \quad (5.12)$$

where the upcrossing rate ν of the level ζ is given by

$$\nu = \nu_0 e^{-\frac{\zeta^2}{2m_{R0}}} \quad (5.13)$$

with the zero upcrossing rate ν_0 given by Eq. (5.9).

5.2.2 Quadratic Frequency Response

The response determined from the quadratic strip theory analysis contains in addition to the linear response amplitude operator two quadratic response amplitude operators. These quadratic response operators are given as described in Section 3.3.1. They are functions of sum and difference frequencies, respectively. The operator related to the difference frequencies represent a slowly varying contribution to the solution and the operator related to the sum frequencies represents a rapidly varying contribution. Given a wave spectrum at equidistantly spaced frequencies of encounter and the quadratic frequency response functions in Eqs. (3.51) and (3.52) the response can be written in the compressed form

$$\frac{M(x, 0)}{\lambda} = \sum_{j=1}^{2n} \lambda_j \chi_j + \epsilon \sum_{j=1}^{2n} \sum_{k=1}^{2n} \Lambda_{jk} \chi_j \chi_k \quad (5.14)$$

where the independent stochastic variables χ_j are defined as

$$\chi_j = \frac{\xi_j}{\sqrt{V_j}} \quad (5.15)$$

The amplitude and phase lag of each wave component are, as in Section 3.3.1, expressed as $\xi_j = a_j \cos(\theta_j)$ and $\xi_{j+n} = a_j \sin(\theta_j)$ and with a variance given by $V_j = V_{j+n} = S_{\eta}^e(\omega_{e_j})$ corresponding to the frequency ω_{e_j} . The response has been normalised by the standard deviation of the first order contribution, denoted λ , and given by

$$\lambda = \left[\sum_{r=1}^n \{ (M_r^c)^2 + (M_r^s)^2 \} V_r \right]^{1/2} = \sqrt{m_{R0}} \quad (5.16)$$

The linear standard deviation referring to each frequency of encounter becomes

$$\lambda_j = \begin{cases} M_j^c \frac{\sqrt{V_j}}{\lambda} & \text{for } j \leq n \\ -M_{j-n}^s \frac{\sqrt{V_{j-n}}}{\lambda} & \text{for } j > n \end{cases} \quad (5.17)$$

Using $t = 0$, which is applicable as the response is stationary in a statistical sense. Finally, the second order coefficients become

$$\Lambda_{jk} = \begin{cases} (M_{jk}^{c+} + M_{jk}^{c-}) \cdot \sqrt{V_j V_k} & \text{for } j, k \leq n \\ (-M_{j,k-n}^{s+} + M_{j,k-n}^{s-}) \cdot \sqrt{V_j V_{k-n}} & \text{for } j \leq n \text{ and } k > n \\ -(M_{j-n,k}^{s+} + M_{j-n,k}^{s-}) \cdot \sqrt{V_{j-n} V_k} & \text{for } j > n \text{ and } k \leq n \\ (-M_{j-n,k-n}^{c+} + M_{j-n,k-n}^{c-}) \cdot \sqrt{V_{j-n} V_{k-n}} & \text{for } j, k > n \end{cases} \quad (5.18)$$

These coefficients have been normalised by the non-linearity parameter ϵ to fulfil

$$\sum_{j=1}^{2n} \sum_{k=1}^{2n} \Lambda_{jk} = 1 \quad (5.19)$$

By reference to the work by Jensen and Dogliani [23], the first four moments of the response become

$$\mu = K_1 = \lambda \epsilon \sum_{i=1}^{2n} \Lambda_{ii} \quad (5.20)$$

$$\sigma^2 = K_2 = \lambda^2 (1 + 2\epsilon^2) \quad (5.21)$$

$$\kappa_3 \sigma^3 = K_3 = \lambda^3 \left(6\epsilon \sum_{i=1}^{2n} \sum_{j=1}^{2n} \lambda_i \Lambda_{ij} \lambda_j + 8\epsilon^3 \sum_{i=1}^{2n} \sum_{j=1}^{2n} \sum_{k=1}^{2n} \lambda_{ij} \Lambda_{jk} \Lambda_{ki} \right) \quad (5.22)$$

$$(\kappa_4 - 3)\sigma^4 = K_4 = \lambda^4 48\epsilon^2 \left(\sum_{i=1}^{2n} \sum_{j=1}^{2n} \sum_{k=1}^{2n} \lambda_i \Lambda_{ij} \Lambda_{jk} \lambda_k + \epsilon^2 \sum_{i=1}^{2n} \sum_{j=1}^{2n} \sum_{k=1}^{2n} \sum_{l=1}^{2n} \Lambda_{ij} \Lambda_{jk} \Lambda_{kl} \Lambda_{li} \right) \quad (5.23)$$

Different methods can be used for the extreme value prediction as discussed in Jensen and Dogliani [23]. The approximate procedure applied here is a simple cubic Hermite polynomial transformation. For a Gaussian process the distribution of peaks is simple to determine from Eq. (5.7). The Hermite series approximation method takes advantage of this by a functional transformation of a non-linear response into a standard Gaussian process. The non-linear response $M(t)$ is used to determine a polynomial $g(U(t))$ of the standard Gaussian process $U(t)$. The procedure is to determine the four deterministic coefficients c_0 , c_1 , c_2 and c_3 in

$$M(t) \simeq g(U(t)) = c_0 + c_1 U + c_2 U^2 + c_3 U^3 \quad (5.24)$$

so that the mean value μ , the variance σ^2 , the skewness κ_3 and the kurtosis κ_4 are the same for $M(t)$ and $g(U(t))$. Thus, see [22]:

$$E[M] = \mu_M = c_0 + c_2 \quad (5.25)$$

$$E[(M - \mu_M)^2] = \sigma_M^2 = c_1^2 + 6c_1 c_3 + 2c_2^2 + 15c_3^2 \quad (5.26)$$

$$E[(M - \mu_M)^3] = \kappa_3 \sigma_M^3 = c_2 (6c_1^2 + 8c_2^2 + 72c_1 c_3 + 270c_3^2) \quad (5.27)$$

$$E[(M - \mu_M)^4] = \kappa_4 \sigma_M^4 = 60c_2^4 + 3c_1^4 + 10395c_3^4 + 60c_2^2 c_1^2 + 4500c_2^2 c_3^2 + 630c_1^2 c_3^2 + 936c_1 c_2^2 c_3 + 3780c_1 c_3^3 + 60c_1^3 c_3 \quad (5.28)$$

This set of algebraic equations is solved by a Newton-Raphson scheme.

The distribution of the extremes can now be formulated simply by use of the transformation to the standard Gaussian distribution.

The peak distribution for the non-linear response ζ thus becomes

$$F_p(\zeta) = 1 - e^{-\frac{u^2(\zeta)}{2}} \quad (5.29)$$

where $u(\zeta)$ is the inverse function of $g(U)$ given by the real solution to

$$\zeta = \sum_{i=0}^3 c_i u^i \quad (5.30)$$

The upcrossing rate is found in a similar way as in the linear case except for a more complicated relation between the response and its time derivative. From an expression of the same form as Eq. (5.14) for the time derivative of the response the upcrossing rate can be calculated as in [23], by

$$\nu_0 = \frac{1}{2\pi} \frac{\dot{\sigma}}{\sigma} \left(1 + \frac{1}{8}(\kappa_4 - 3) \right) \quad (5.31)$$

The extreme value prediction is determined as in the linear case by Eq. (5.12) but using the transformation in the relation between zero upcrossing and the upcrossing rate at $u(\zeta)$:

$$\nu = \nu_0 e^{-\frac{u^2(\zeta)}{2}} \quad (5.32)$$

5.2.3 Fatigue Analysis

As the local loads are related to the global loads, the fatigue analysis becomes relevant in this context. There are several models for relating the cyclic stress/strain state at a structural detail to the fatigue strength of the material. The basic assumption is that the fatigue performance of the detail can be described by a small-scale laboratory specimen when it is exposed to the same stress history.

The S-N Approach

The S-N approach is based on fatigue tests which describe the relation between a constant cyclic stress range $\Delta\sigma$ and the corresponding number of load cycles N leading to failure. The procedure assumes that it is only necessary to consider the range $\Delta\sigma$ in the principal stresses when the fatigue endurance is estimated. Thus, the influence of the mean stress level is neglected. The result from the S-N fatigue test is described on the following form

$$N_e(\Delta\sigma)^m = \bar{a} \quad (5.33)$$

where N_e is the number of cycles for failure at the stress range $\Delta\sigma$ and m is the negative slope of the S-N curve. Finally, \bar{a} is a scale parameter. To extend this constant amplitude test result to a load sequence of varying amplitude, the linear Palmgren-Miner fatigue damage model [33] is used. It states that the total damage experienced by the structure may be expressed by the accumulated damage from each load cycle at different stress levels. A load sequence consisting of different amplitudes or stress ranges can be divided into j levels of constant stress amplitude and the expected accumulated damage D is calculated as

$$D = \sum_{i=1}^j \frac{n_i}{N_{c,i}} = \sum_{i=1}^j \frac{n_i \Delta\sigma_i^m}{\bar{a}} \quad (5.34)$$

where n_i is the number of stress cycles at the load level i and $N_{c,i}$ is the corresponding critical number of load cycles. Failure is assumed to occur when the damage index D is equal to 1.0. The Palmgren-Miner approach [33] assumes that the cumulative damage D is independent of the sequence of the applied stress. This is generally not the case. However, the Palmgren-Miner rule is still one of the most accurate models for cumulative damage calculations.

For a symmetric, slightly non-Gaussian stress response the fatigue damage per cycle can be estimated on the basis of the Palmgren-Miner [33] rule as given by Winterstein [66]:

$$d = \frac{\Gamma(1 - \frac{m}{2})}{\bar{a}(2\sqrt{2}\sigma)^m} \left(1 + \frac{1}{24}(m^2 + m)(\kappa_4 - 3) \right) \quad (5.35)$$

where $\Gamma()$ is the Gamma function, \bar{a} and m the scale and slope parameters in the S-N curve and σ and κ_4 the standard deviation and kurtosis of the stress response. The total expected damage D during a time period T can finally be calculated as

$$D = T\nu_0 d \quad (5.36)$$

5.3 Long-Term Response Statistics

The long-term analysis covers the lifetime of a ship, say 20 years. The applied concept is that the long-term analysis is modelled as a sequence of stationary short-term periods. The determination of the spectral moments for the short-term responses has been described in previous sections.

As the wave spectrum is a function of the square of the significant wave height it is in the linear case only necessary to determine the variance for a single significant wave height and all relevant zero upcrossing periods. Similarly, for the second order response a relation is used between the significant wave height and the cumulants K_i , given in Eq. (5.20)-Eq. (5.23). In this case it involves calculation of the spectral moments at only two different significant wave heights. The details can be found in [23].

The probability of exceedance becomes

$$Q(M_p(T)) = P(\max_T M_p > \zeta) \quad (5.37)$$

$$= 1 - \prod_{i=1}^p e^{-\nu_i(\zeta)T_i} \quad (5.38)$$

$$= 1 - \prod_{i=1}^p e^{-\nu_{0i} f_{s_i} T e^{-\frac{1}{2} u_i^2(\zeta)}} \quad (5.39)$$

$$= 1 - e^{(-T \sum_{i=1}^p \nu_{0i} f_{s_i} T e^{-\frac{1}{2} u_i^2(\zeta)})} \quad (5.40)$$

using the Poisson upcrossing description. For second order responses the transformation $u(\zeta)$ is given by Eq. (5.30), whereas for the linear response no transformation is needed. f_{s_i} is the fraction of the time in a given sea state T_i out of the total period T . Further, p is the number of stationary combinations of the parameters.

- Significant wave height H_s .
- Zero upcrossing period T_z .
- Forward speed U .
- Heading angle β .

ν_{0i} is the zero upcrossing rate in the combination number i out of the total number p . Each of the combinations above is experienced by the ship in a certain fraction of time f_{s_i} given by

$$f_{s_i} = f_s \Delta H_s \Delta T_z \Delta U \Delta \beta \quad (5.41)$$

where

$$f_S(H_s, T_z, U, \beta) = f_M(H_s, T_z) f_U(U|H_s) f_\beta(\beta|H_s) \quad (5.42)$$

and ΔH_s , ΔT_z , ΔU and $\Delta \beta$ are the discretization of H_s , T_z , U and β . The fraction f_M of time spent in the different combinations of H_s and T_z is determined by the operational profile given by a number of scatter diagrams and the corresponding time distribution. Based on the selected scatter diagrams, a normalised scatter diagram is determined as

$$f_M(H_s, T_z) = \sum_{j=1}^n P_j f_{Mj}(H_s, T_z) \quad (5.43)$$

where n is the number of scatter diagrams, P_j is the fraction of time in diagram j and f_{Mj} is the distribution of short-term sea states given by the j th scatter diagram.

The speed distribution f_U can also be interpreted as a speed reduction because it takes into account deviations from the design speed. The speed reduction can be divided into two terms a voluntary and an involuntary speed reduction.

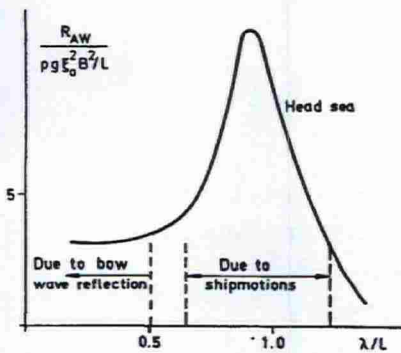


Figure 5.2: The added resistance in waves as a function of the wave length [41].

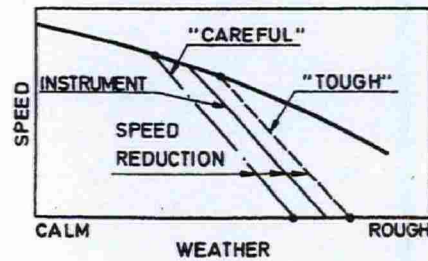


Figure 5.3: Example of speed reductions as a function of the weather roughness [30].

The involuntary speed reduction can be seen in Figure 5.2 as the increased resistance due to the waves and the ship motions. The upper curve in Figure 5.3 indicates how the ship speed slowly decreases as the weather roughness increases. This curve indicates the speed given a constant thrust. However, a lot of ships have a power reserve to account for this kind of situation, which might eliminate the involuntary speed reduction. The voluntary speed reduction is indicated in Figure 5.3 as the linear, decreasing lines. This applies to situations where the master of the ship estimates the sea state to be too rough on the ship and eases it

by reducing the speed. As shown in Figure 5.3 the decision when to reduce speed is highly dependent on the experience of the master of the ship. This experience is modelled by a number of threshold values for the significant wave height, which make it possible to define a number of ranges where different speeds are applied.

The heading distribution f_β is given in a similar manner with a set of probabilities as in Eq. (5.44) for each range of the significant wave height:

$$f_\beta(\beta) = \{p_{\beta=\beta_1}, p_{\beta=\beta_2}, \dots, p_{\beta=\beta_n}\} \quad (5.44)$$

This page is intentionally left blank.

Chapter 6

Verification and Validation of the Code

This chapter is dedicated to verification and validation of the code. Emphasis is put on the verification against results from other codes, but also validation against model tests is made.

A very precise verification, which would require an exact match of the results, could have been made with a program using the same theory and the same algorithms. However, such results are not always available and even if the type of strip theory was the same, the method for determining added mass and damping could be different. Besides, differences in the modelling of the ship, in terms of geometry and weights, could lead to minor deviations. Parts of the verification are made with results from ordinary strip method (OSM) and new strip method (NSM), which are variants of the present methods. The reason is that they seem more widely used and are therefore found more frequently in articles. The results from the three analysed ships are, however, the best available. A comparison with a sample of results from an in-house software at Registro Italiano Navale has also been made. This program is denoted SGN80 and is based on the theory by Salvesen, Tuck and Faltinsen. Finally, results from a commercial program denoted SHIPMO has been used for comparison. This program is also based on the theory by Salvesen, Tuck and Faltinsen.

The linear strip theory program (LIST) is based on the theory by Salvesen, Tuck and Faltinsen (STF). Both STF and Gerritsma and Beukelman (GB) are options for the quadratic strip theory (SOST). The non-linear time-domain strip theory, also based on GB, is denoted NLST.

The two methods for determination of added mass and damping using the simple Green function have not been found sufficiently robust for general use. The reason is that the present method for discretization of the additional boundaries is not sufficiently general to handle the entire frequency range used for the analyses. Two methods for the determination of added mass and damping are used in this section. The Lewis transformation, denoted LT

and the Frank Close Fit method, denoted FCF. All results of motions refer to the centre of gravity and phases refer to a wave crest at the centre of gravity.

Emphasis is put on the response amplitude operators because they are often available for comparison and, furthermore, the following short- and long-term calculations are theoretically more straightforward. As regards the quadratic strip theory only the linear part of the transfer function is verified. The second order contribution is included in the long-term calculation.

6.1 Analysis of a Container Ship

A relevant ship type for non-linear analyses is a container ship, due to the bow flare. A good test example is the container ship S-175, which has been subject to several model tests and computer studies. The ship has a block coefficient of 0.572, a bulbous bow, and a relatively high design speed of 22 knots corresponding to a Froude number of 0.275. Its principal particulars are given in Table 6.1

Principal Particulars			
Length between perpendiculars	L_{pp}	m	175.0
Breadth	B	m	25.4
Side height	H	m	15.4
Design draught	T	m	9.5
Trim ($T_{aft} - T_{fore}$)		m	0.03
Displacement	Δ	t	24856.6
Block coefficient	C_B		0.59
Longitudinal centre of buoyancy	LCB/L_{pp}	%	-1.42
Transverse metacentric height	GM_T	m	1.0
Vertical centre of gravity (from baseline)	z_g	m	9.5
Longitudinal radius of gyration	r_y/L_{pp}		0.251
Roll period	T_r	sec	18.0

Table 6.1: Principal particulars for the container ship S-175.

The results used for verification are based on the work by the ITTC78 Committee [17] on the comparison of results obtained by computer programs to predict ship motions. Twenty-two organisations submitted results from their computations and model tests were carried out. None of the organisations used the same program. The main part of the analyses was performed by use of the ordinary strip method (OSM) and two analyses were made on the basis of the theory of Salvesen, Tuck and Faltinsen. The results are presented as a lower

and upper quartile of the results from all the participants and thus also give a measure of the spreading of the results. The reason for this spreading can be divided into two. First the comparison involves results from different methods. Secondly the code from different institutions does not give identical results, even though the same theory has been applied. This might be due to differences in modelling or use of different algorithms.

6.1.1 Geometry

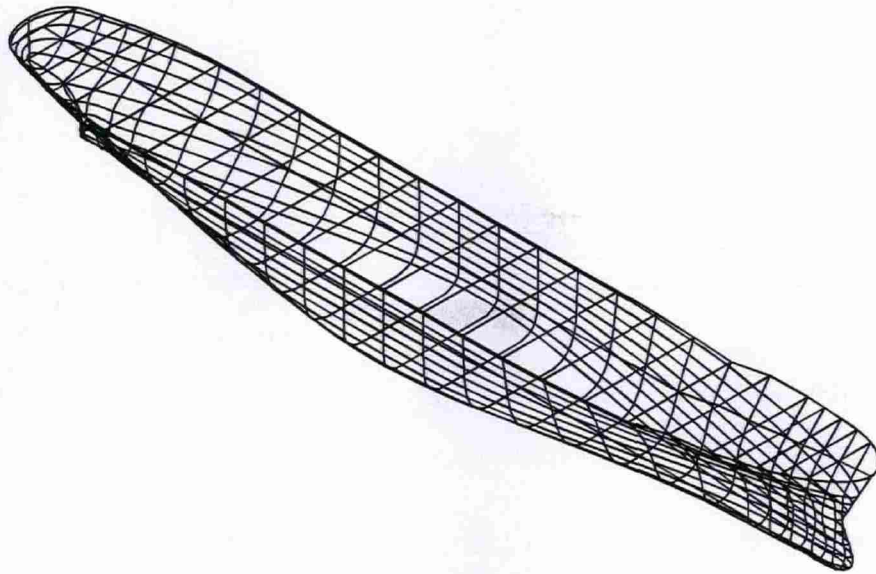


Figure 6.1: Geometrical description of the container ship S-175.

The geometry of the ship is described by 25 station curves with an increased density in the aft and fore part of the ship. The geometry is shown in Figure 6.1.

6.1.2 Weight Condition

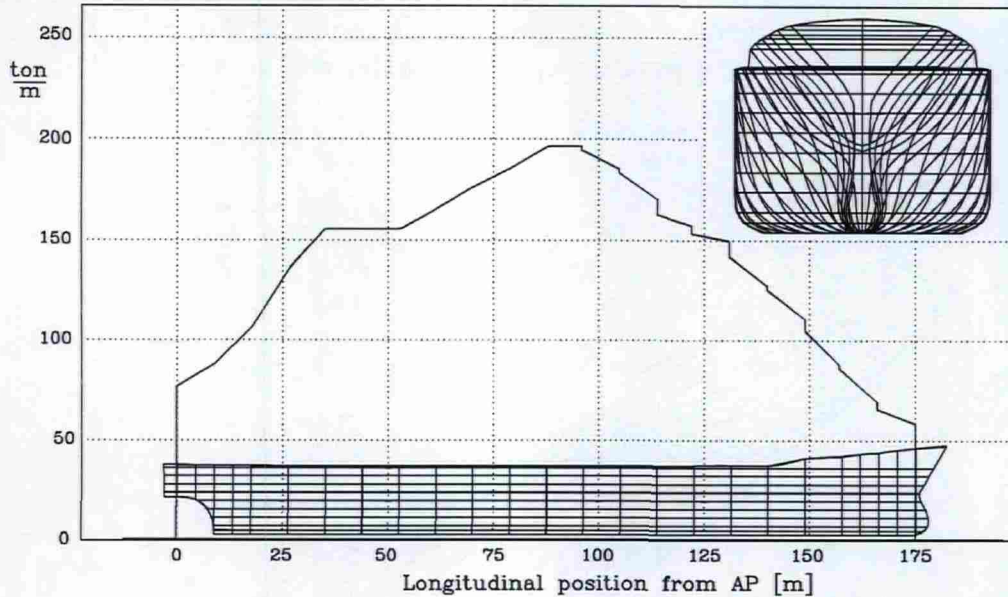


Figure 6.2: Weight distribution and body plan for the container ship S-175.

The weight condition shown in Figure 6.2 has been determined on the basis of the displacement, trim and longitudinal radius of gyration. No data has been found on the vertical distribution. Therefore, all the sectional weights have the centre of gravity at the same vertical level.

6.1.3 Motions

The motions in the vertical plane have been analysed for the S-175. Both transfer and phase functions are compared. In Figure 6.3 the response amplitude operator and the phase function for the heave motion of the ship S-175 in head waves are shown. The results from three of the present results are in between the quartiles. The results from SOST can be divided into analyses using STF strip theory and analyses based on GB strip theory. The response calculated using SOST, STF is generally larger than the SOST, GB. The heave response amplitude determined by SOST, STF is above the upper quartiles. The reason for the difference between LIST, STF and SOST, STF is that the use of the diffraction potential in the former has been replaced by the relative motion concept in the latter, however, still including the speed-dependent terms similar to STF.

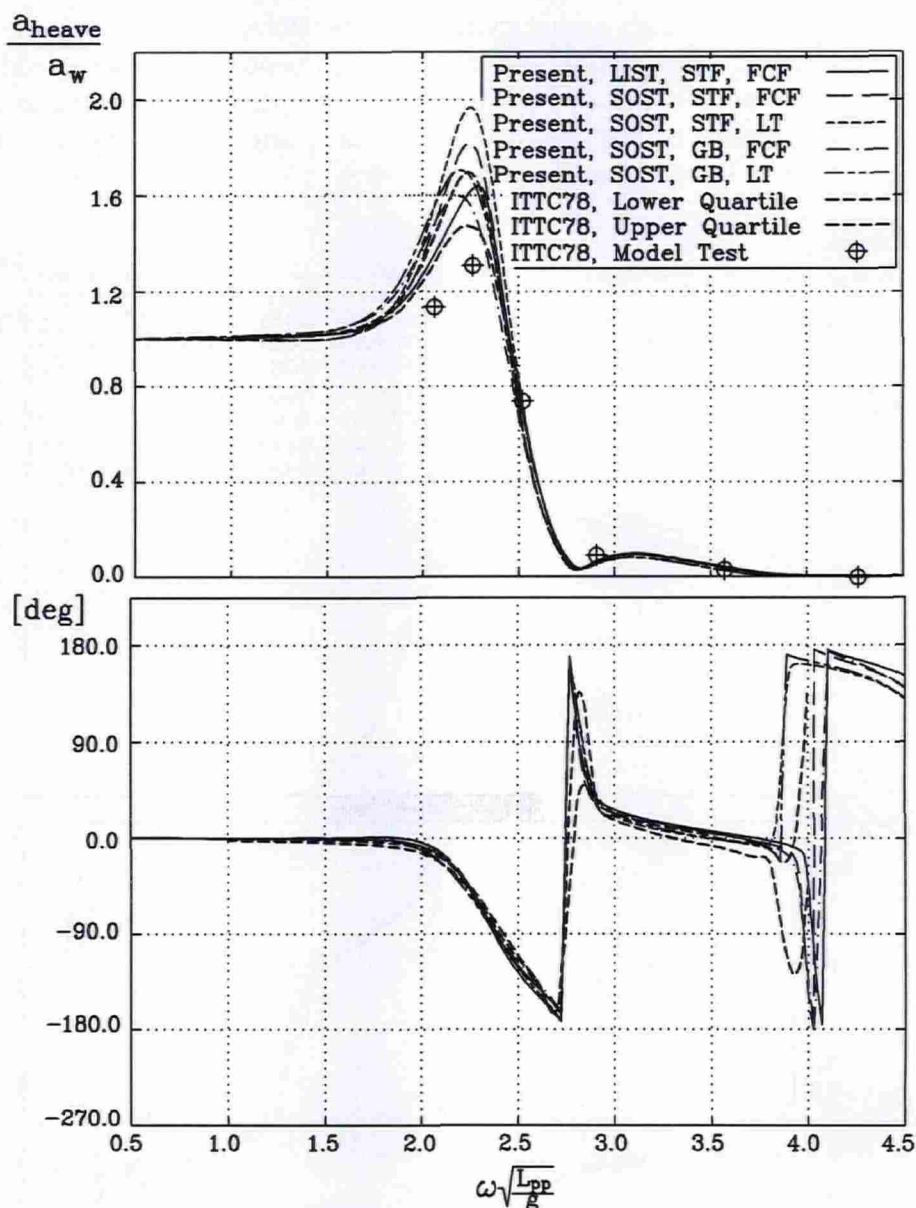


Figure 6.3: Comparison of the heave response amplitude operator and phase function for S-175 in head sea at a speed of 22 knots.

The present methods give the same results for zero forward speed. An example of this is given in Appendix A. It is indicated that the speed dependent terms are the source to the difference.

The phases are defined in relation to a wave crest in the centre of gravity and correspond well with the predictions except in the high-frequency region. At the frequencies where the folding to the range ± 180 degrees takes place, there are some deviations. However, the

response is very small in the high frequency region. Therefore, the deviation does not have any impact on the results for practical purposes. The present results correspond well with the results from the model test outside the frequency range, where the dynamic amplification occurs. In the range where the response is amplified the computed results overestimate the heave response compared to the model test.

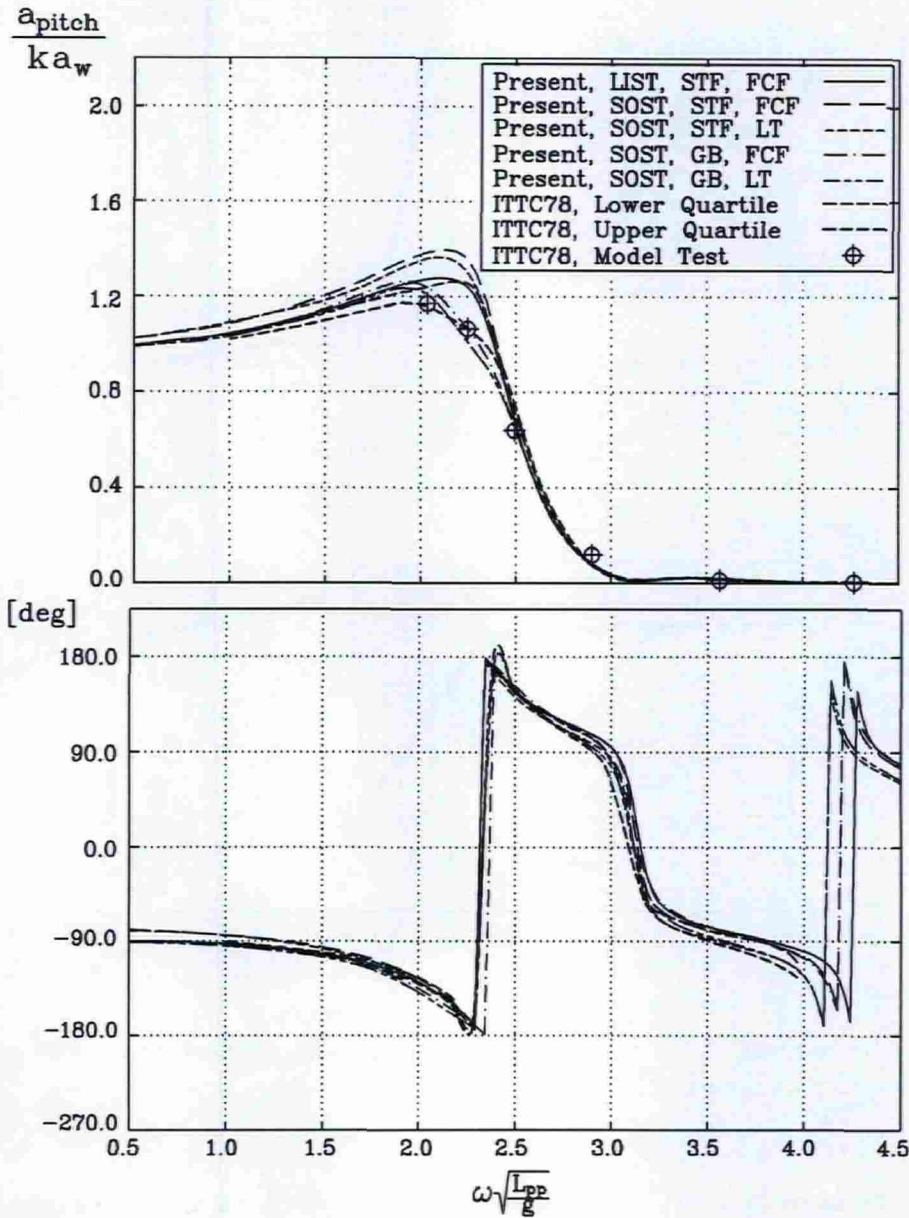


Figure 6.4: Comparison of the pitch response amplitude operator and phase function for S-175 in head sea at a speed of 22 knots.

In Figure 6.4 the pitch response amplitude operator and the phase function are shown. The

response amplitude operator corresponds well with the quartiles, however, as for the heave response, the two SOST, STF calculations overpredict to some extent. The LIST, STF follows the upper quartile, while the two SOST, GB calculations follow the lower quartile. The difference between the two SOST, GB calculations is the method used to determine added mass and damping. The results show no or very small sensitivity to this. The model test follows the lower quartile quite well and a very good prediction can be observed with the SOST, GB, FCF and the SOST, GB, LT.

As in the case of the heave phases, also the pitch phases show good agreement with the quartiles. The high-frequency part folds at different frequencies, which makes the deviation seem larger. However, as for the heave motion the response is insignificant in this range.

6.1.4 Loads

The loads on the hull were subsequently compared by an ITTC Committee, ITTC81 [18]. The comparison is presented in terms of plots of the results from all the participants. To go into detail about all this data would require a large description, which has been avoided. Instead the results are included for the purpose of showing an example of the spreading which may occur in computed results of this type. The results from the participants are shown with different symbols. The large circles are results from model tests and finally the present results are shown by curves.

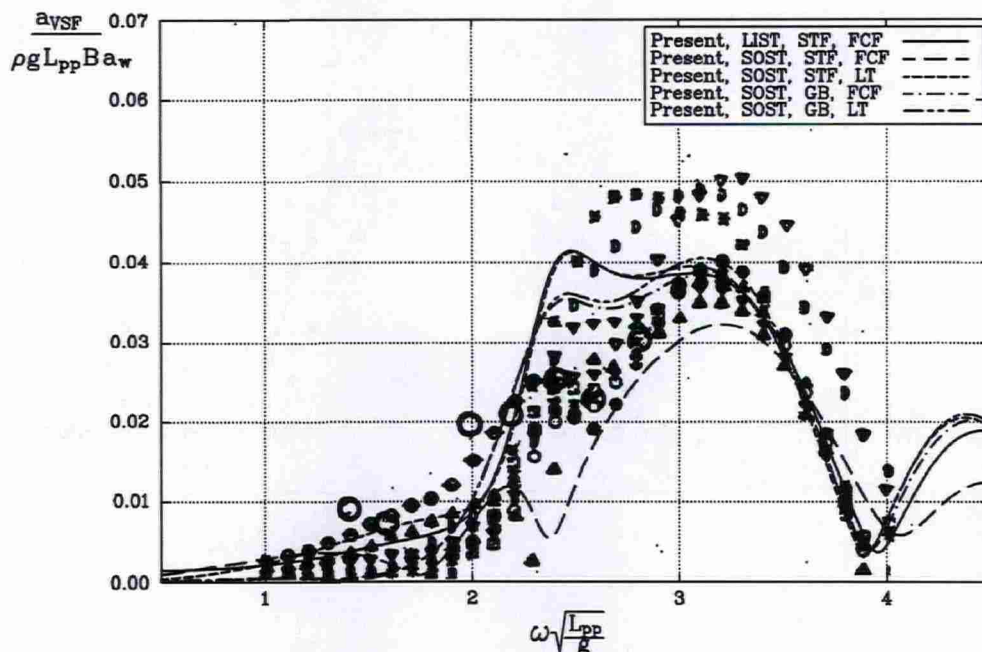


Figure 6.5: Comparison of the response amplitude operators for the midship vertical shear force for S-175 in head sea at a speed of 22 knots.

In Figure 6.5 the response amplitude operator for the vertical shear force amidship is shown. Generally, the present results are within the relatively large scatter of the results. The present results can be divided into three groups. The SOST, STF, LT corresponds well with the LIST, STF, FCF, despite differences in the motions, and form the upper level of the predictions. The SOST, GB, LT and the SOST, GB, STF again show a very small difference due to the method of added mass and damping. Finally, the SOST, STF, FCF give a rather poor prediction compared to the remaining methods.

In Figure 6.6 the response amplitude operator for the midship vertical bending moment is shown. The results from the ITTC participants are distributed into two groups. The LIST, STF, FCF and the SOST, STF, LT correspond well with the upper level, while the SOST, GB, LT and SOST, GB, FCF correspond well with the lower level. The SOST, STF, FCF again deviate both in level and in tendency from the remaining results.

The results from the model tests show roughly the same tendency as the calculations. The scatter of the calculated responses is also found in the results from the model tests. However, not to the same extent. The model tests show responses in the upper part of the scatter of the calculated results. The results are therefore generally found to be acceptable both with respect to comparisons with other programs and with respect to comparisons with model tests.

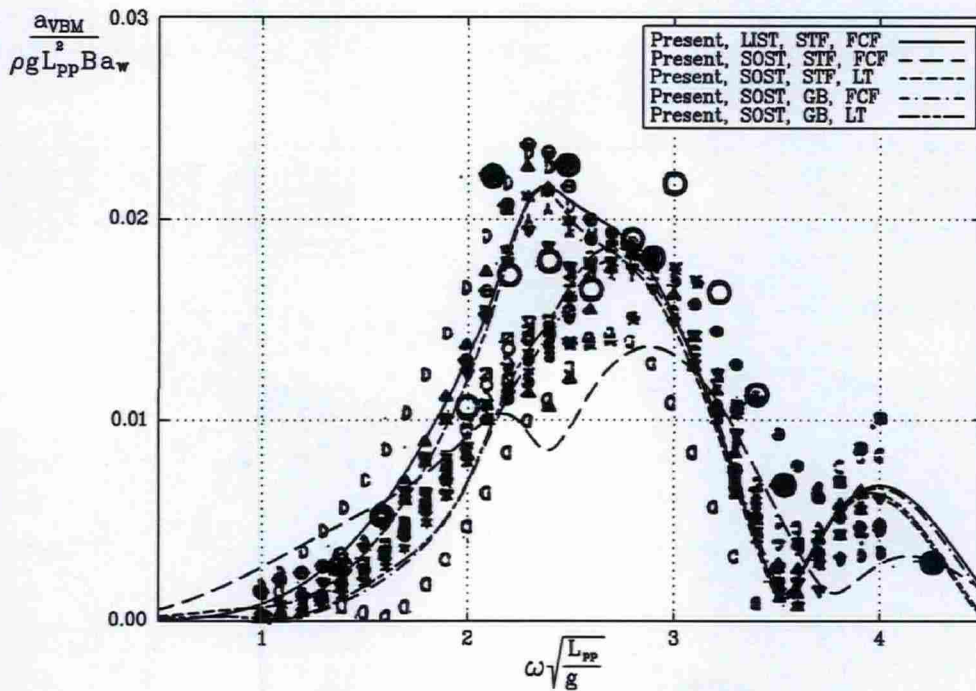


Figure 6.6: Comparison of the response amplitude operators for the midship vertical bending moment for S-175 in head sea at a speed of 22 knots.

6.1.5 Long-Term Predictions

A long-term calculation has been performed on the basis of a 20 year period. The frequency response functions are calculated for various headings, in increments of 45 degrees from following sea (0 degrees) to head sea (180 degrees). Two speeds have been used: the design speed and a reduced speed. Normally, a long-term prediction involves all the weight conditions the ship will experience. However, in this example only the weight condition corresponding to full load has been used. The heading distribution is shown in Table 6.2. It is

Heading	0	45	90	135	180
$0m \leq H_s \leq 4m$	0.071	0.143	0.143	0.429	0.214
$4m \leq H_s \leq 15m$	0.071	0.143	0.143	0.429	0.214

Table 6.2: Heading distribution of time in the sea states.

similar to what has been used by Jensen and Dogliani, [23]. The speed distribution is given in Table 6.3. The design speed is used in sea states with a significant wave height less than 4m, and a reduced speed of 8 knots is used in the severer sea states. The applied range of the

Speed	22 knots	8 knots
$0m \leq H_s \leq 4m$	1.0	0.0
$4m \leq H_s \leq 15m$	0.0	1.0

Table 6.3: Speed distribution of time in the sea states.

frequencies of encounter is 0.01 rad/s to 4.0 rad/s and 50 frequencies have been distributed equidistant in the range. The fraction of time the ship is in the different Marsden areas is shown in Table 6.4. The numbers in the scatter diagrams refer to Hogben et al. [14].

Marsden area	10	11	15	16	23	25	33	35	48
Fraction of time	0.083	0.083	0.083	0.083	0.083	0.250	0.083	0.083	0.167

Table 6.4: Distribution of time in the Marsden areas.

The result of the long-term calculation is shown in Figure 6.7 in terms of probability of exceedance curves for the response.

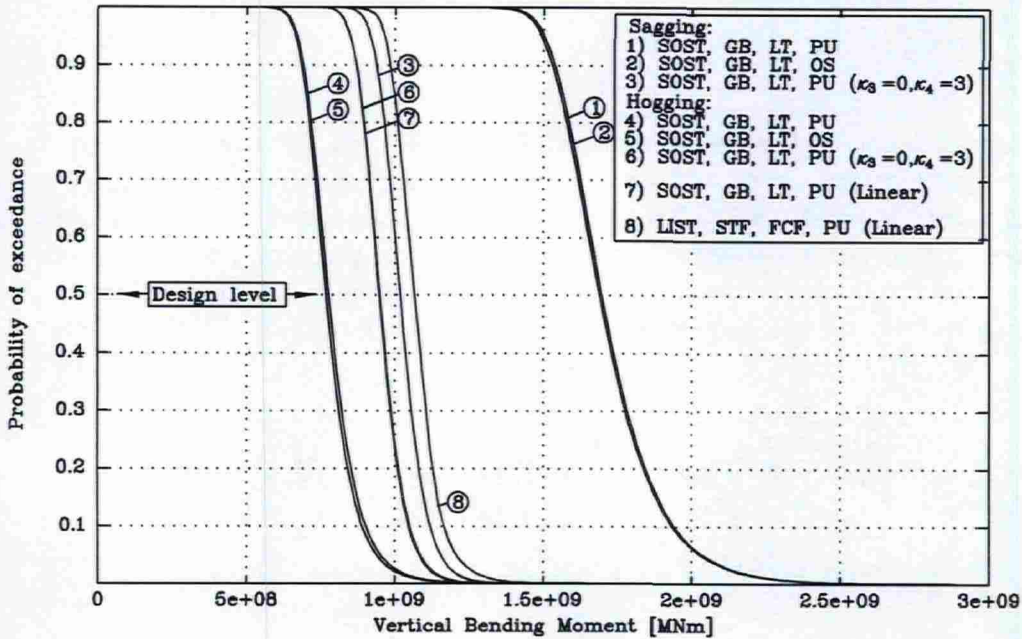


Figure 6.7: Comparison of present long-term predictions. The results are the vertical bending moments (PU: Poisson upcrossing. OS: Order statistics).

For Poisson upcrossing and order statistics the return period of a given response will correspond to the duration in question roughly at an exceedance level equal to 0.5. This level of the vertical bending moment with a return period of 20 years is indicated by *design level*. The calculations with SOST are made using GB, LT. It is seen that the Poisson upcrossing and order statistics give almost identical results both for hogging and sagging. The second order response with the skewness set to 0 and the kurtosis set to 3 indicated by 3) and 6) has thus been made Gaussian, leading to a reduced sagging bending moment and an increased hogging bending moment. This is mainly because the skewness is reduced to zero, which causes probability to move from the tail in the sagging part to the tail in the hogging part to become Gaussian distributed.

The linear part of the second order response is identical to the hogging bending moment with $\kappa_3 = 0$ and $\kappa_4 = 3$. The reason that the linear part is not larger than the above-mentioned hogging bending moment is that the now Gaussian distributed response has a nonzero mean value.

The results from the LIST show a higher level than SOST, GB, LT, PU. Generally, the vertical bending moment is larger when it is determined using the theory of LIST, STF, FCF than with the SOST, GB, LT. Therefore, also a larger response level for the long-term prediction can be expected.

The long-term calculation is compared with results determined according to the International Association of Classification Societies, IACS requirement S11, [40], which include a

	Unit	Hogging	Sagging
IACS [40]	MNm	814	1237
SOST, GB, LT. PU.	MNm	775	1642
SOST, GB, LT. OS.	MNm	756	1660
SOST, GB, LT. PU. ($\kappa_3 = 0, \kappa_4 = 3$)	MNm	948	1013
SOST, GB, LT. Linear	MNm	940	940
LIST, STF, FCF. OS.	MNm	1080	1080

Table 6.5: Comparison of design midship vertical bending moments.

unified requirement for longitudinal strength. The comparison is shown in Table 6.5. The hogging bending moment from the SOST corresponds well with the hogging bending moment determined according to the IACS rules. However, the sagging bending moment deviates by 30 % , which is also of the order found in Jensen and Dogliani, [23]. Part of the reason for this could be that the second order theory is suited for determination of the response in low to mediate sea states. In the severer sea states the immersion dependence, in terms of the vertical slope of the hull in the waterline, is extrapolated below the keel and above the deck. This is the case for the linear methods as well. However, for the second order strip theory the extrapolation is not vertical but corresponds to the vertical slope, which makes the difference between the modelled and the real ship larger.

Since the linear vertical bending moment has been shown to deviate to some extent from the model tests, also a deviation from the IACS rules could be expected. Further, the long-term predictions given above are based on an operational profile, which does not necessarily correspond to reality and neither to the operational profile, the design values from IACS are based on, which could be a reason for the deviation. Long crested seas have been used also. If short crested seas, which applies a certain spreading to the sea from a certain direction, were used, a probable reduction of the response would have been the result.

With respect to the deviation from the IACS rules, good correspondence cannot necessarily be expected as the rules are empirical. The aim of this work has been to make a tool which could be used to investigate reasons for differences, but not necessarily determine them. The subject has therefore not been pursued further.

6.1.6 Results from the Non-linear Time-domain Strip Theory

The non-linear time-domain strip theory has been used to analyse the response of the container ship S-175 in head sea. To present the results in a form comparable to the linear results, the minimum and the maximum of the time-domain response in regular seas has

been determined, from which an average amplitude has been determined as

$$a = \frac{resp_{max} + resp_{min}}{2} \quad (6.1)$$

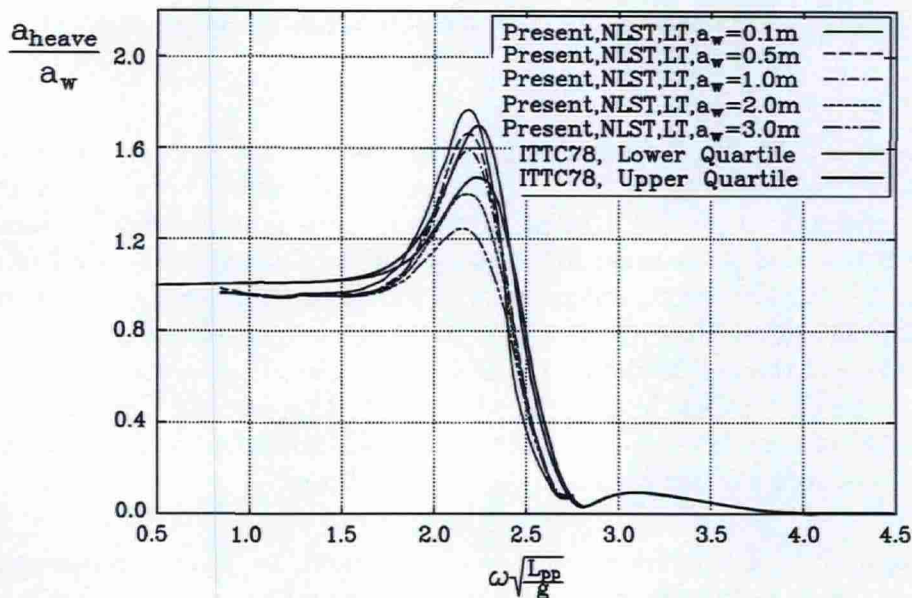


Figure 6.8: Heave response amplitude operators determined by the non-linear time-domain strip theory. The heading corresponds to head sea and the speed is 22 knots.

In Figure 6.8 the response amplitude operators for heave are shown on the basis of different wave amplitudes with the quartiles as in Figures 6.3 and 6.4. For decreasing wave amplitudes the response amplitude operators should converge towards the result from a linear analysis. The heave response amplitude operators based on the small wave amplitude ($a_w = 0.1$) are slightly shifted in comparison with the results from the ITTC81 Committee. Also the peak exceeds the upper quartile. For increasing wave amplitudes the response amplitude operator decreases due to non-linearities.

The response amplitude operators for pitch are shown in Figure 6.9, also with the above-mentioned quartiles. The magnitude of the response for the small wave amplitudes corresponds well with the quartiles provided the shift in frequency is neglected. The reason for this shift has been sought but no explanation has been found.

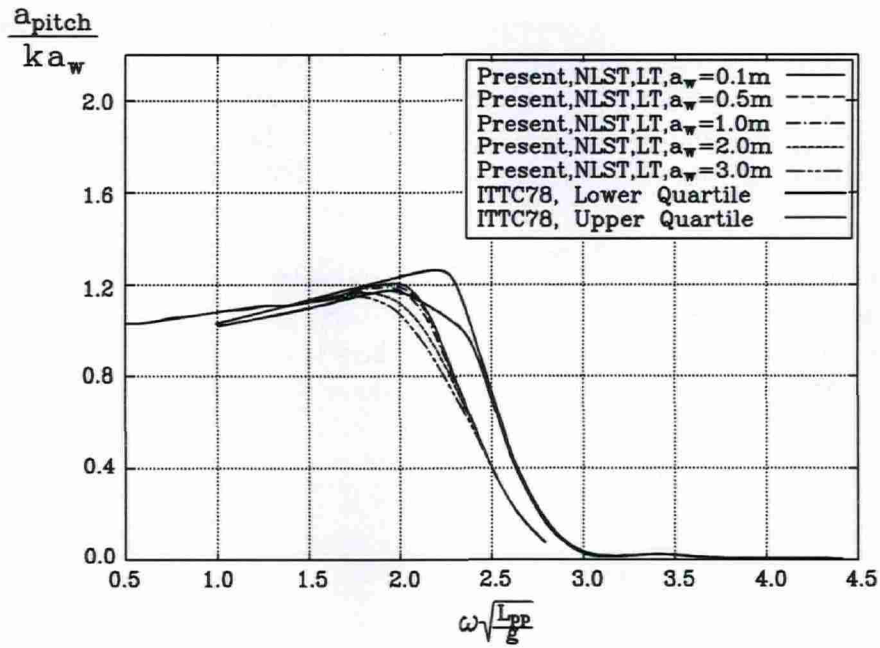


Figure 6.9: Pitch response amplitude operators determined by the non-linear time-domain strip theory. The heading corresponds to head sea and the speed is 22 knots.

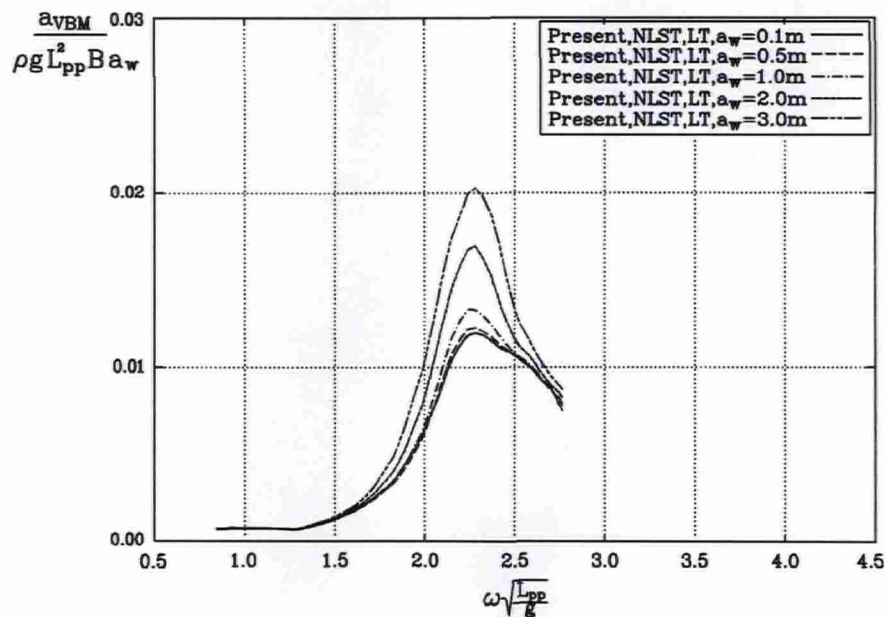


Figure 6.10: Response amplitude operators for the vertical bending moment amidship determined by the non-linear time-domain strip theory. The heading corresponds to head sea and the speed is 22 knots.

In Figure 6.10 the response amplitude operators for the vertical bending moment amidship are shown. A larger dependence on the wave amplitude is found reflecting larger nonlinearities. Compared to the corresponding linear frequency domain results in Figure 6.6, the magnitude of the response is generally too low for the small amplitude ($a_w = 0.1$) response amplitude operator. The reason for this low level could be the deviating pitch response.

The results from the implemented time-domain strip theory are generally not found satisfactory for practical use. The heave motion for small wave amplitudes shows good agreement slightly above the upper quartiles from ITTC81. The pitch motion in small wave amplitudes shows a poor agreement and, finally, the magnitude of the vertical bending moment is too low.

6.2 Analysis of a VLCC

The tanker used for validation is a Very Large Crude Carrier (VLCC). The validation has been made by comparing the present results with results obtained by use of NSM and results from model tests, both from Tanizawa et al. [57]. Moreover, a comparison with results from SGN80 and a commercial program denoted SHIPMO has been made, both based on the theory by Salvesen, Tuck and Faltinsen.

The weight distribution is different for the analyses made with SGN80, however, the longitudinal centre of gravity and the radius of gyration are the same. Therefore, only motions have been compared with this program.

The data on the ship is given as dimensions of a model. This has been converted to a full scale ship with a displacement of 264,000 t. However, as all results have been made non-dimensional the actual dimensions have no effect on the calculations.

The principal particulars are given in Table 6.6.

Principal particulars			Ship	Model
Length between perpendiculars	L_{pp}	m	306.0	4.500
Beam	B	m	53.9	0.793
Depth	H	m	30.9	0.430
Design draught	T	m	19.3	0.285
Trim ($T_{aft} - T_{fore}$)		m	-0.48	0.0
Displacement	Δ	t	264.000	0.821
Longitudinal centre of buoyancy	LCB/L_{pp}	%	0.033	-
Vertical centre of gravity (from baseline)	z_g	m	15.3	0.225
Longitudinal metacentric height	GM_L	m	6.80	0.100
Longitudinal radius of gyration	r_y/L_{pp}		0.253	0.241
Transverse radius of gyration	r_x/B		0.33	-
Roll period	T_r	sec	15.35	1.861

Table 6.6: *Principal particulars for model and full-scale tanker. The scale ratio is 68.0.*

The vertical distribution of the weights has not been available, so a uniform distribution at the level of the given centre of gravity has been assumed. No transverse radius of gyration has been given. However, from the roll period the moment of inertia can be determined including the added mass. By subtracting the calculated added mass moment of inertia at the given frequency the radius of gyration for the dry model has been approximated.

6.2.1 Geometry

The geometry of the tanker is shown in Figure 6.11. The tanker has been subdivided into 22 station curves.

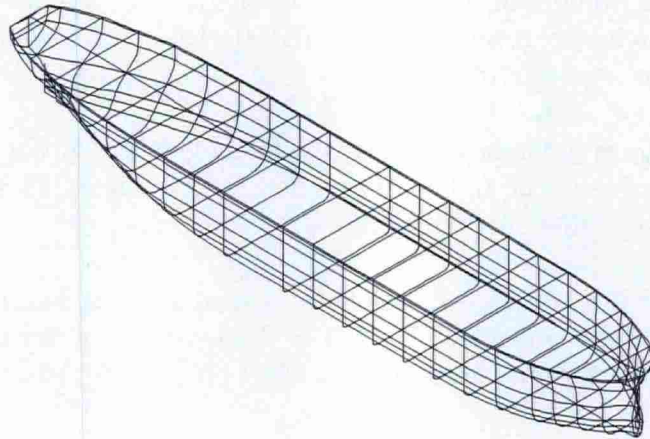


Figure 6.11: Geometrical description of the VLCC tanker.

6.2.2 Weight Condition

The weight condition given for the ship is shown in Figure 6.12.

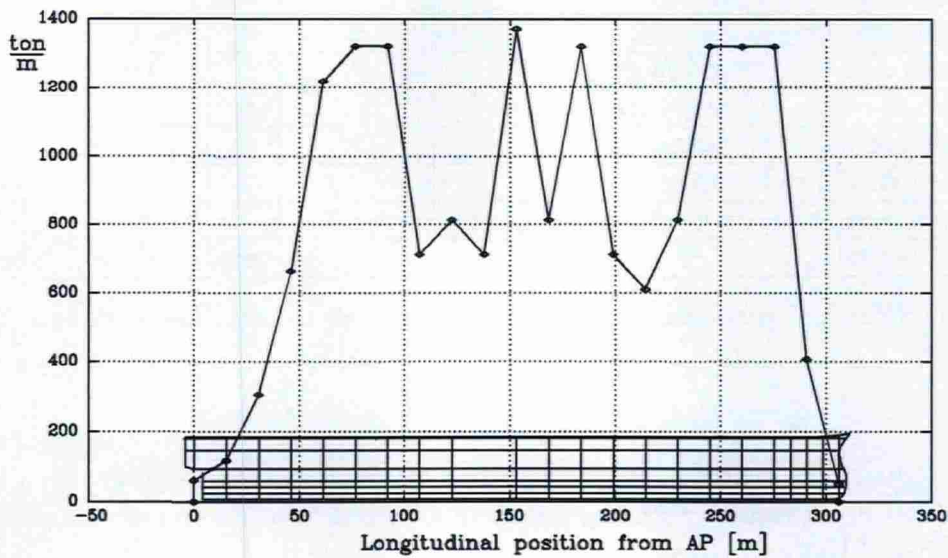


Figure 6.12: Analysed weight condition of the VLCC.

6.2.3 Motions

The motions have been compared for four headings at the design speed of 14.3 knots.

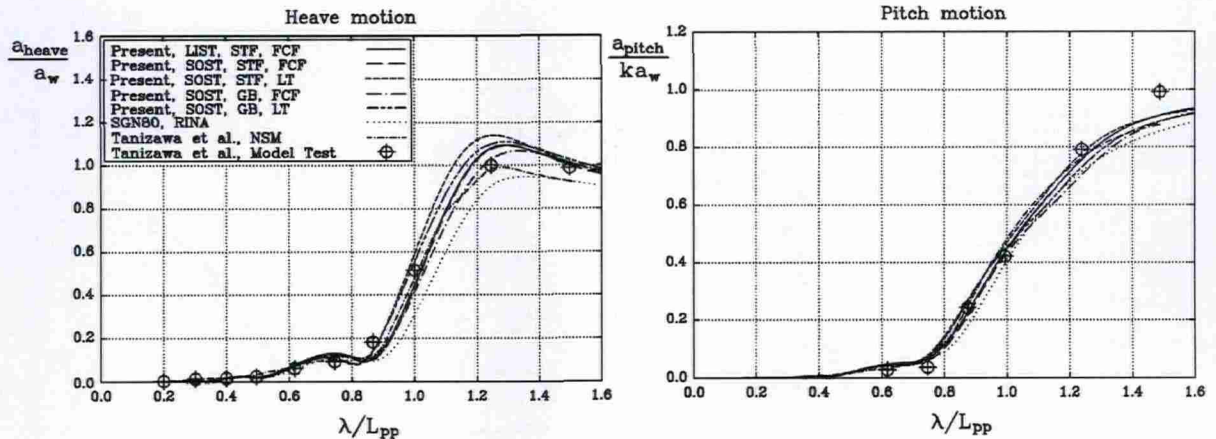


Figure 6.13: Comparison of the response amplitude operators for the heave and pitch motions of a VLCC in head sea at a speed of 14.3 knots.

In Figure 6.13 the response amplitude operators for heave and pitch in head sea are shown. The present results for heave show a relatively small scatter, however, deviate to some extent from the SGN80 and the NSM, which predict a lower heave response in the peak region. The results from the model test are in the region in between the two groups of curves. For the pitch response a very small scatter in the present results can be seen. The results correspond well with both the SGN80 and the NSM. The model tests are predicted well except in the long-wave range where the theories generally underpredict the response. Generally, a good agreement has been found.

In Figure 6.14 the response amplitude operators for the motions of the ship with a heading of 150 degrees are shown. The characteristics of the comparison for heave and pitch in head sea are also valid for this heading. The present results predict larger heave response than the NSM. However, the present results correspond well with the results from the model tests. For sway, roll and yaw only the LIST, STF, FCF has been compared to NSM and to the results from the model tests. Generally, the results from the LIST and the NSM are very close and correspond very well with the results from the model tests. An exception is the result from the model test in the long-wave region for sway, where the predicted response is half the response measured in the model test. The roll motions has been determined by use of an additional damping of 15 % of the critical damping in the full frequency range.

In Figure 6.15 the response amplitude operators for the motions of the ship with a heading of 90 degrees are shown. For heave, the present results agree well with the NSM, except for the LIST, STF, FCF, which overestimates largely in the peak region compared to the other calculations. However, the method corresponds better with the model test in this region.

The pitch motion is small and the calculations generally underestimate the response. For sway, roll and yaw the response is not predicted as well as for the vertical motions. The sway motion deviates in the long-wave region.

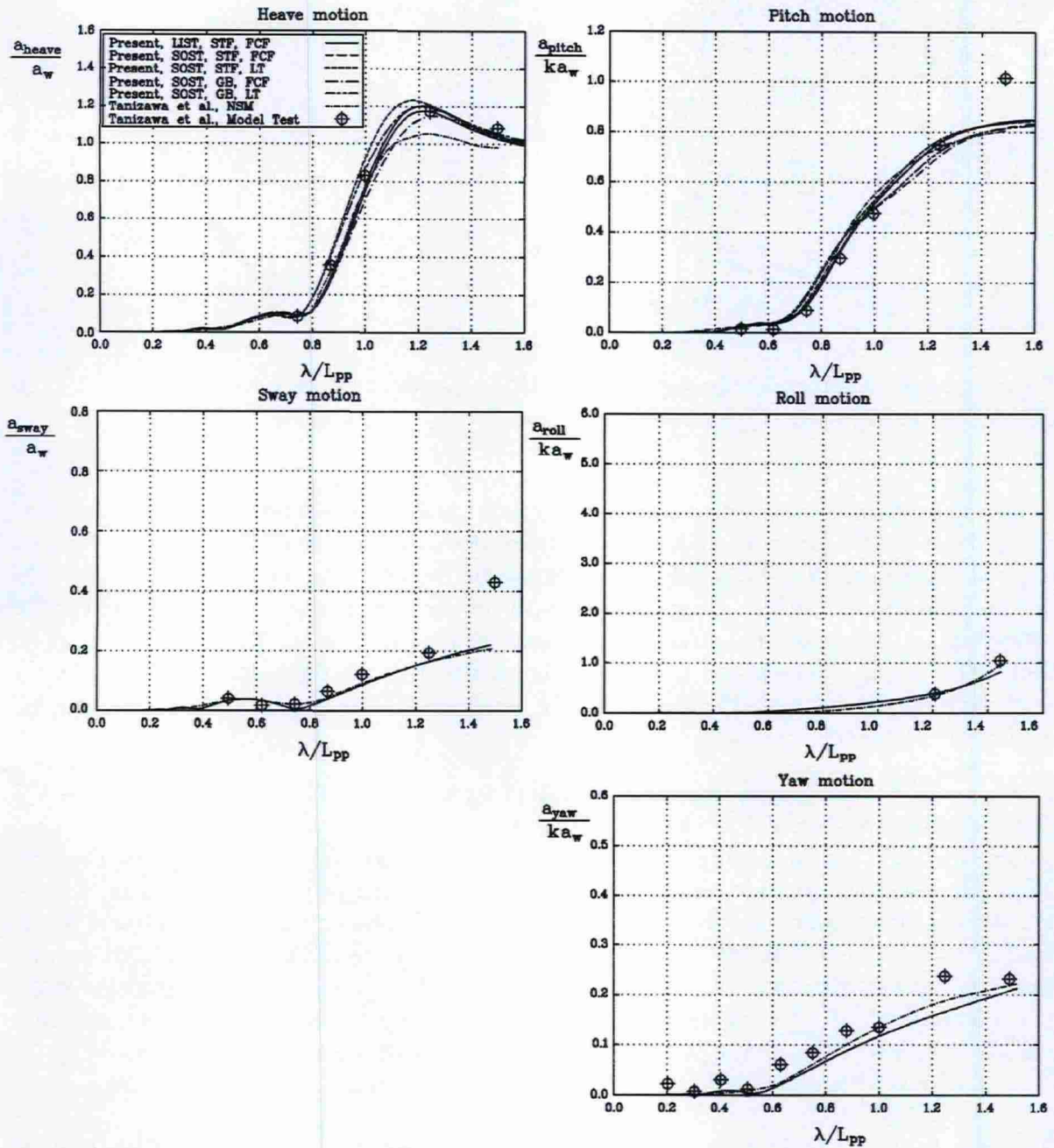


Figure 6.14: Comparison of the response amplitude operators for the heave, pitch, sway, roll and yaw motions of a VLCC. The heading is 150 degrees and the speed 14.3 knots.

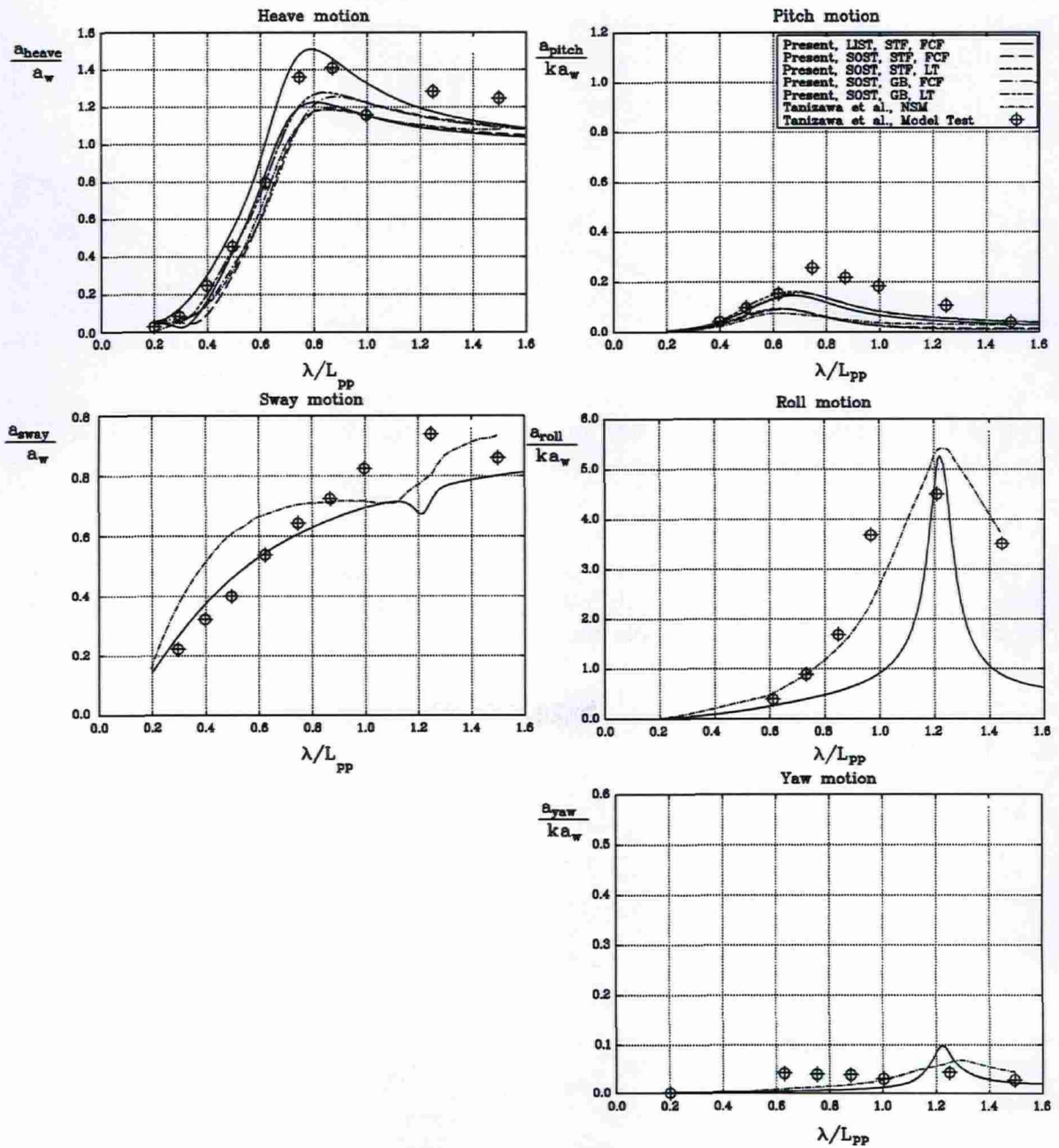


Figure 6.15: Comparison of the response amplitude operators for the heave, pitch, sway, roll and yaw motions of a VLCC. The heading is 90 degrees and the speed 14.3 knots.

A small peak can be seen due to the coupling to the roll motion, which peaks at the corresponding wave length. The roll motion follows the same tendency but the results from the LIST show a more pronounced peak than both those from the NSM and the model tests. To improve this prediction the additional damping could be changed to a more advanced method.

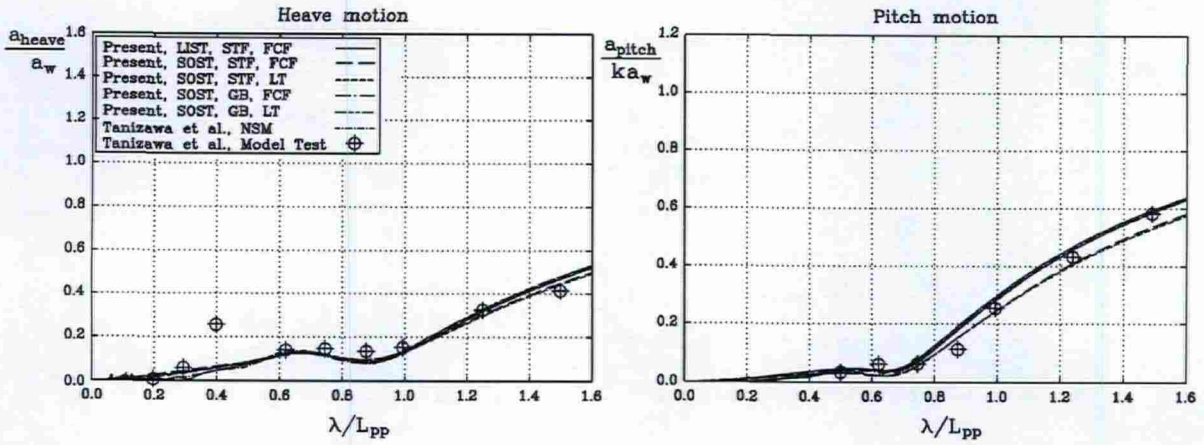


Figure 6.16: Comparison of the response amplitude operators for the heave and pitch motions of a VLCC in following sea at a speed of 14.3 knots.

In Figure 6.16 the response amplitude operators for heave and pitch in following sea are shown. With an exception of one result from the model test a very good agreement between the calculations and the model tests is found.

6.2.4 Loads

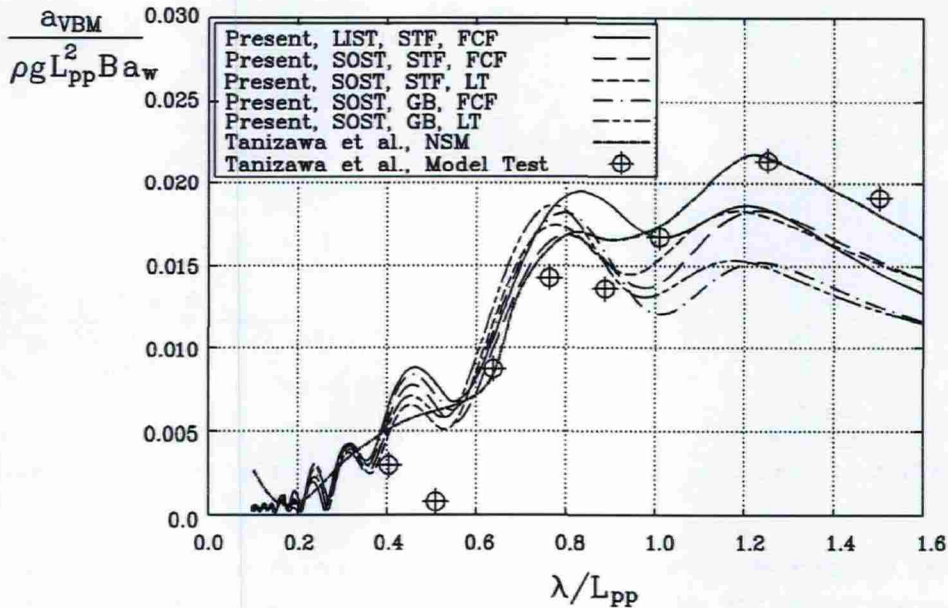


Figure 6.17: Comparison of the response amplitude operators for the midship vertical bending moment for a VLCC in head sea at a speed of 14.3 knots.

In Figure 6.17 the response amplitude operators for the vertical bending moment for the ship in head sea are shown. For the short-wave lengths the predicted response forms a relatively narrow band in good agreement with the model tests. For the long-wave range three levels are found. The NSM gives the largest predictions and corresponds well with the model tests. The three computations using STF underpredict the response. The two computations using GB predict the lowest response.

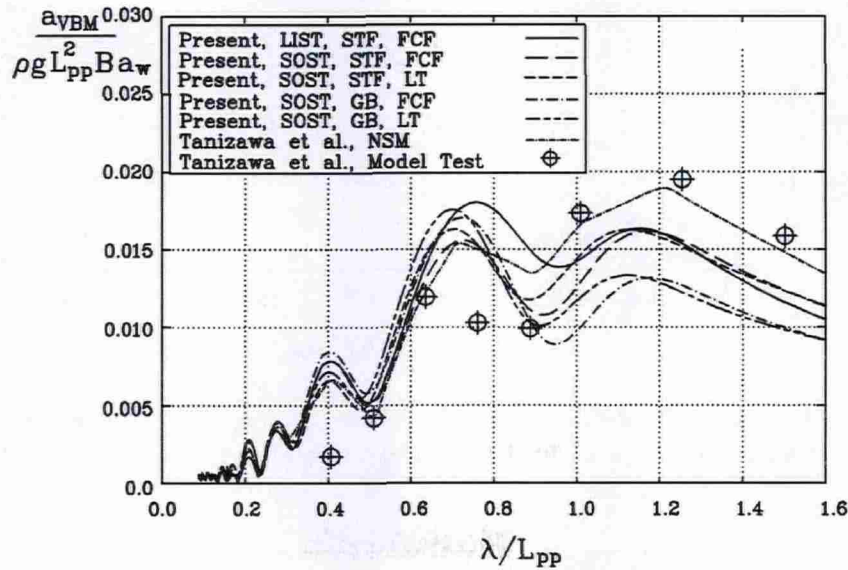


Figure 6.18: Comparison of the response amplitude operators for the midship vertical bending moment for a VLCC. The heading is 150 degrees and the speed is 14.3 knots.

In Figure 6.18 the response amplitude operators for the vertical bending moment for the ship with a heading of 150 degrees are shown. The same characteristics for the comparison for head sea are valid for the heading of 150 degrees. It is a general tendency that the response is overpredicted in an intermediate range of wave lengths and underpredicted in the long-wave range.

In Figure 6.19 the response amplitude operators for the horizontal bending moment for the ship with a heading of 150 degrees are shown. The NSM gives larger predictions than the LIST. The LIST corresponds well with the model test.

In Figure 6.20 the response amplitude operators for the horizontal bending moment for the ship in following sea are shown. The present results form a rather wide band. The LIST predicts a response slightly larger than the NSM and the two calculations with SOST, GB a slightly smaller one. The two calculations with SOST, STF predict an even smaller response. Further, it is found that for head sea the SOST, STF gives larger vertical bending moment than the SOST, GB, similarly to what has been found for the container ship. For following sea the opposite has been observed.

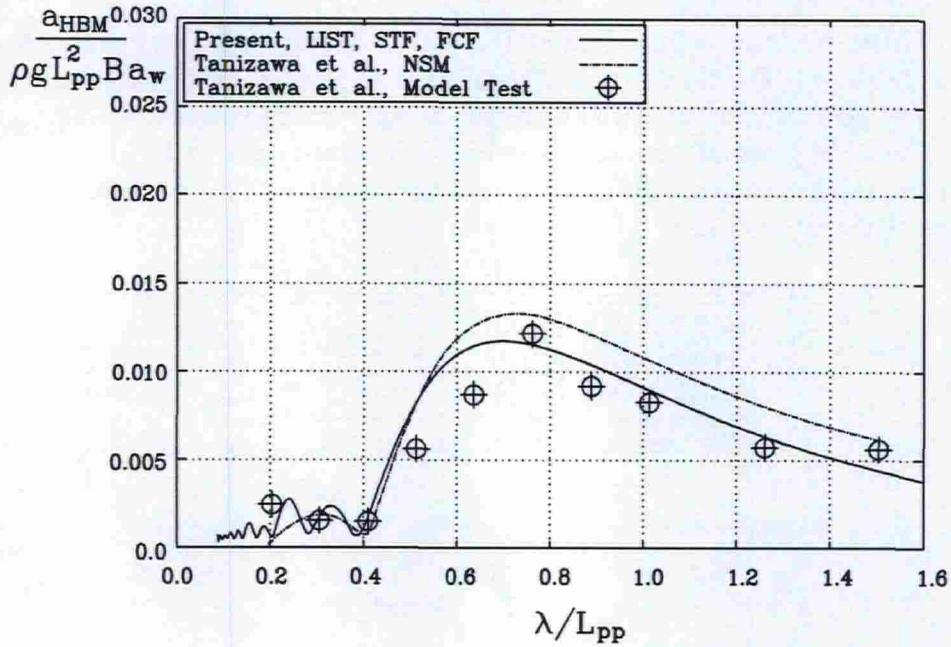


Figure 6.19: Comparison of the response amplitude operators for the midship horizontal bending moment for a VLCC. The heading is 150 degrees and the speed is 14.3 knots.

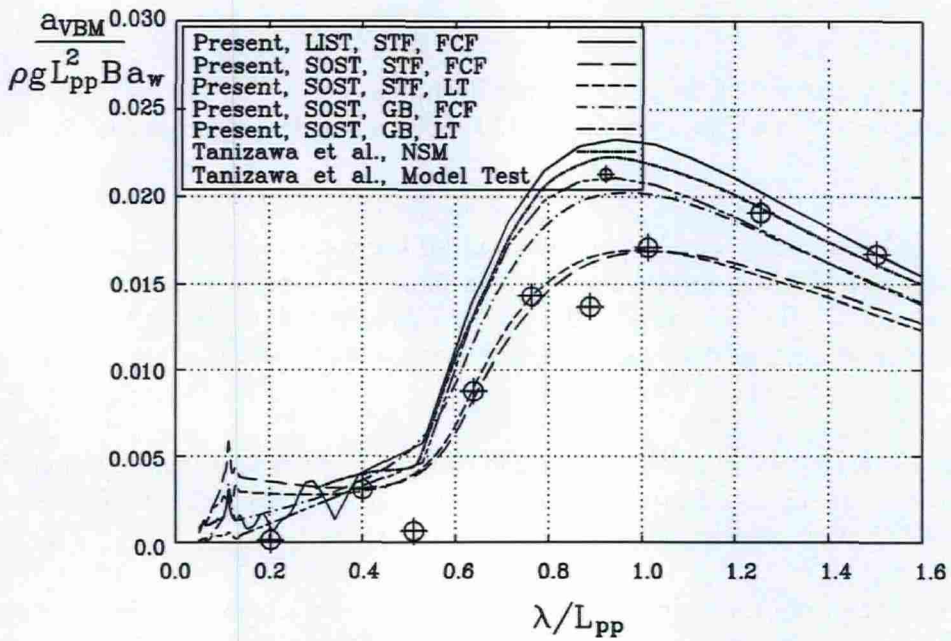


Figure 6.20: Comparison of the response amplitude operators for the midship vertical bending moment for a VLCC in following sea at a speed of 14.3 knots.

6.3 Analysis of a Fast Ferry

Analysis of a fast ferry using conventional low speed strip theory may seem to be a use of the program outside its capabilities. However, it has been shown by e.g. Blok and Beukelman [4] that this theory yields reasonable results even at very high Froude numbers. Therefore, the fast ferry has been included among the three ship types. A similar study where the results have been compared with full-scale measurements have been reported in Wang et al. [63].

The monohull fast ferry used for validation and verification has the approximate data as listed below. This ship has been selected because both results from other programs and a sample of short term statistical results from model tests has been available. The full-scale ferry has active fins to reduce the motions. This is not included in any of the calculations and the model tests used for comparison were carried out without fins.

The vessel has an approximate length of 100m. Beam of about 17m and a displacement about 1700t.

The dynamic sinkage and trim has been measured in the model tests and used in the analyses of motions and accelerations. For analyses determining loads, no dynamic sinkage and trim has been applied.

6.3.1 Weight Condition

The weight condition given for the ship is shown in Figure 6.21.

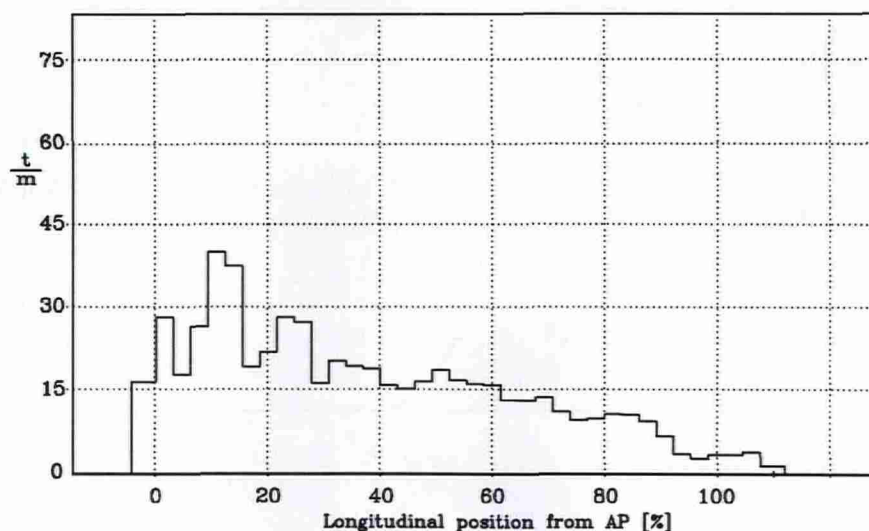


Figure 6.21: Weight distribution of the analysed fast ferry.

6.3.2 Motions

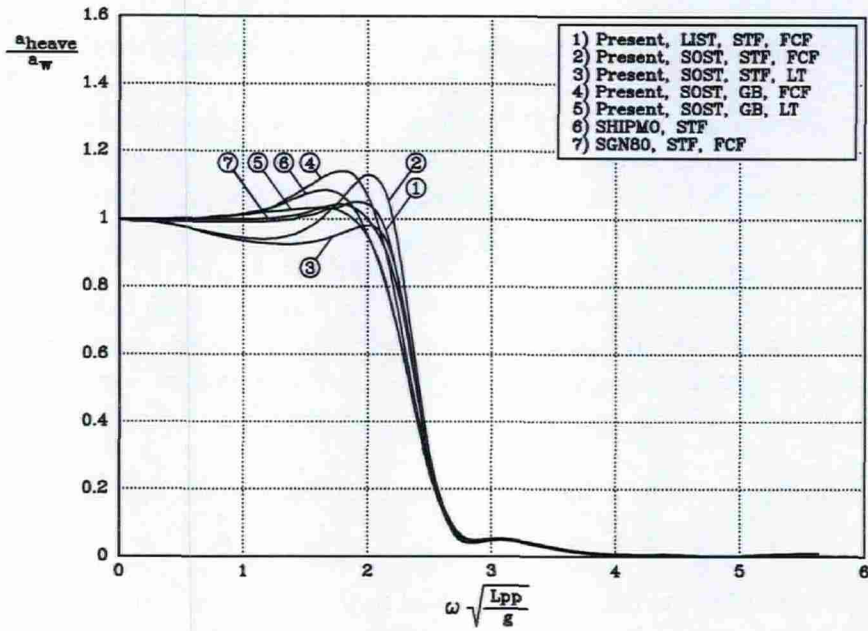


Figure 6.22: Comparison of the heave response amplitude operators for a fast ferry advancing in head sea at a speed of 35 knots.

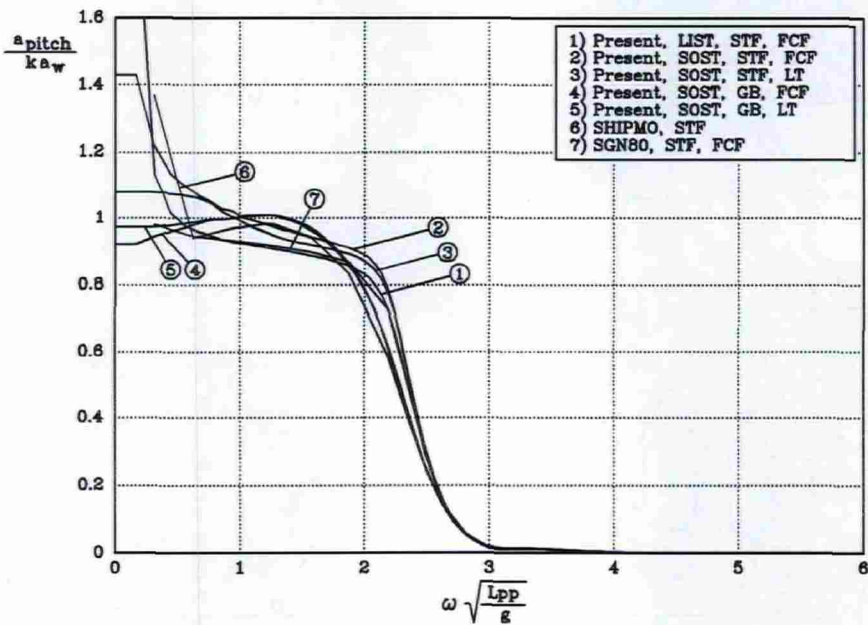


Figure 6.23: Comparison of the pitch response amplitude operators for a fast ferry advancing in head sea at a speed of 35 knots.

The response amplitude operators for the heave motion shown in Figure 6.22 can be divided into three groups. The three programs LIST, SGN80 and SHIPMO are based on the same theory and therefore the results should also be very close. The LIST and the SGN80 correspond well, while SHIPMO gives slightly larger heave response. The two sets of results from the SOST, STF have the same tendency, however, the dynamic amplification deviates almost 20 percent. This is also the case for the two sets of results from the SOST, GB. The difference between the programs is that the one uses the Lewis transformation and the other the Frank Close Fit method. An explanation of this could be that the hull shape of the fast ferry deviates from the Lewis shapes.

The pitch response amplitude operators shown in Figure 6.23 agree generally well. The same pattern of the methods for heave is valid for pitch. In the low-frequency range some of the codes give a pitch response, which deviates from the wave slope. A reason for the deviation could be that, as pointed out in Section 3.2.1, an assumption of a high frequency of encounter has been used in the derivation, which is violated for the frequencies in question. However, the response in this range is dominated by the restoring forces and the hydrodynamic forces are small.

The behaviour of the response in the low frequency region normally has no effect on the response because no waves are present at these wave frequencies.

6.3.3 Accelerations

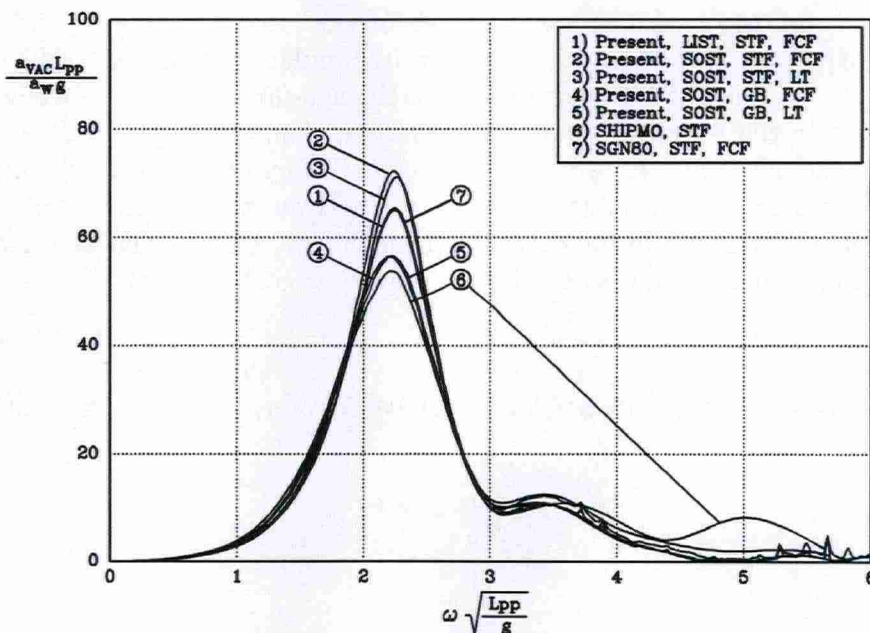


Figure 6.24: Comparison of the response amplitude operators for the vertical acceleration in FP for a fast ferry advancing in head sea at a speed of 35 knots.

The response amplitude operators for the vertical accelerations in the FP are shown in Figure 6.24. Because the accelerations are derived from the heave and pitch, a similar pattern as for those is expected. The grouping is, however, more significant.

In Figure 6.25 a comparison between predicted root mean square values (rms) of the vertical acceleration and results from model tests is shown. The comparison has been performed at three longitudinal positions on the ship and for different speeds, headings, wave spectra and sea states. The left column of the plots is for head sea and the right column is for a heading of 135 degrees. A definite pattern is difficult to find because the model tests have only been available for the shown cases. From one case to another both the speed and sea state parameters change and in the lower plot also the wave spectrum is changed from JONSWAP to Pierson Moskowitz.

Generally, the predictions of the acceleration levels for the LIST, STF and SGN80 are very close. For head sea a relatively good agreement between the predictions and the results from the model tests is found. The calculated responses correspond well for the speed of 25 knots. However, some deviation is found for the high speed.

For the heading of 135 degrees a very good agreement between calculations and model experiments is found for the high speed and the low sea state shown in Figure 6.25f. Less good agreement is found for the remaining sea states at this heading. Generally, the agreement between the model tests and the predictions is less good than for the head sea case.

This comparison depends on where the peak of the wave spectrum is located relative to the peak of the response amplitude operator. For the calculations based on the Pierson Moskowitz spectrum the zero upcrossing periods of 4.3 s and 5.5 s correspond to the non-dimensional frequencies of 2.5 and 3.2, respectively. Similarly for the JONSWAP spectrum, the zero upcrossing period of 7.8 s corresponds to the non-dimensional frequency of 1.9. The agreement between the response amplitude operators, shown in Figure 6.24, for the LIST, STF, FCF and the SGN80 is very good in this range. Therefore, also a good correspondence between the root mean square values is expected. However, the integration of the response spectrum sums up deviations in the entire frequency range, which could be a reason for the agreement in Figure 6.25c is not so good between the two calculations.

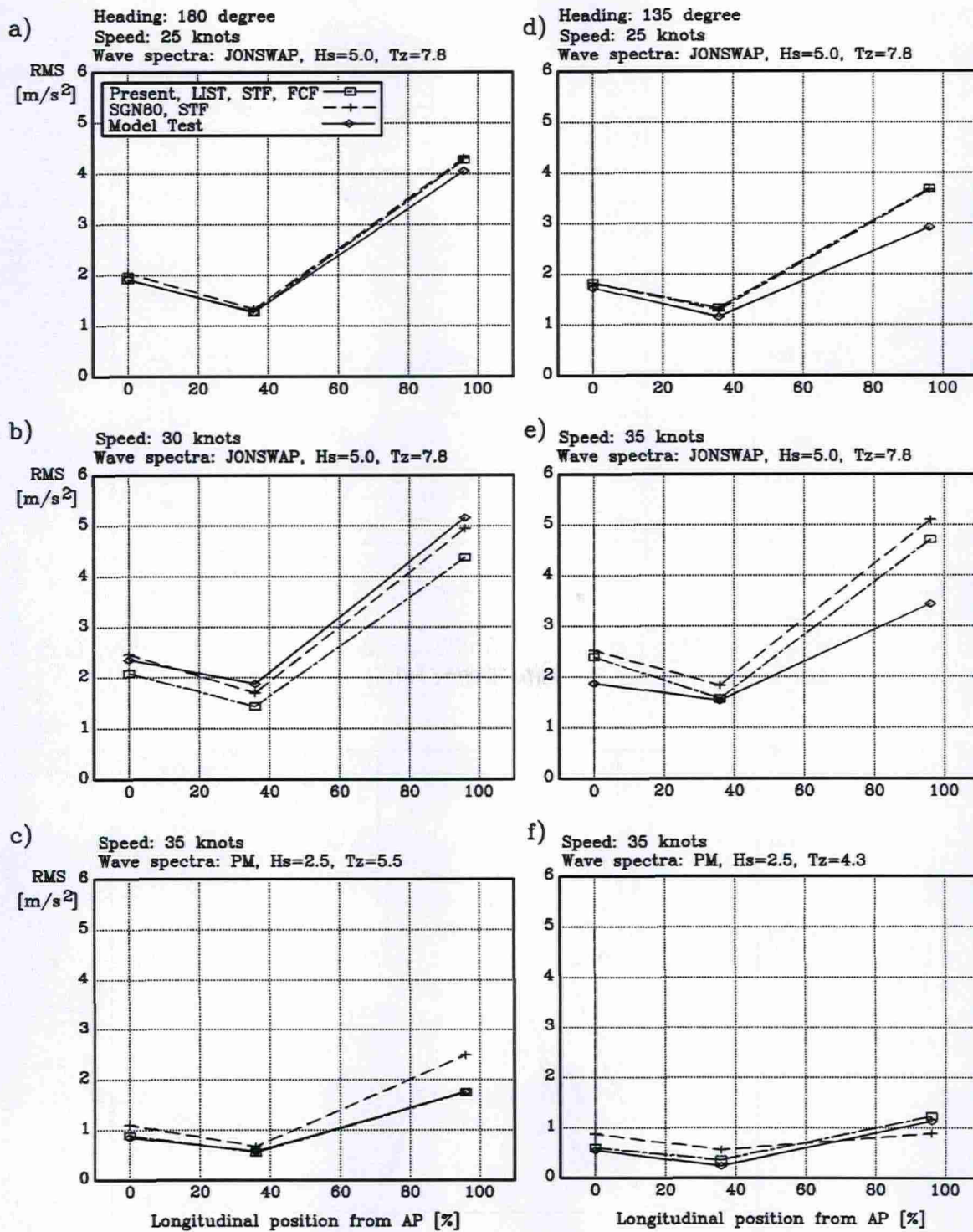


Figure 6.25: Comparison of the longitudinal distributions of the rms value of the vertical acceleration for a fast ferry in different sea states.

6.3.4 Loads

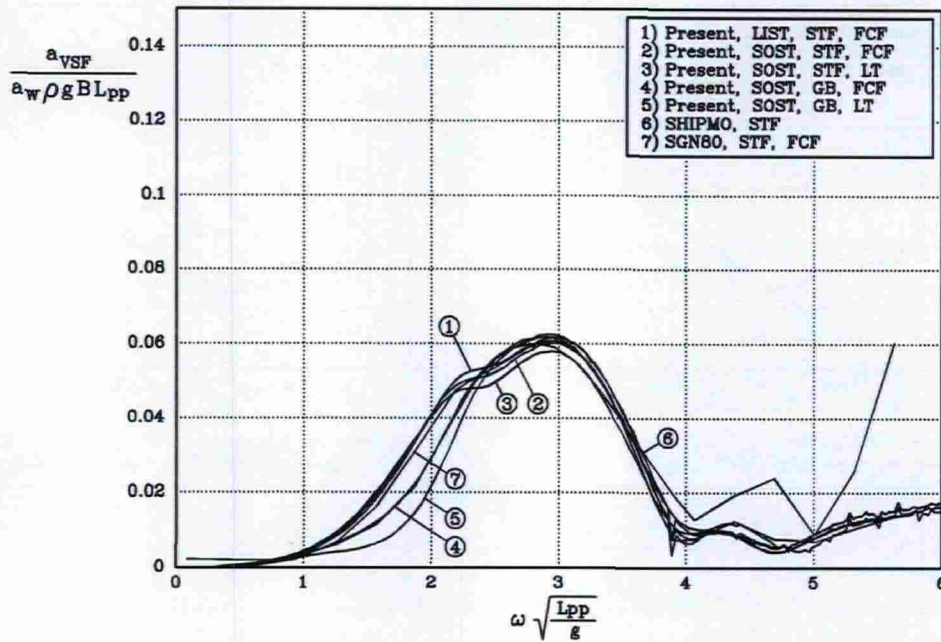


Figure 6.26: Comparison of the response amplitude operators for the vertical shear force in the COG for a fast ferry advancing in head sea at a speed of 35 knots.

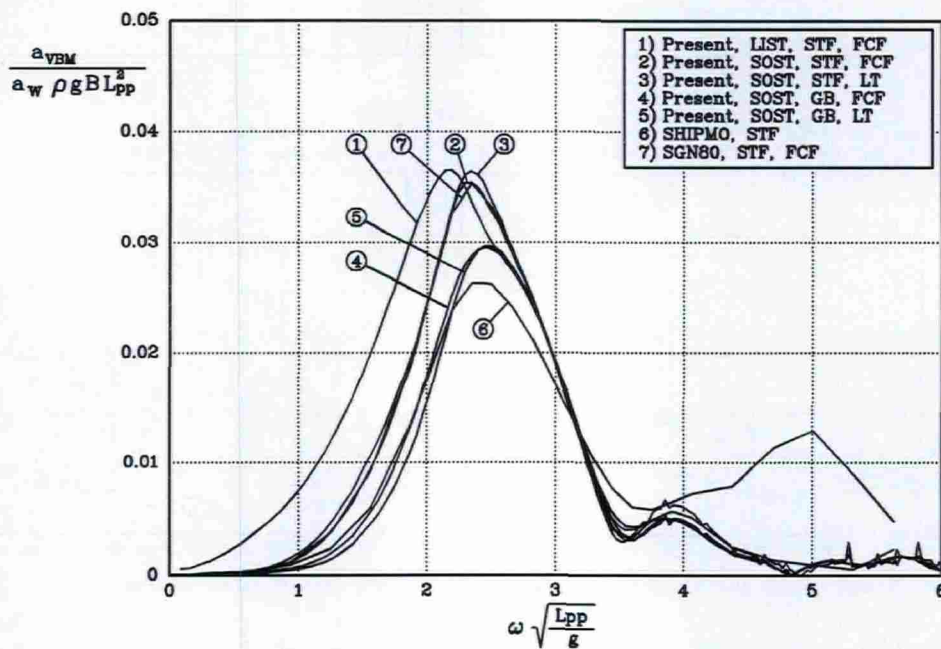


Figure 6.27: Comparison of the response amplitude operators for the vertical bending moment in the COG for a fast ferry advancing in head sea at a speed of 35 knots.

In Figure 6.26 the response amplitude operators for the vertical shear force at the longitudinal position of centre of gravity is shown. Normally, the shear force is not of interest at this position because it is not the position where it is at its maximum. However, for the purpose of performing a comparison the shear force is as useful here. The results from the different programs show a relatively narrow band. SHIPMO deviates at the high frequencies from the remaining calculations. This is also the case in the low-frequency range for the two calculations using SOST, GB. However, generally the results agree very well.

In Figure 6.27 the response amplitude operators for the vertical bending moment at the position of the centre of gravity are shown. The pattern is found as for the motions. However, the calculation with LIST shows the level as the calculations with SOST, STF and SGN80 but it is shifted with respect to the frequencies. The reason for this shift has been sought for without success.

6.4 Summary of the Verification and Validation

Generally, some spreading has been found between the compared programs. As shown by the ITTC78 [17] and ITTC81 [17], committee differences occur, even between programs based on the same theory. The aim of this verification has been to show that the programs give results within the limits expected by the applied methods. This aim has been reached from an overall point of view. There are, however, some exceptions. The SOST, STF, FCF deviates largely at some points. For the LIST, STF, FCF a shift of the vertical bending moment for the fast ferry has been found. Also for the roll motion some deviation has been found. However this is expected to be due to the rather simple implementation of additional damping. The NLST has been shown not to converge towards the linear results for decreasing wave amplitudes for pitch and the vertical bending moment. This implementation of the theory has therefore not been found suitable for practical purposes.

A validation to draw definite conclusions upon must include a larger number of cases based on more weight conditions, headings and speeds. The heave response in head sea determined theoretically in the region with dynamic amplification is generally overestimated compared to results from model tests. A relatively good prediction of pitch in head sea has been found, however, some of the methods overestimate. For the horizontal motions the agreement is good. However, as the headings approach beam sea the agreement becomes less good. As regards the loads the predictions on the container ship is fairly good taking the spreading on the results from the model tests into account. For the tanker there is proper agreement in the lower part of the considered frequency range but underprediction is found in the upper part.

For the fast ferry the different programs correspond well and the short-term calculations on the vertical acceleration show good agreement with the model tests.

Since the quadratic strip theory is not widely used, it has been difficult to find results for verification. A comparison with the design values based on the IACS unified rules of

classification, [40] for longitudinal strength shows good agreement with the hogging bending moment but an overpredicted sagging bending moment. Similar agreement has been found by Jensen and Dogliani, [23].

The reason for the different predictions the methods give could be treated more in detail by comparing the different terms in the calculations for a given frequency. However, the scope of this work has been to validate and verify the code and not to perform a parameter study on the methods available. The conclusion therefore becomes that the different methods deviate to some extent depending on both the type of result and the type of ship. It has, however, been found that the methods, with the exception of the SOST, STF, FCF for the container ship give reasonable results and correspond to some extent well with the model tests.

Chapter 7

System Design

7.1 Introduction

The present work has focused on the implementation of practical methods for prediction of wave loads on ships and much effort has been made to implement the program system into a comprehensive integrated rational ship design package, I-ship (see Baatrup et al. [2] and Michelsen et al. [32]). The design package is organised in a number of program modules for related tasks in preliminary ship design. Each of these modules are divided into submodules for more specific tasks.

7.2 General

The I-ship program system is at present divided into five main program modules:

1. Geometry definition.
2. Hydrostatic calculations.
3. Resistance and propulsion.
4. Wave load prediction.
5. Midship section/hull girder response.

Figure 7.1 shows a more detailed list of the modules and submodules available for preliminary ship design in the system. This report covers the program module *Wave load prediction*.

<u>Geometry definition</u>		<u>Hydrostatic calculations</u>	
PRFL	Definition of 2D profiles	CAPA	Compartment capacity calculations
FMDA	Definition of initial lines from standard shapes	WGHT	Definition of loading condition
LINE	Definition of hull lines and surfaces	STCT	Definition of stability criteria
BSRF	Definition of B-spline surfaces from hull lines	HYTB	Intact and damaged stability calculations
APDG	Definition of hull appendages	LGST	Longitudinal strength calculations
CPDF	Definition of hull compartmentation		
GMIF	Interface of geometry via neutral file formats		
<u>Wave load prediction</u>		<u>Resistance and propulsion</u>	
STPE	Strip theory preprocessor	PROP	Hull resistance and propeller calculations
STSL	Strip theory solver		
STPP	Strip theory postprocessor		
		<u>Midship section/hull girder response</u>	
		SCTM	Definition of midship sections
		CRSC	Calculation of cross-sectional constants
		HVTR	Static/dynamic hull girder response

Figure 7.1: I-ship modules and submodules for preliminary ship design.

The module *Wave load prediction* includes three submodules: a *Strip theory preprocessor*, a *Strip theory solver* and a *Strip theory postprocessor*. The concept has been to develop a pre- and postprocessor applicable in general to strip theory calculations. The solver contains the theories described in the previous sections and the basic idea is that it should be suited for extensions to be added.

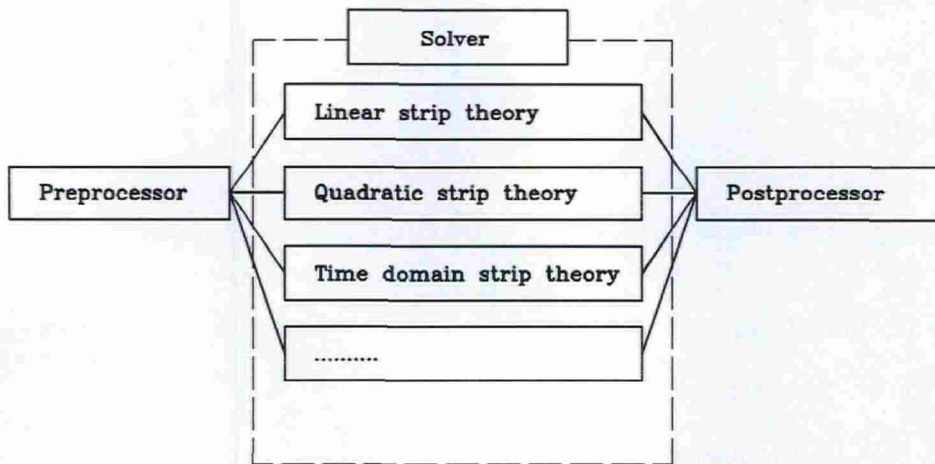


Figure 7.2: Basic concept of the wave load module.

A more detailed description will be given in the following sections.

7.3 The Preprocessor

In the *Strip theory preprocessor* different input is given and relevant ship data is determined for the strip theory calculations based on the predefined ship. The predefined input required as a minimum, is the geometry of the ship, defined in the *Geometry definition* module, and a weight condition, defined in the *Hydrostatic calculation* module.

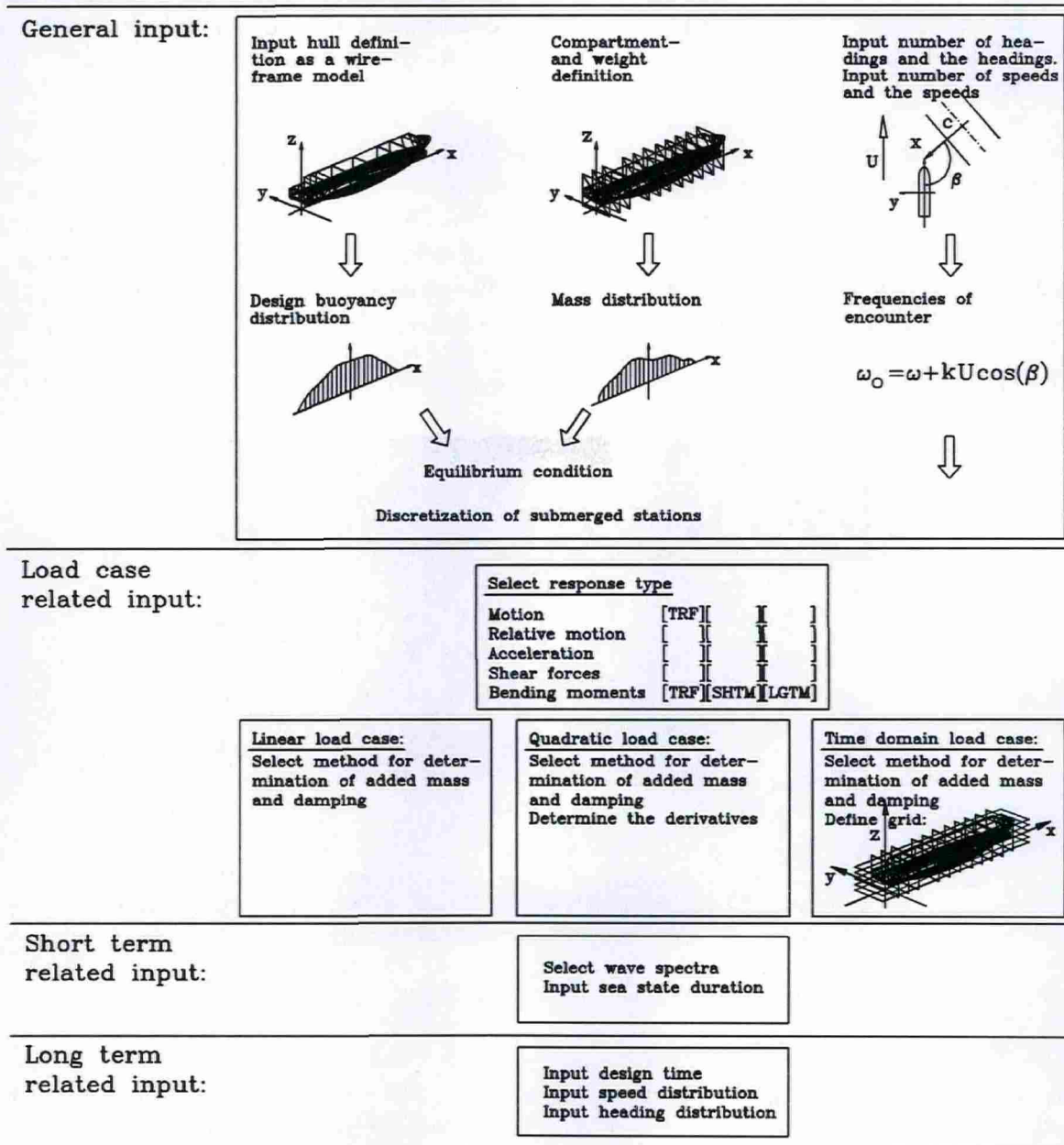


Figure 7.3: Diagram of the Strip theory preprocessor.

As shown in Figure 7.3 the input can be divided into four groups, which will be addressed in the following.

7.3.1 General Input

The general input is common for any type of calculation and the initial input is the physical constants, the acceleration of gravity and the density of the sea water. Then a hydrostatic calculation follows to determine the equilibrium condition of the ship, based on a selected weight condition. It is possible to use a manipulated condition as equilibrium, which e.g. takes dynamic sinkage and trim into account.

The submerged stations are described by a sequence of straight line segments. The segments are of equal length except when knuckle points are present. In such cases the station curve is treated as a number of subcurves ensuring that knuckle points are preserved as endpoints to segments. The input is given as the number of segments on each station or a single number giving the same number of segments on all stations. During inspection of the grid it is possible to adjust the grid by increasing or decreasing the number of segments.

The grid is determined in the discretization dialogue window as shown in Figure 7.4.

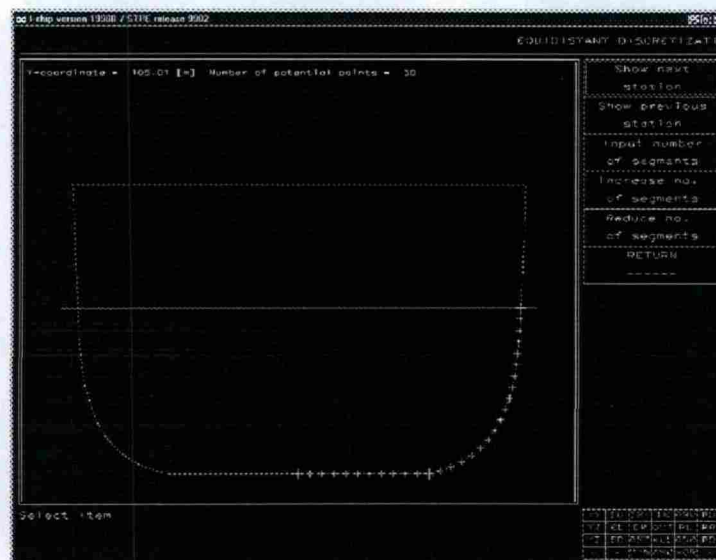


Figure 7.4: Discretization dialogue window.

By setting the number of points on a certain station equal to 0 it is possible to ignore the station from the calculation. This is a very useful facility as a large number (~ 100) is often used for the hydrostatic calculation, whereas about 30 – 40 is sufficient for strip theory calculations.

A part of the general input also includes the operational data for the ship in terms of number of speeds, headings and either wave or frequencies of encounter as well as the corresponding ranges.

Finally, the type of the response of interest is specified. The response has been divided into a number of types and three calculation levels as shown in Table 7.1.

Response type:	Level		
	FRF	SHTM	LGTM
Motions			
Relative motions			
Accelerations			
Shear forces			
Bending moments			

Table 7.1: *Types and calculation levels of the response (FRF: Frequency response function, SHTM: Short-term response statistics, LGTM: Long-term response statistics).*

The relative motions are the motions of the ship relative to the undisturbed wave surface for given longitudinal positions. The accelerations are the horizontal and vertical acceleration levels at a certain longitudinal position corresponding to the absolute motions of the ship. The shear forces refer to the horizontal and vertical directions. Finally, the bending moments refer to a horizontal and vertical plane and the torsional moment is included in this item.

The types of output described above refer to the horizontal and vertical plane. Only the linear analysis includes both of these planes. The non-linear calculations only consider the vertical plane, which limits the degrees of freedom within each item.

7.3.2 Load Case Related Input

Each calculation is defined as a load case. It is possible to define three different types of load cases:

1. Linear frequency-domain load case.
2. Quadratic frequency-domain load case.
3. Non-linear time-domain load case.

The selection of the method for determining the added mass and damping coefficients is common for all the load case types. Five methods are available and listed below.

1. Lewis (1-dof, symmetric).
2. Lewis/Yamamoto (1-dof, symmetric).
3. Frank Close Fit (3-dof, symmetric).
4. Simple Green function I (3-dof, symmetric).
5. Simple Green function II (3-dof, limited depth).

In connection with the input of each load case more specific input has to be given as well. The Green function II require a water depth and a width of a rectangular domain, which along with the hull section encloses the domain. Based on a given number of points a grid will be made on the boundaries.

Linear Frequency Domain Load Case

The simplest load case is the linear frequency-domain load case. The selection of the method for determination of added mass and damping is the only input for this load case.

Quadratic Frequency-Domain Load Case

The same information as in the linear case is needed for the quadratic frequency domain load case.

Two options for the linear part of the quadratic calculations are available: either the theory according to Gerritsma and Beukelman, [6], or that derived by Salvesen, Tuck and Faltinsen, [49]. The quadratic strip theory requires also the sectional derivatives with respect to immersion. The draughts to be applied for the numerical determination of these derivatives must be given. The selection of either a rigid body analysis or a hydroelastic analysis is done through the number of modes selected. Two modes, as a minimum, indicate rigid body analysis (heave and pitch). A mode number equal to three includes the two-node vibration and so forth. For hydroelastic calculations the vertical bending and the shear rigidities are required at the longitudinal positions where the station curves are defined. Finally, the structural damping is needed to complete a hydroelastic calculation.

Non-Linear Time-Domain Load Case

The procedure for the non-linear time-domain load case is somewhat different from the frequency-domain procedures. In order to be able to evaluate the hydrodynamic and hydrostatic coefficients for any sectional immersion, a table is established for each station. This

table consists of added mass, damping and restoring coefficients for each discrete immersion according to the grid.

The analysis consists of transfer functions for a number of specified wave amplitudes in a prior defined frequency range.

7.3.3 Short-Term Related Input

The short-term related input is the selection between a Pierson-Moskowitz wave spectrum or a JONSWAP spectrum. Auxiliary input for fatigue damage analysis is given as the ratio between the response and the stress at the structural detail in question. Also the slope and the scale factor for the S-N curve have to be given. This facility is only available for the vertical bending moment.

7.3.4 Long-Term Related Input

The long-term related input concerns the distribution of speeds and headings during the time in question. The aim of the analysis is to determine the extreme value distribution for a certain response type during the lifetime of a ship. First the duration in question is given in years. A normalised scatter diagram is determined on the basis of input of a number of Marsden areas and a corresponding distribution of time in the respective areas. The general approach used for the input of heading and speed distribution is that they can be given different in ranges of the significant wave height. This facility makes it possible to define different philosophies concerning weather-influence reduction in the operational profile.

```

%1 ship
HEADING DISTRIBUTION
+-----+-----+-----+-----+
| Heading | Wave range | Wave range | Wave range |
| Eleycccc | 0.0KHz< 5.0 | 5.0KHz<10.0 | 10.0KHz<15.0 |
+-----+-----+-----+-----+
| 0.0 | 0.000 | 0.000 | 0.000 |
| 30.0 | 0.157 | 0.157 | 0.157 |
| 60.0 | 0.187 | 0.187 | 0.187 |
| 90.0 | 0.192 | 0.192 | 0.192 |
| 120.0 | 0.157 | 0.157 | 0.157 |
| 150.0 | 0.092 | 0.092 | 0.092 |
+-----+-----+-----+-----+
The sum of the probabilities in the columns
must equal 1.0
To continue press RETURN

```

Figure 7.5: Example of a heading distribution

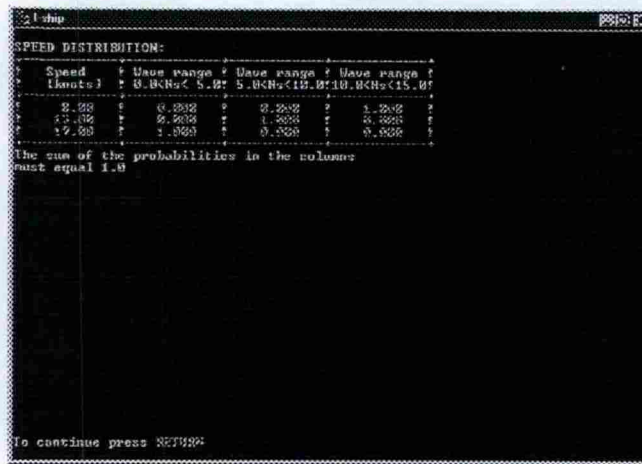


Figure 7.6: Example of a speed distribution.

In Figures 7.5 and 7.6 an example is shown where three ranges for the significant wave height have been defined, each with different distributions of heading and speed. This can model common practice in navigation in heavy weather to reduce the loads on the ship and ease it either by changing the heading or by reducing the speed.

7.4 The Strip Theory Solver

The *Strip theory solver* calculates the response for the predefined load cases. The response corresponding to the defined load cases is determined by calling the respective subprograms in the solver shown in Figure 7.2.

7.5 The Postprocessor

In the *Postprocessor* the responses can be printed and plotted. The files shown in Table 7.2 are used for storage.

```

c1ship
RAD for HEAVE
Heading: 1.000E+02 [deg] Speed : 7.725E+00 [m/s], (Fn= 1.501E-01)
-----+-----+-----+-----+-----+-----+-----+
No | Om. of ent. | Om. of wave | Lw/lpp | Amplitude | Phase |
  | [rad/s]    | [rad/s]    |        |           | [deg] |
-----+-----+-----+-----+-----+-----+
 1 | 2.610E-02 | 2.579E-02 | 3.445E+02 | 9.960E-01 | 1.498E-03 |
 2 | 5.255E-02 | 5.054E-02 | 8.908E+01 | 9.800E-01 | 2.620E-03 |
 3 | 1.051E-01 | 9.760E-02 | 2.307E+01 | 8.894E-01 | -2.555E-03 |
 4 | 1.577E-01 | 1.418E-01 | 1.155E+01 | 8.310E-01 | -2.735E-02 |
 5 | 2.102E-01 | 1.880E-01 | 6.765E+00 | 9.823E-01 | -7.036E-02 |
 6 | 2.628E-01 | 2.334E-01 | 4.573E+00 | 9.628E-01 | -1.241E-01 |
 7 | 3.153E-01 | 2.615E-01 | 3.039E+00 | 8.302E-01 | -1.028E-01 |
 8 | 3.679E-01 | 2.880E-01 | 2.572E+00 | 8.826E-01 | 1.015E-01 |
 9 | 4.204E-01 | 3.131E-01 | 2.058E+00 | 8.198E-01 | 8.730E-01 |
10 | 4.730E-01 | 3.369E-01 | 1.696E+00 | 7.437E-01 | 1.084E+00 |
11 | 5.255E-01 | 3.597E-01 | 1.402E+00 | 6.602E-01 | 4.105E+00 |
12 | 5.781E-01 | 3.815E-01 | 1.228E+00 | 5.770E-01 | 7.819E+00 |
13 | 6.306E-01 | 4.023E-01 | 1.088E+00 | 5.058E-01 | 1.266E+01 |
14 | 6.832E-01 | 4.223E-01 | 9.419E-01 | 4.437E-01 | 1.558E+01 |
15 | 7.357E-01 | 4.418E-01 | 8.093E-01 | 3.893E-01 | 1.873E+01 |
16 | 7.883E-01 | 4.600E-01 | 7.548E-01 | 3.509E-01 | 2.206E+01 |
17 | 8.408E-01 | 4.779E-01 | 6.837E-01 | 3.224E-01 | 2.549E+01 |
18 | 8.934E-01 | 4.954E-01 | 6.090E-01 | 2.911E-01 | 2.925E+01 |
19 | 9.459E-01 | 5.117E-01 | 5.721E-01 | 2.697E-01 | 3.356E+01 |
20 | 9.985E-01 | 5.278E-01 | 5.278E-01 | 2.138E-01 | 4.037E+01 |
21 | 1.051E+00 | 5.439E-01 | 4.880E-01 | 1.448E-01 | 2.655E+01 |
-----+-----+-----+-----+-----+
Heave non-dimensionalized by: wave amp.
Input +, -, NNN, +NNN, -NNN or <R> to quit ?

```

Figure 7.7: Print output example.

Description	Type
Project file	projectname.pjc
Analysis definition file	projectname.ste
Hydrodynamic data file	projectname.amd
Linear load case output file	projectname.lst
Quadratic load case output file	projectname.sst
Time-domain load case output file	projectname.tme

Table 7.2: Input and output files.

An analysis is a part of a project contained in a project file. The definition of the analysis undertaken and the corresponding ship data are stored in the analysis definition file. For a linear load case as well as a quadratic load case the hydrodynamic data in terms of added mass and damping is stored in the hydrodynamic data file and can be plotted and printed in the postprocessor. This is very useful in cases where reasons for deviations are sought. A good start is a plot of the added mass and damping for all the stations, which will very quickly show if a station gives unrealistic results. The station curve can then be identified and usually a modification of the grid will improve the results.

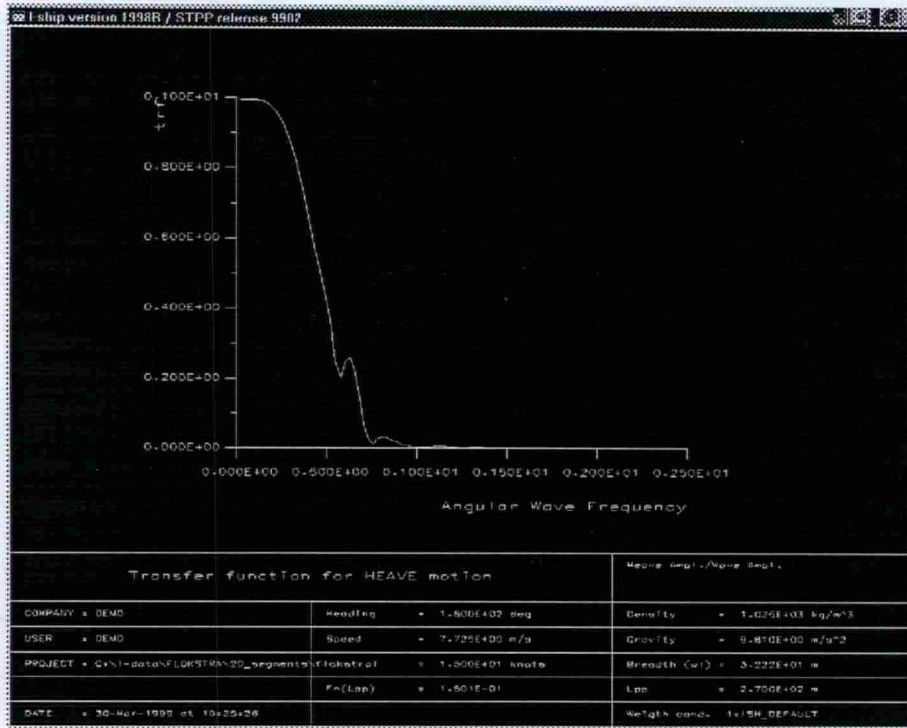


Figure 7.8: Plot output example.

The results from the defined load cases are stored in the three load case output files. These output files can one at a time be loaded in the postprocessor and results can be plotted and printed. The form of the output for plot as well as print is the standard in I-ship as illustrated in Figures 7.7 and 7.8.

Chapter 8

Conclusion and Recommendations

8.1 Conclusion

The objective of the present work has been to develop a rational computer software system to predict design wave loads on ships. From a survey of available theoretical formulations, a number has been selected and a system design for an analysis tool have been developed. The theoretical background and the structure of program have been described. To verify and validate the procedures, a number of comparisons with other methods and results from model tests have been carried out.

The conclusions drawn will be described in the following.

From a survey of available theoretical formulations, three theoretical approaches have been selected: the linear strip theory, the quadratic strip theory and a non-linear time-domain strip theory. The linear strip theory program for basic calculations and for analyses requiring motions and loads in both the vertical and the horizontal plane. Then, in order to include non-linearities and hydroelasticity the quadratic strip theory has been implemented, with the advantage of being formulated in the frequency domain. Finally, for more detailed studies a non-linear time-domain strip theory has been implemented. A common part of strip theory calculations is the determination of added mass and damping. Therefore, a library of methods for determination of these has been developed to include different types of effects. The theoretical background to the applied theories has been described in the first part of the thesis.

The ship definition has been based on the I-ship system. Therefore, a large number of facilities has been available initially. However, this also applies some constraints on the system. The I-ship system is structured in modules and this architecture has been adopted for consistency in a preprocessor, a solver and a postprocessor.

- A preprocessor with the main purpose of extracting ship data from the I-ship modules, interpret user input and prepare an input file for the solver module.
- A solver including the strip theory formulations along with a library of routines to determine added mass and damping.
- A postprocessor, where input and output can be printed and for the main part also plotted.

The system design has been described and the interface of the developed modules have been documented.

The results from the solver have been verified against results from other applications by analyses of three ships. Also a validation has been performed by comparison with model tests. The conclusions drawn on this part of this work are

- The library of routines for determination of added mass and damping consists of five methods. Three methods have been found to be suitable for strip theory calculations. The methods denoted Green function I and II have been found to be very sensitive to the used grid. The present method for discretization of the additional boundaries has not been sufficiently general to handle a large frequency range, which is relevant for analyses. Therefore, the present implementation of these methods has not been judged to be sufficiently robust for general use.
- The linear strip theory (LIST) has been found generally to predict motions and loads well in comparison to other programs and model tests. However, deviations have been found in the determination of the vertical bending moment on a fast ferry. The present implementation of roll damping has been found to be too simple leading to a less good prediction of roll motion in beam seas.
- In the verification and validation also the quadratic strip theory (SOST) has generally been found to predict linear motions and loads in good agreement with other programs and model tests. A single combination of the use of the program (SOST, GB, FCF) have been found to deviate generally, however, this is only a small part of the available combinations. For the second order part of the response, a comparison with the design values based on the IACS unified rules of classification [40] for longitudinal strength shows good agreement with the hogging bending moment, but an overpredicted sagging bending moment. A similar agreement has been found by Jensen and Dogliani [23].
- The time-domain strip theory (NLST) has been implemented only for analysis in regular waves. It has been shown to give satisfactory heave motion but unsatisfactory pitch motion leading to too low wave-induced loads on the hull. This part of the program has therefore not been found to be suitable for analyses. It has, however, been demonstrated that the system can handle time-integration methods.

Generally, the developed system has been shown to be a useful tool for determination of wave loads on ships. The included facilities has been narrower than originally intended. The task of implementing and test a complete application including time-domain strip theory and hydroelasticity has been too ambitious. The emphasis has therefore been put on a robust well tested application including the linear strip theory and the quadratic strip theory with the described statistical facilities to perform short- and long-term predictions.

8.2 Recommendations for Future Work

The developed system has been considered a suitable frame for existing and future applications based on strip theory. The recommendations for future work therefore focus on improvements of the existing methods and extensions of the system to include new methods.

The improvements include

- **The linear strip theory:** The motion and load derived from the roll motion can be improved by a more advanced method to include viscous roll damping. Pressure distributions on the hull are another very useful extension. The surge motion can be added to the existing five degrees of freedom.
- **The quadratic strip theory:** The present validation has focused on rigid body motions at the expense of the hydroelastic part of the method. More effort should be made to validate this part of the program.
- **The time-domain strip theory:** More effort put into the present implementation should be able to make it give satisfactory results. Provided this is done, improved facilities for the input wave signal could be made, e.g. analysis in irregular waves and corresponding statistical postprocessing.

The recommended extension of the theoretical methods implemented so far would be to include the strip theories which are developed to a level suitable for practical use in general.

This includes

- Extending the linear strip theory to the unified slender body theory and thus eliminating the frequency limitation.
- Improving the time-domain strip theory to take memory effects and hydroelasticity into account as e.g. Wang [62].

This page is intentionally left blank.

Bibliography

- [1] Andersen, P. and He, W. On the Calculation of Two-Dimensional Added Mass and Damping Coefficients by Simple Green's Function Technique. DCAMM report no. 287, Technical University of Denmark, June 1984.
- [2] Baatrup, J. and Jensen, J. J. Dynamic Analysis of Offshore Jacket Platforms Subjected to Non-Gaussian Wave Loads. *Proceedings of International Symposium on Offshore Engineering*, September 1991.
- [3] Bertram, V. and Iwashita, H. Comparative Evaluation of Seakeeping Prediction Methods. *Schiff und Hafen*, 6:54-58, June 1996.
- [4] Blok, J. J. and Beukelman, W. The High-Speed Displacement Ship Systematic Series Hull Forms Seakeeping Characteristics. *Trans. SNAME*, 92:125-150, 1984.
- [5] Cummins, W. E. The Impulse Response Function and Ship Motions. *Schiffstechnik*, 9:101-109, June 1962.
- [6] Gerritsma, J. and Beukelman, W. The distribution of the hydrodynamic forces on a heaving and pitching shipmodel in still water. Technical Report 22, Technological University, Delft, June 1964.
- [7] Gerritsma, J. and Beukelman, W. Analysis of the modified strip theory for the calculation of ship motions and wave bending moments. *International Shipbuilding Progress*, (14):319-337, 1967.
- [8] Gerritsma, J., Beukelman, W. and Glansdorp, C. C. The Effect of Beam on the Hydrodynamic Characteristics of Ship Hulls. *Tenth Symposium on Naval Hydrodynamics*, pages 3-29, 1974.
- [9] Grim, O. Berechnung der durch Schwingungen eines Schiffskörpers erzeugten hydrodynamischen Kräfte. *Jahrbuch der Schiffbautechnischen Gesellschaft*, 47:277-299, 1953.
- [10] Gunsteren, F.F. van. *Springing of ships in waves*. PhD thesis, Technische Hogeschool, Delft, November 1978.
- [11] Hanaoka, T. On the reverse flow theorem concerning wave-making theory. *Proc. 9th Japan National Congress for App. Mech.*, pages 223-226, 1959.

-
- [12] Hansen, P. F. *Reliability Analysis of a Midship Section*. PhD thesis, Technical University of Denmark, Department of Naval Architecture and Offshore Engineering, January 1994.
- [13] Haskind, M. D. The exciting forces and wetting of the ships in waves. *DTMB, Translation*, (307), March 1962.
- [14] Hogben, N., Dacunha, N. M. C. and Olliver, G. F. *Global Wave Statistics*. Unwin Bros. Ltd, 1984.
- [15] ISSC. Proceedings of Int. Ship & Offshore Structures Congress, St. John's, Canada. 1994.
- [16] ISSC. Proceedings of Int. Ship & Offshore Structures Congress, Trondheim, Norway. 1997.
- [17] ITTC. Proceedings of Int. Towing Tank Conference, the Hague, the Netherlands. 1978.
- [18] ITTC. Proceedings of Int. Towing Tank Conference, Leningrad, USSR. 1981.
- [19] ITTC. Proceedings of Int. Towing Tank Conference, Göteborg, Sweden. 1984.
- [20] ITTC. Proceedings of Int. Towing Tank Conference, Kobe, Japan. 1987.
- [21] ITTC. Symbols and Terminology List. 1993.
- [22] Jensen, J. J. Dynamic Amplification of Offshore Steel Platform Responses due to Non-Gaussian Wave Loads. *Marine Structures*, (7):91-105, 1994.
- [23] Jensen, J. J. and Dogliani, M. Wave-induced Ship Hull Vibrations in Stochastic Seaways. *Marine Structures*, (9):353-387, 1996.
- [24] Jensen, J. J. and Pedersen, P. T. Wave-induced Bending Moments in Ships - A Quadratic Theory. *The Royal Institution of Naval Architects*, pages 151-165, 1978.
- [25] Jensen, J. J., Petersen, J.B. and Pedersen, P. T. Prediction of Non-linear Wave-induced Loads on Ships. *Dynamics of Marine Vehicles and Structures in Waves*, 1991.
- [26] Kashiwagi, M. Prediction of Surge and Its Effect on Added Resistance by Means of the Ship Motion Based on Three-Dimensional Theories. *Trans. of West-Japan Soc. Nav. Arch.*, (89):77-89, 1995.
- [27] Krylov, A. A new theory for the pitching and heaving motion of ships in waves. *Transactions of Royal Institute of Naval Architects*, 1896.
- [28] Lee, C. H. and Sclavounos, P. D. Removing the Irregular Frequencies from Integral Equations in Wave-Body Interactions. *Journal of Fluid Mechanics*, 207:393-418, 1989.
- [29] Lewis, F. M. The Inertia of the Water Surrounding a Vibrating Ship. *Trans. SNAME*, 37:1-20, 1929.

- [30] Lindemann, K. Possible Warning Conditions and System for Ship Handling in Rough Weather. *Ship Operation Automation*, pages 3–10, 1976.
- [31] Meyerhoff, W. K. and Schlachter. An Approach for the Determination of Hull-Girder Loads in a Seaway Including Hydrodynamic Impacts. *Ocean Engineering*, 7(6):305–332, 1980.
- [32] Michelsen, J., Baatrup, J. and Jensen, J. J. Development of a CAD System for Ship Design in a University Environment. *IMAM, IV Congress, Bulgaria*, 1993.
- [33] Miner, M. A. Cumulative Damage in Fatigue. *Journal of Applied Mechanics, Trans. A.S.M.E.*, 12:A159–A164, September 1945.
- [34] Nakos, D. E. and Sclavounos, P. D. Ship Motions by a Three-Dimensional Rankine Panel Method. *18th Symposium on Naval Hydrodynamics*, pages 21–39, 1991.
- [35] Nakos, D. E., Kring, D. C. and Sclavounos, P. D. Rankine Panel Methods for Time-Domain Free Surface Flows. *6th Intl. Conference on Numerical Ship Hydrodynamics, University of Iowa*, 1993.
- [36] Newman, J. N. The Exciting Forces on Fixed Bodies in Waves. *Journal of Ship Research*, 6(3):10–18, December 1962.
- [37] Newman, J. N. The Theory of Ship Motions. *Advances in Applied Mechanics*, 18, 1978.
- [38] Newman, J. N. The quest for a three-dimensional theory of ship-wave interactions. *Phil. Trans. Royal Society London, series A*, (334):213–227, 1990.
- [39] Newman, J. N. and Sclavounos, P. D. The Unified Theory for Ship Motions. *Proceedings, 13th Symposium on Naval Hydrodynamics, Tokyo*, 1980.
- [40] Nitta, A., Hironori, A. and Atsushi, M. Basis of IACS Unified Longitudinal Strength Standard. *Marine Structures*, 5(1):1–21, 1992.
- [41] Nordforsk. Assessment of Ship Performance in a Seaway. Nordforsk, Sortedam Dossering 19, Kbh. N., DK-2200, 1987.
- [42] Ohmatsu, S. On the Irregular Frequencies in the Theory of Oscillating Bodies. *Papers, Ship Res. Inst.*, (48), 1975.
- [43] Pereira, R. Simulation Nichtlinearer Seegangslasten, (in German). *Ship Technology Research*, 35:173–193, 1988.
- [44] Petersen, J. B. *Non-Linear Strip Theories for Ship Response in Waves*. PhD thesis, Dept. of Ocean Engineering, Technical University of Denmark, March 1992.
- [45] Potash, L. R. Second-Order Theory of Oscillating Cylinders. Technical report, College of Engineering, University of California, Berkeley, June 1970.

- [46] Price, W. G. and Bishop, R. E. D. *Probabilistic Theory of Ships Dynamics*. Chapman and Hall Ltd., 1. edition, 1974.
- [47] Rice, S. O. Mathematical Analysis of Random Noise. *Bell System Technical Journal*, 23:282-332, 1944.
- [48] Russo, V. L. and Sullivan, E. K. Design of the Mariner-Type Ship. *Trans. SNAME*, 61:98-218, 1953.
- [49] Salvesen, N., Tuck, E. O. and Faltinsen, O. Ship Motion and Sea Loads. *Trans. SNAME*, 78:250-287, 1970.
- [50] Schmitke, R. T. Ship Sway, Roll and Yaw Motions in Oblique Seas. *Trans. SNAME*, 86:26-46, 1978.
- [51] Slavounos, P. D. The Diffraction of Free-Surface Waves by a Slender Ship. *Journal of Ship Research*, 28(1):29-47, 1984.
- [52] Slavounos, P. D. The Unified Slender-body Theory: Ship Motion in Waves. *Office of Naval Research Symposium on Naval Hydrodynamics*, (15):177-192, August 1984.
- [53] Shin, Y., Cung, J. S., Lin, W. M., Zhang, S. and Engle, A. Dynamic Loadings for Structural Analysis of Fine Form Container Ship Based on a Non-linear Large Amplitude Motions and Loads Method. *SNAME, Transactions*, 105:127-154, 1997.
- [54] Söding, H. Leckstabilität im Seegang. Report no. 429, Institut für Schiffbau, Hamburg, 1982.
- [55] St. Denis, M. and Pierson, W. J. Jr. On the Motions of Ships in Confused Seas. *Trans. SNAME*, 61:280-358, 1953.
- [56] Tanaka, N. A Study on the Bilge Keels, Part 4. On the Eddy-making Resistance to the Rolling of a Ship Hull. *Japan Society of Naval Architects*, 109, 1960.
- [57] Tanizawa, K., Saruta, T., Taguchi, H. and Watanabe, I. Experimental Study of Wave Pressure on a VLCC Running in Short Waves. *Journal of the Society of Naval Architects of Japan*, 174:233-242, 1993.
- [58] Tasai, F. On the Damping Force and Added Mass of Ships Heaving and Pitching. *Research Institute for Applied Mechanics*, XII(26):131-152, 1959.
- [59] Tasai, F. Improvements in the Theory of Ship Motions in Regular Waves. *Appendix 2 the of Seakeeping Committee Report, 12th ITTC*, 1969.
- [60] Tick, L. J. Differential Equations with Frequency Dependent Coefficients. *Journal of Ship Research*, 3(2):45-46, October 1959.
- [61] Ursell, F. On the heaving motion of a circular cylinder on the surface of a fluid. *Quarterly Journal of Mech. and Applied Math.*, II(pt2), 1949.

-
- [62] Wang, Z. *Hydroelastic Analysis of High-Speed Ships*. PhD thesis, Dept. of Naval Architecture and Offshore Engineering, Lyngby, Denmark, 2000.
- [63] Wang, Z., Folsø, R., Bondini, F. and Pedersen, T. Linear and Non-linear Numerical Sea-keeping Evaluation of a Fast Monohull Ferry Compared to Full Scale Measurements. *FAST99*, 1999.
- [64] Wehausen, J. and Laitone, E. V. *Surface Waves*, volume IX of *Encyclopedia of Physics*, page 483. Springer-Verlag, 1960.
- [65] Weinblum, G. and St. Denis, M. On the Motions of Ships at Sea. *Trans. SNAME*, 58:184-248, 1950.
- [66] Winterstein, S. R. Non-linear Vibration Models for Extremes and Fatigue. *Journal of Engineering Mechanics*, 114(10):1772-1790, October 1988.
- [67] Xia, J., Wang, Z. and Jensen, J. J. Non-linear wave loads and ships responses by a time-domain strip theory. DCAMM report no. 569, Technical University of Denmark, March 1998.
- [68] Yamamoto, Y., Sugai, K., Inoue, H., Yoshida, K., Fujino, M. and Ohtsubu, J. Wave loads and response of ships and offshore structures from the viewpoint of hydroelasticity. *Intl. Conf. on Advances in Marine Structures*, May 1986.
- [69] Yeung, R. W. A Singularity-Distribution Method for Free-Surface Flow Problems with an Oscillating Body. Technical Report NA 73-6, College of Engineering, University of California, Berkeley, August 1973.

This page is intentionally left blank.

List of Figures

3.1	<i>Sketch illustrating the sign convention for translatory and angular displacements.</i>	11
3.2	<i>Sketch illustrating the sign convention for loads on the hull</i>	12
3.3	<i>Plot of the frequency response function for heave and pitch for Mariner [48] in head sea at $Fn = 0.2$ shown as an example of results from the linear strip theory. The plots are compared with results from Salvesen, Tuck and Faltinsen [49].</i>	19
3.4	<i>Plot of the frequency phase function for heave and pitch for Mariner [48] in head sea at $Fn = 0.2$ shown as an example of results from the linear strip theory. The plots are compared with results from Salvesen, Tuck and Faltinsen [49].</i>	19
3.5	<i>Plot of an example of the response determined with the quadratic strip theory in the form of the frequency response functions for the midship bending moment for the container ship S175. The ship is advancing in head sea at a forward speed of 22 knots.</i>	24
3.6	<i>Plot of an example of results from the quadratic strip theory in terms of a time serie of the midship vertical bending moment for the container ship S175. The ratio $L/\lambda = 1.1$, the wave amplitude a is 3m and the ship is advancing in head sea at a forward speed of 22 knots.</i>	25
3.7	<i>Plot showing the measured natural frequency of the 2-node vertical vibration as a function of ship length (van Gunsteren [10])</i>	26
3.8	<i>Plot showing a comparison of heave frequency response functions for a fast ferry of Froude number 0.55 with and without dynamic sinkage and trim. . .</i>	29
3.9	<i>Plot showing a comparison of pitch frequency response functions for a fast ferry of Froude number 0.55 with and without dynamic sinkage and trim. . .</i>	30

3.10	Plot showing a comparison of acceleration frequency response functions at $3/4L_{pp}$ for a fast ferry of Froude number 0.55 with and without dynamic sinkage and trim	30
3.11	Plot showing the difference the low frequency of encounter modification makes for the response amplitude operators for heave, pitch, vertical shear force and vertical bending moment. The ship is a fast ferry with a Froude number of 0.55 and a heading of 0 degrees.	31
3.12	Plot showing the difference the low frequency of encounter modification makes for the response amplitude operators for heave, pitch, vertical shear force and vertical bending moment. The ship is a fast ferry with a Froude number of 0.55 and a heading of 30 degrees.	32
3.13	Plot showing the difference the low frequency of encounter modification makes for the response amplitude operators for heave, pitch, vertical shear force and vertical bending moment. The ship is a fast ferry with a Froude number of 0.55 and a heading of 60 degrees.	33
4.1	Sketch showing the corresponding experimental setup to determine the hydrodynamic coefficients for heave	35
4.2	Plot showing the non-dimensional coefficient k_4 as a function of $\frac{T}{B}$ and the non-dimensional frequency of encounter.	38
4.3	Sketch showing the two-dimensional fluid domain and the boundaries for the deep-water case.	41
4.4	Sketch showing the principle for the discretization of the boundary for the infinitely deep-water case.	48
4.5	Plot of results from the method using Green function for restricted water depth. The example is non-dimensional added mass and damping of a rectangular symmetric section with $B/T = 2$ and different depth/draught-ratios.	50
4.6	Plot of results from the method using Green function for infinite water depth. The example is non-dimensional added mass and damping for a rectangular symmetric section with $B/T = 2$ and different heeling angles.	51
5.1	Sketch showing the effect of skewness and kurtosis in the Gaussian distribution through different combinations.	56
5.2	Plot showing the added resistance in waves as a function of the wave length [41].	64

5.3	Plot showing an example of speed reduction as a function of the weather roughness [30].	64
6.1	Sketch showing the geometrical description of the container ship S-175. . . .	69
6.2	Plot showing the analysed weight condition of the container ship S-175. . . .	70
6.3	Plot showing a comparison between present results and computed results made by the ITTC78 Committee. The results are the heave response amplitude operator and the phase function for S-175 in head sea at a speed of 22 knots.	71
6.4	Plot showing a comparison between present results and computed results made by the ITTC78 Committee. The results are the pitch response amplitude operator and the phase function for S-175 in head sea at a speed of 22 knots.	72
6.5	Plot showing a comparison between present results and computed results made by the ITTC81 Committee. The results are the response amplitude operators for the midship vertical shear force for S-175 in head sea at a speed of 22 knots.	73
6.6	Plot showing a comparison between present results and computed results made by the ITTC81 Committee. The results are the response amplitude operators for the midship vertical bending moment for S-175 in head sea at a speed of 22 knots.	74
6.7	Plot showing a comparison of present long-term predictions. The results are the vertical bending moments.	76
6.8	Plot showing present results and computed results made by the ITTC81 Committee. The results are the response amplitude operators for the heave motion determined by the non-linear time-domain strip theory. The ship is S-175 in head sea at a speed of 22 knots.	78
6.9	Plot showing present results and computed results made by the ITTC81 Committee. The results are the response amplitude operators for the pitch motion determined by the non-linear time-domain strip theory. The ship is S-175 in head sea at a speed of 22 knots.	79
6.10	Plot showing present results of the response amplitude operators for the vertical bending moment amidship determined by the non-linear time-domain strip theory. The ship is S-175 in head sea at a speed of 22 knots.	79
6.11	Sketch showing the geometrical description of the VLCC tanker used for validation and verification.	82
6.12	Plot of the analysed weight condition of the VLCC.	82

-
- 6.13 Plot showing a comparison between present results and computed results by Tanizawa [57]. The results are the heave and pitch response amplitude operator for a VLCC in head sea at a speed of 14.3 knots. 83
- 6.14 Plot showing a comparison between present results and computed results by Tanizawa [57]. The results are the heave, pitch, sway, roll and yaw response amplitude operators for a VLCC. The heading is 150 degrees and the speed 14.3 knots. 84
- 6.15 Plot showing a comparison between present results and computed results by Tanizawa [57]. The results are the heave, pitch, sway, roll and yaw response amplitude operators for a VLCC. The heading is 90 degrees and the speed 14.3 knots. 85
- 6.16 Plot showing a comparison between present results and computed results by Tanizawa [57]. The results are the heave and pitch response amplitude operators for a VLCC in following sea at a speed of 14.3 knots. 86
- 6.17 Plot showing a comparison between present results and computed results by Tanizawa [57]. The results are the response amplitude operator for the mid-ship vertical bending moment for a VLCC in head sea at a speed of 14.3 knots. 86
- 6.18 Plot showing a comparison between present results and computed results by Tanizawa [57]. The results are the response amplitude operator for the mid-ship vertical bending moment for a VLCC. The heading is 150 degrees and the speed is 14.3 knots. 87
- 6.19 Plot showing a comparison between present results and computed results by Tanizawa [57]. The results are the response amplitude operator for the mid-ship horizontal bending moment for a VLCC. The heading is 150 degrees and the speed is 14.3 knots. 88
- 6.20 Plot showing a comparison between present results and computed results by Tanizawa [57]. The results are the response amplitude operator for the mid-ship vertical bending moment for a VLCC in following sea at a speed of 14.3 knots. 88
- 6.21 Plot of the analysed weight distribution of the fast ferry. 89
- 6.22 Plot showing a comparison between present results and computed results made by SHIPMO and SGN80. The results are the heave response amplitude operators for a fast ferry advancing in head sea at a speed of 35 knots. 90
- 6.23 Plot showing a comparison between present results and computed results made by SHIPMO and SGN80. The results are the pitch response amplitude operators for a fast ferry advancing in head sea at a speed of 35 knots. 90

-
- 6.24 Plot showing a comparison between present results and computed results made by SHIPMO and SGN80. The results are the response amplitude operator for the vertical acceleration in FP for a fast ferry advancing in head sea at a speed of 35 knots. 91
- 6.25 Plot showing a comparison between present results and computed results made by SGN80. The results are the longitudinal distribution of the rms value of the vertical acceleration for a fast ferry in different sea states. 93
- 6.26 Plot showing a comparison between present results and computed results made by SHIPMO and SGN80. The results are the response amplitude operators for the vertical shear force in the COG for a fast ferry advancing in head sea at a speed of 35 knots. 94
- 6.27 Plot showing a comparison between present results and computed results made by SHIPMO and SGN80. The results are the response amplitude operators for the vertical bending moment in the COG for a fast ferry advancing in head sea at a speed of 35 knots. 94
- 7.1 List of the modules and submodules in the software system, I-ship 98
- 7.2 Sketch showing the concept of the wave load module. 98
- 7.3 Sketch showing a diagram over the Strip theory preprocessor. 99
- 7.4 Picture showing the discretization dialogue window. 100
- 7.5 Display from the program showing a heading distribution for a long-term statistics calculation 103
- 7.6 Display from the program showing a speed distribution for a long-term statistics calculation. 104
- 7.7 Display of an example of output in tables. 105
- 7.8 Display of an example of output as plots. 106
- A.1 Plot showing a comparison between present methods for a speed of zero knots. The results are the response amplitude operators for the vertical bending moment amidship for S-175 in head sea. 125

This page is intentionally left blank.

List of Tables

6.1	<i>Principal particulars for the container ship used for validation and verification.</i>	68
6.2	<i>Heading distribution of time in the sea states.</i>	75
6.3	<i>Speed distribution of time in the sea states.</i>	75
6.4	<i>Distribution of time in the Marsden areas.</i>	75
6.5	<i>Comparison of design midship vertical bending moment (IACS refer to control for buckling).</i>	77
6.6	<i>Principal particulars for the model and the full-scale tanker used for validation and verification.</i>	81
7.1	<i>A List showing the possible combinations of type and calculation level of the response.</i>	101
7.2	<i>List of files contained in a project.</i>	105

This page is intentionally left blank.

Appendix A

Additional Results on the Container Ship

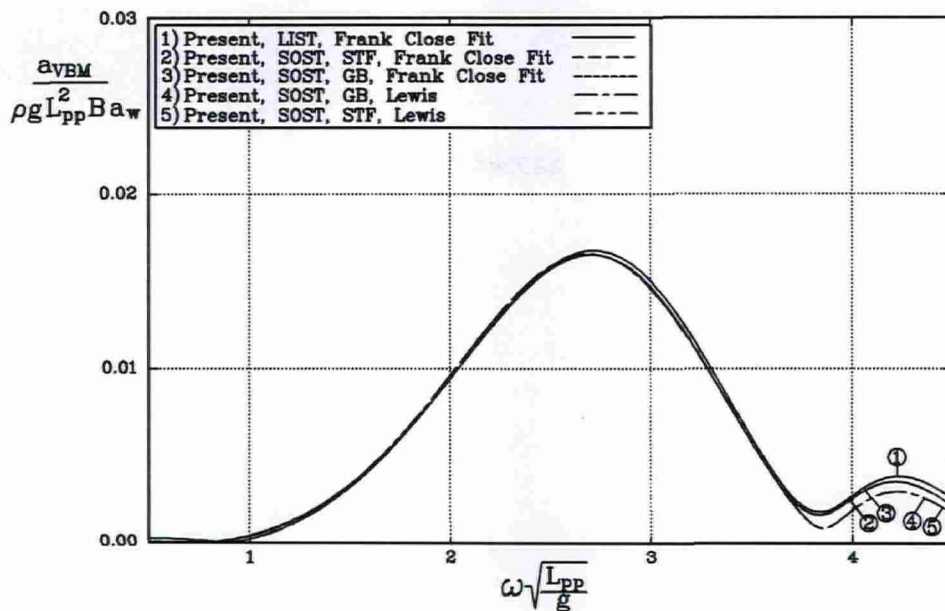


Figure A.1: Response amplitude operators for the vertical bending moment amidship for S-175 in head sea at a speed of zero knots.

The vertical bending moments amidship for the different methods are seen to be identical when the speed is set to zero. The difference in the results from the present methods could therefore be related to speed dependent damping terms.

This page is intentionally left blank.

Appendix B

Documentation of the User Interface

This documentation describes the use of the modules for determination of wave loads. The modules are denoted STPE, LIST, SOST, NLST and STPP and they are a part of the I-ship design system. The pre- and postprocessor consist of the single modules STPE and STPP, while the solver includes the three modules LIST, SOST and NLST, each capable of performing different types of analyses. The documentation is divided into three sections describing the use of the preprocessor, the solver and the postprocessor, respectively.

The use of the modules requires a prior definition of the ship geometry and the weight condition. This is done by use of the modules WGHT and LINE, which is also included in the I-ship design system. Separate documentation is available on these modules. An important requirement related to the LINE module is that the station curves must be defined from the keel to the line of symmetry in the deck.

In the main documentation of the I-ship design system the general guide to the use of the system can be found. The most important information on the general use of the system is shortly summarised in the following.

The file structure is gathered in a project. By the selection of a project the files, which are necessary for the module in question are autoloaded. The general philosophy is that menu items are to be selected in the order from top and down, which also refers to the item numbers. A supplement to this documentation is provided by the help related to each menu. The help is invoked by the input of ?. It is also possible to abort a menu by the input of \$.

B.1 The Preprocessor

The main entry of the preprocessor consists of the menu labelled THE PREPROCESSOR. The menu items 1-3 divides the input into three categories. The first and the second include *General input* in Figure 7.3 and the third covers *Load case related input*.

THE PREPROCESSOR
1. Input ship data
2. Input operational parameters
3. Specify analysis
4. Miscellaneous
5. Setup
6. File
7. EXIT

Menu item 4 makes it possible to determine added mass and damping directly in the preprocessor and is intended for use where the output of interest is the added mass and damping, e.g for use in another program. Menu item 5 is a standard I-ship module menu. It is used for project file manipulation and it is documented in the main I-ship documentation. Menu item 6 is used for manipulation of input and output files. It is important to note that the last action in the preprocessor is to save the output file and it is done using this menu item. The menu items will be described further in the following.

B.1.1 Input Ship Data

Input ship data
1. Environmental data
2. Hydrostatic data
3. Define sinkage and trim (OPTIONAL)
4. Hull discretization
5. RETURN

Environmental data includes the gravitational acceleration and the density of the water used for the analysis.

Hydrostatic data makes it possible to choose a weight condition for the analysis and the equilibrium position of the ship is determined. Prior to the return to the shown menu all relevant input data is listed.

Define sinkage and trim (OPTIONAL) consists of the possibility of basing the analysis on a deviation from the equilibrium condition. This is given in terms of an input of sinkage and trim.

Hull discretization covers the menu item for input of data for determination of the grid of segments on the station curves. It is possible to

Hull discretization
1. Automatic grid generation
2. Modify grid
3. Plot grid
4. Auxiliary
5. RETURN

use the automatic grid generation to distribute a given number of points on all the stations. This is normally the initial step. A following inspection or modification of the grid can be performed by selecting *Modify grid* or *Plot grid*. In the *Modify grid* it is possible to step through the station curves and decrease or increase the number of points. The grid is updated automatically after each modification. If the number of points on a station curve is set to zero it will be neglected from the analysis. This may be convenient, e.g. if a station curve has a characteristic shape which gives unphysical results.

B.1.2 Input Operational Parameters

Input operational parameters
1. Input speed(s)
2. Input heading(s)
3. Input frequencies
4. Input frequency distribution
5. RETURN

Input speed(s) is possible both in terms of [m/s], [knots] or based on a Froude number. The Froude number is based on the length between perpendiculars.

Input heading(s) is possible by specifying a lower and upper limit along with the number of equidistantly distributed headings. Generally, seven headings are sufficient, but in some cases, especially in studies of accelerations, a larger number of headings may be feasible.

Input frequencies cover the range and number of frequencies for the analysis. It can be given both in terms of wave and encounter frequency. The range must cover the wave spectrum in the considered sea states.

Input frequency distribution makes it possible to manipulate the distribution of the frequencies of encounter. It is possible to choose from an equidistant and a weighted distribution. The former is self-explaining and compulsory for quadratic analyses. The latter takes into account for a given range of frequencies of encounter the fact that the corresponding wave frequencies are shifted depending on the headings. The frequencies of encounter are distributed in a way which makes the wave frequencies in an overall sense more evenly distributed.

B.1.3 Specify Analysis

When the input for the analysis has been defined, the next step is to define the analysis in terms of methodology and output of interest.

Specify analysis
1. Specify output
2. Select methods
3. Short-term statistics (OPTIONAL)
4. Long-term statistics (OPTIONAL)
5. RETURN

The first two menu items are necessary for a basic analysis, while the selection of short- and long-term statistics is optional. The output from the analysis is specified by selecting the first menu item. If this includes short-term or long-term statistics the default or the specified input under menu items 3 and 4 will be used.

Specify Output

All output except the motions is related to a longitudinal position. These positions are given as input by selecting the first menu item.

Specify output	
1. Specify longitudinal positions	[3]
2. Ship motions	[FRF][SHTM][LGTM]
3. Relative motions	[FRF][SHTM][LGTM]
4. Accelerations	[FRF][SHTM][LGTM]
5. Shear forces	[FRF][SHTM][LGTM]
6. Bending moments	[FRF][SHTM][LGTM]
7. RETURN	

The input is given in the following form. Initially, the square brackets on the right side of the menus are empty. Each time a menu item is selected an additional set of brackets is filled for the selected menu item. The abbreviations are FRF, Frequency response function, SHTM, Short-term statistics and finally LGTM, Long-term statistics. The dependence of some selections on others is taken into account by adding contents to the brackets from the left to the right. A selection of a menu item having the full selection listed in brackets resets the menu item.

Select Methods

The method for the analysis is selected by means of the menu shown below.

Select methods	
1. Linear load case	[n]
2. Quadratic load case	[y]
3. Time-domain load case	[n]
4. Reset load cases	
5. RETURN	

The [y] or [n] indicates whether the input has been completed or not. The first two methods have input in common, therefore the same basic menu is invoked, however, not all menu items are active. These menu items are indicated by an italic font. The third method has a separate menu due to a different input.

Linear Load Case

Linear load case
1. <i>Strip theory</i>
2. Methods for added mass and damping
3. <i>Derivatives</i>
4. <i>Modes</i>
5. RETURN

The input for a linear load case consists of the selection of the method for determining added mass and damping. This selection is the same for the quadratic load case and will be described separately in a following section.

Quadratic Load Case

Quadratic load case
1. Strip theory
2. Methods for added mass and damping
3. Derivatives
4. Modes
5. RETURN

Because the quadratic strip theory can be based on both the theory according to Gerritsma and Beukelman [6] as well as Salvesen, Tuck and Faltinsen [49], the first menu item makes it possible to select from the two. The selection of the method for determining added mass and damping will be described below. The draught variation for the determination of the derivatives with respect to immersion is given as input by selecting menu item 3. Menu item 4 makes it possible to perform a hydroelastic analysis by including a given number of elastic modes. Heave and pitch refer to mode one and two, while selection of a higher number of modes includes the corresponding elastic modes. Sectional shear and bending rigidities as well as the structural damping must be given as input too, if a mode number larger than two is selected.

Added Mass and Damping

A part of the module consists of a library of methods for determining added mass and damping. The methods are listed below.

Added mass and damping	
1. 1-dof theory according to Lewis	()
2. 1-dof theory according to Lewis/Yamamoto	()
3. 3-dof Frank Close Fit	()
4. 3-dof Green function I	()
5. 3-dof Green function II (Finite depth)	()
6. Additional roll damping	
7. RETURN	

For load case selections including only heave and pitch all methods are available, while for the remaining only menu items 3-5 are available. The first menu item indicates Lewis transformation. The second determines added mass using Lewis transformation and damping according to Yamamoto et al. [68]. The methods under menu items 3-5 are described in Chapter 4. The Green function I refers to the method for infinite depth and the Green function II refers to finite water depth. Selection of the 3-dof Green function II requires an input of the size of the domain in terms of depth and distance to radiation boundaries.

For load cases including roll there is a possibility of including additional roll damping. The input is given as a fraction of the critical damping.

Time-Domain Load Case

The input specific for a time-domain load case is as shown below.

Time-domain load case	
1. No. of stations	
2. No. of waterlines	
3. No. of wave amplitudes	
4. Green water implementation	
5. RETURN	

For the time-domain analysis a grid is made on the basis of interpolation. The grid consists of a given number of stations and waterlines. The analysis includes determination of the response amplitudes in regular waves with the amplitudes specified by selecting menu item 3. The frequencies refer to the input given in the *Input ship data* menu. Menu item 4 makes it possible to include the green water on deck in the d'Alembert force in the analysis. An input between zero and one can be given. The input indicates the fraction of the green water which is to be included in the d'Alembert force.

Short-Term Statistics

Short-term statistics	
1. Spectrum	[ISSC]
2. Duration	10000.0 sec
3. No. of Hs	15
4. Limits for Hs	1.0-15.0 m
5. No. of Tz	15
6. Limits for Tz	1.0-15.0 sec
8. RETURN	

Input of the short-term statistics is only required if output of this type is selected. The spectrum can be specified to be ISSC or JONSWAP. The duration of the sea state is given in seconds under menu item 2. The number of significant wave heights and zero upcrossing periods is fifteen and should not be modified. This will cover regular scatter diagrams.

Long-Term Statistics

Long-term statistics
1. Period
2. Route data
3. Speed and heading distribution
4. Auxiliary
5. RETURN

The input to the long-term statistics is as in the preceding case only necessary if output of this kind has been specified. The operational period for the analysis is usually twenty years but can be modified by use of menu item 1. The route data is given in menu item 2 as the number of the scatter diagrams and a corresponding distribution of the time. The distribution of the speeds and headings specified for the analysis can be given by use of menu item 3.

Speed and heading distribution	
1. No. of speeds	2
2. No. of headings	5
3. No. of limits for the significant wave heights	2
4. Modify speed distribution	
5. View speed distribution	
6. Modify heading distribution	
7. View heading distribution	
8. RETURN	

Menu items 1 and 2 list the numbers of speeds and headings earlier specified. Menu item 3 is used to define the range for the significant wave height where it is possible to define different distributions for the speed and heading. The distributions are given by using menu items 4 and 6 and can be viewed by using menu items 5 and 7.

Auxiliary	
1. Stress/response ratio	
2. Slope of SN curve	
3. Scale of SN curve	
4. Ranges for probability of exceedance	
5. RETURN	

Menu items 1, 2 and 3 cover input to fatigue calculations. The stress/response ratio is given between the vertical bending moment and a structural detail on the ship. Menu item 4 is used to modify the output of the probability of exceedance curves. The input is the lower and upper limit for the response and the number of calculation points.

B.2 The Strip Theory Solver

The solver covers the three modules LIST, SOST and NLST. Only one load case type can be selected for each analysis.

THE SOLVER
1. Compute load cases
2. Setup
3. File
4. EXIT

B.3 The Postprocessor

The main menu of the postprocessor has the menu items shown below.

THE POSTPROCESSOR
1. Load data
2. Print data
3. Plot data
4. Setup
5. RETURN

The first step is to load data, which gives the options listed below.

Load data
1. General data on the ship [.STE]
2. Added mass and damping [.AMD]
3. Linear strip theory load case [.LST]
4. Quadratic strip theory load case [.SST]
5. Time domain strip theory load case [.TME]
6. View load cases
7. RETURN

First menu item 1 is to be selected. Secondly, the result corresponding to the load case type defined can be loaded. To view the main parameters of the analysis menu item 6 can be used.

Returning to the main menu and selecting *Print data* give the following options:

Print data
1. Input for this analysis
2. Hydrodynamic data
3. Response amplitude operators
4. Short-term response
5. Long-term response
6. RETURN

The results can be printed in tables as shown in Figure 7.7. Help is provided at each menu point for guidance.

By selection of the *Plot data* menu item in the main menu the following option becomes available:

Plot data
1. Hydrodynamic data
2. Response amplitude operators
3. RETURN

An example of the plots is shown in Figure 7.8. The response amplitude operators include transfer and phase functions. Phases are defined relative to a wave crest in the centre of gravity. Usually, the preferred form of the output is different. Therefore, a facility to manipulate the units on the axes is available. An example of this is shown below for the abscissa on a plot of a transfer function.

Manipulate settings
1. Angular frequency of encounter
2. Angular wave frequency
3. Wave length
4. Ship to wave length ratio
5. Wave to ship length ratio
6. Non-dimensional frequency w. respect to L_{pp}
7. Non-dimensional frequency w. respect to B

The current selection has a different colour and is marked by an increased vertical space to the remaining menu items.

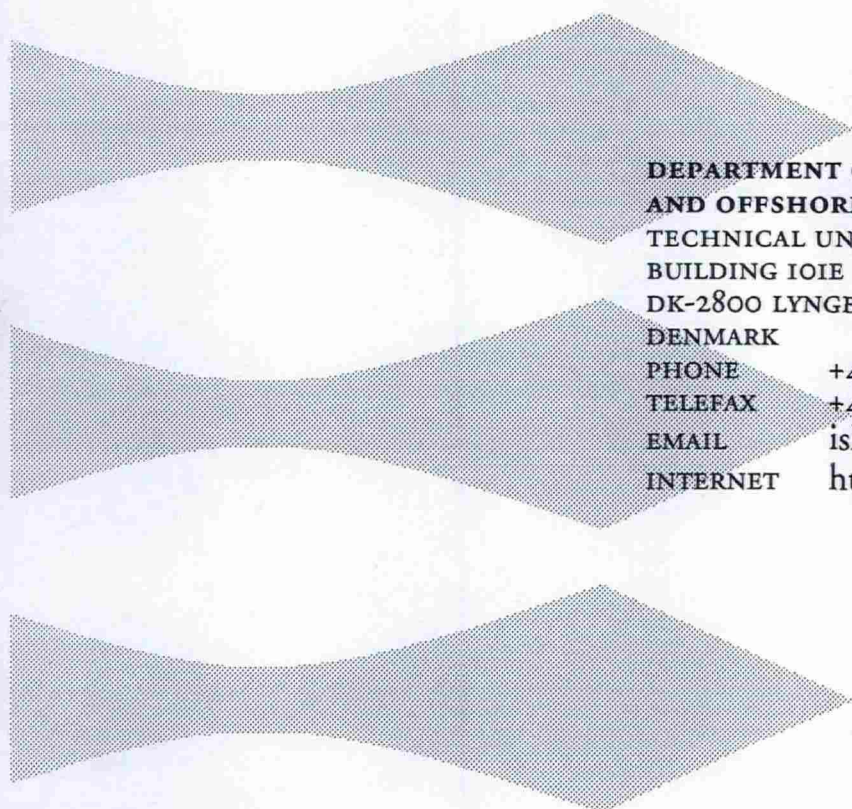
Ph.D. Theses
Department of Naval Architecture and Offshore Engineering
Technical University of Denmark · Lyngby

- 1961 Strøm-Tejsen, J. *Damage Stability Calculations on the Computer DASK.*
- 1963 Silovic, V. *A Five Hole Spherical Pilot Tube for three Dimensional Wake Measurements.*
- 1964 Chomchuenchit, V. *Determination of the Weight Distribution of Ship Models.*
- 1965 Chislett, M.S. *A Planar Motion Mechanism.*
- 1965 Nicordhanon, P. *A Phase Changer in the HyA Planar Motion Mechanism and Calculation of Phase Angle.*
- 1966 Jensen, B. *Anvendelse af statistiske metoder til kontrol af forskellige eksisterende tilnærmelsesformler og udarbejdelse af nye til bestemmelse af skibes tonnage og stabilitet.*
- 1968 Aage, C. *Eksperimentel og beregningsmæssig bestemmelse af vindkræfter på skibe.*
- 1972 Prytz, K. *Datamatorienterede studier af planende bådes fremdrivningsforhold.*
- 1977 Hee, J.M. *Store sideportes indflydelse på langskibs styrke.*
- 1977 Madsen, N.F. *Vibrations in Ships.*
- 1978 Andersen, P. *Bølgeinducerede bevægelser og belastninger for skib på lægt vand.*
- 1978 Römeling, J.U. *Buling af afstivede pladepaneller.*
- 1978 Sørensen, H.H. *Sammenkobling af rotations-symmetriske og generelle tre-dimensionale konstruktioner i elementmetode-beregninger.*
- 1980 Fabian, O. *Elastic-Plastic Collapse of Long Tubes under Combined Bending and Pressure Load.*
- 1980 Petersen, M.J. *Ship Collisions.*
- 1981 Gong, J. *A Rational Approach to Automatic Design of Ship Sections.*
- 1982 Nielsen, K. *Bølgeenergimaskiner.*
- 1984 Rishøj Nielsen, N.J. *Structural Optimization of Ship Structures.*
- 1984 Liebst, J. *Torsion of Container Ships.*
- 1985 Gjersøe-Fog, N. *Mathematical Definition of Ship Hull Surfaces using B-splines.*

-
- 1985 Jensen, P.S. *Stationære skibsbølger.*
- 1986 Nedergaard, H. *Collapse of Offshore Platforms.*
- 1986 Yan, J.-Q. *3-D Analysis of Pipelines during Laying.*
- 1987 Holt-Madsen, A. *A Quadratic Theory for the Fatigue Life Estimation of Offshore Structures.*
- 1989 Andersen, S.V. *Numerical Treatment of the Design-Analysis Problem of Ship Propellers using Vortex Lattice Methods.*
- 1989 Rasmussen, J. *Structural Design of Sandwich Structures.*
- 1990 Baatrup, J. *Structural Analysis of Marine Structures.*
- 1990 Wedel-Heinen, J. *Vibration Analysis of Imperfect Elements in Marine Structures.*
- 1991 Almlund, J. *Life Cycle Model for Offshore Installations for Use in Prospect Evaluation.*
- 1991 Back-Pedersen, A. *Analysis of Slender Marine Structures.*
- 1992 Bendiksen, E. *Hull Girder Collapse.*
- 1992 Petersen, J.B. *Non-Linear Strip Theories for Ship Response in Waves.*
- 1992 Schalck, S. *Ship Design Using B-spline Patches.*
- 1993 Kierkegaard, H. *Ship Collisions with Icebergs.*
- 1994 Pedersen, B. *A Free-Surface Analysis of a Two-Dimensional Moving Surface-Piercing Body.*
- 1994 Hansen, P.F. *Reliability Analysis of a Midship Section.*
- 1994 Michelsen, J. *A Free-Form Geometric Modelling Approach with Ship Design Applications.*
- 1995 Hansen, A.M. *Reliability Methods for the Longitudinal Strength of Ships.*
- 1995 Branner, K. *Capacity and Lifetime of Foam Core Sandwich Structures.*
- 1995 Schack, C. *Skrogudvikling af hurtiggående færger med henblik på sødygtighed og lav modstand.*
- 1997 Simonsen, B.C. *Mechanics of Ship Grounding.*
- 1997 Riber, H.J. *Response Analysis of Dynamically Loaded Composite Panels.*
- 1997 Olesen, N.A. *Turbulent Flow Past Ship Hulls.*

- 1998 Andersen, M.R. *Fatigue Crack Initiation and Growth in Ship Structures.*
- 1998 Nielsen, L.P. *Structural Capacity of the Hull Girder.*
- 1999 Zhang, S. *The Mechanics of Ship Collisions.*
- 1999 Birk-Sørensen, M. *Simulation of Welding Distortion in Ship Sections.*
- 1999 Jensen, K. *Documentation and Analysis of Ancient Ships.*

This page is intentionally left blank.



**DEPARTMENT OF NAVAL ARCHITECTURE
AND OFFSHORE ENGINEERING
TECHNICAL UNIVERSITY OF DENMARK
BUILDING IOIE
DK-2800 LYNGBY
DENMARK**

PHONE +45 4525 1360
TELEFAX +45 4588 4325
EMAIL ish@ish.dtu.dk
INTERNET <http://www.ish.dtu.dk>

ISBN 87-89502-17-5